Electron transport barriers in tokamak plasmas

Please check the document version of this publication:

• A submitted manuscript is the version of the article upon submission and before peer-review. There can be important differences between the submitted version and the official published version of record. People interested in the research are advised to contact the author for the final version of the publication, or visit the DOI to the publisher's website.
• The final author version and the galley proof are versions of the publication after peer review.
• The final published version features the final layout of the paper including the volume, issue and page numbers.

[Link to publication](#)

Download date: 16. Nov. 2023

Electron Transport Barriers in Tokamak Plasmas

Marco Richard de Baar

Electron Transport Barriers in Tokamak Plasmas

Electron Transport Barriers in Tokamak Plasmas

PROEFSCHRIFT

ter verkrijging van de graad van doctor aan de
Technische Universiteit Eindhoven, op gezag van de
Rector Magnificus, prof.dr. M. Rem, voor een
commissie aangewezen door het College voor
Promoties in het openbaar te verdedigen
op woensdag 6 januari 1999 om 16.00 uur

door

Marco Richard de Baar

geboren te Woerden

Dit proefschrift is goedgekeurd door de promotoren:

prof.dr. N.J. Lopes Cardozo
en
prof.dr. F.C. Schüller

Copromotor: dr. G.M.D. Hogeweij

FOM   NWO

Soms verman ik mij en begin een fraai gebonden, vers geurend cahier, maar als ik na een paar uur de doorhalingen, de vlekken en bovenal mijn afzichtelijke handschrift tegenkom op die volmaakte gladheid, in dat harmonische formaat, kan ik mijzelf niet vergeven dat ik het niet zo gelaten heb als het uit de winkel kwam en ik stop het weg op een plaats waar ik het nooit terug zal kunnen vinden.

Uit de 'Preambule' van 'Paranoia', W.F. Hermans

Aan Henriëtte

Contents

Chapter 1

Introduction

In this thesis, transport properties of a tokamak plasma under dominant heating with microwaves (electron cyclotron heating or ECH) are investigated. Special attention is paid to the possibility that heat transport by the electrons is inhomogeneous, i.e. that some parts of the plasma act as thermal barriers, that separate regions of high heat conduction. For the reader who is not familiar with the world of thermonuclear plasma physics, we will introduce the abovementioned terminology.

1.1 Plasma

A plasma is a gas of positively and negatively charged particles and neutrals. As a whole, the plasma can be uncharged, but due to the long range Coulomb interaction the particles in the gas are tied together, correlated so to speak, giving rise to collective behaviour. Note that the gas is very thin: $1 \, mm^3$ of solid hydrogen contains typically as many particles as $1 \, m^3$ plasma at fusion temperature.

On earth the occurence of plasmas is rather limited and one might wonder why anybody would be interested in doing plasma physics in the first place. To start, in space, plasma is the predominant state of matter and therefore, to astro-physicists plasma theory is of vital importance. The most famous example of a space plasma is our sun. The sun is an almost perfect sphere. Gravity provides the force that balances enormous pressure gradients leading to conditions at which fusion reactions occur. This naturally introduces what we want to achieve on earth: One of the goals in plasma physics is to simulate the sun on earth in a device in which the pressure gradient needed to achieve fusion conditions is balanced by electromagnetic fields. Today, we are able to routinely produce plasmas with temperatures that exceed that of the sun and we reach conditions at which fusion reactions produce power at the multi MegaWatt level. In the last 40

years the figure of merit (see below) for fusion performance improved by a factor of $\approx 10^7$. Today, we are only a factor of 6 separated from 'ignition,' at which point an economically viable fusion reactor is within reach. The design of an experimental reactor is ready, but the investment required to build it ($\sim 7 \cdot 10^9$ \$) is a major political stumble block, even if such a project is financed as a global collaboration effort.

1.2 Thermonuclear fusion

In nuclear fusion [1, 2, 3, 4], two nuclei of light elements are brought together within the range of their strong interactions. As a consequence the nuclei react and melt together, forming new, energetic particles. In order to bring the two nuclei together, the repelling Coulomb force has to be overcome over a relatively long distance. Consequently, high temperatures are required for fusion reactions.

The most accessible and promising reaction for fusion reactors is the one between deuterium D and tritium T in which helium (^4_2He) and an energetic neutron (n) are formed:

$$D + T \longrightarrow \, ^4_2He + n + 17.58 \, \text{MeV} \, . \tag{1.1}$$
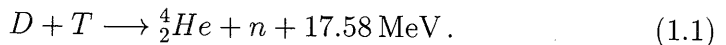
For the $D - T$ reaction the required temperature in a fusion reactor is $\sim 10^8$ K. At these temperatures, the D-T fuel is in the plasma state. For a high energy gain, a high density n_e is required. The volume integral over the pressure is the stored kinetic energy: $W = 3/2k \int [n_e T_e + n_i T_i] dV$, where k is the Boltzmann constant and $T_{e,i}$ denotes the temperature of the electrons and ions respectively. Loss processes (due to Coulomb collisions and turbulence) tend to decrease W. To compensate for the losses, power (P_{in}) is deposited into the plasma. The gross loss processes can be quantified in terms of a typical timescale, the energy confinement time τ_E. The longer τ_E, the better. In steady state, $\tau_E = W/P_{in}$. The triple product $n_e \tau_E T_i$ is a figure of merit for fusion performance. It can be shown that the necessary condition for a steady state reactor is $n_e \tau_E T_i > 6 \, \text{Bar} \cdot \text{s}$ [4].

1.3 Tokamak

Since 1968 a toroidal device called the tokamak [3, 4] is leading the competition for higher values of the triple product. The tokamak (see Fig.1.1) is a system to confine the plasma in a toroidal vacuum vessel with major radius R_0 and minor radius a. The name tokamak stems from the Russian words for Toroidal Chamber and Magnetic Coil, toroidalnaya kamera
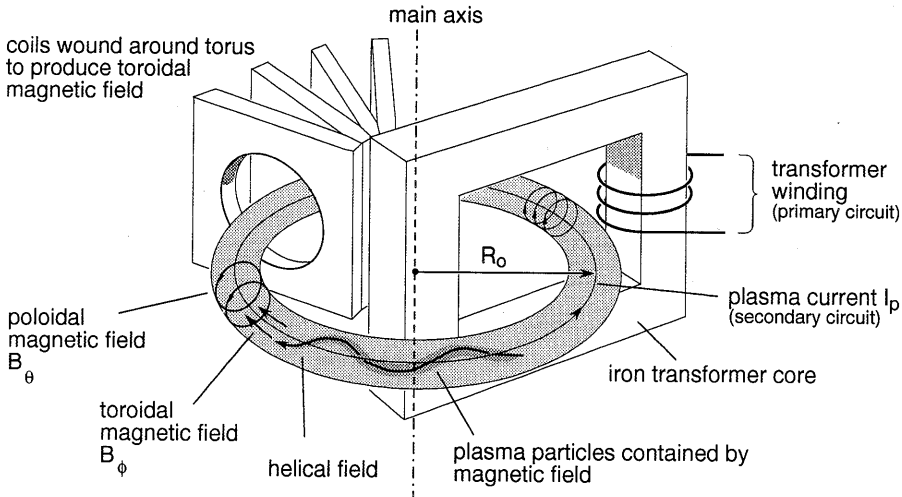
Figure 1.1: *The tokamak, its magnetic fields and some of its subsystems.*

magnitnaya katushka [4]. The achievements of the tokamak are most impressive: Thermal energies are obtained up to 50 keV at reactor relevant densities (up to several times $10^{20}\,\mathrm{m}^{-3}$). Several reactor relevant modes of operation have been identified.

Reactor relevant parameters are achieved in big tokamaks. The largest tokamak in the world, JET, holds many records. Operation in plasmas that consist of deuterium and tritium has been carried out in TFTR and JET. In the fall of 1997, a series of experiments were carried out in JET, showing

- a new record in produced fusion power (16.1 MW),

- a new record in fusion energy of 21 MJ, produced in quasi-steady state in 3 seconds,

- a new record in the ratio between input and fusion power: $P_{\mathrm{fus}}/P_{\mathrm{in}} \approx 0.65$,

1.4   Magnetic field in a Tokamak

Several magnetic fields have to be applied in a tokamak. The dominant magnetic field, the toroidal magnetic field (B_ϕ) is generated by a set of coils. By using the plasma column as the secondary winding of a transformer, a current I_p and the concomittant poloidal magnetic field (B_θ) are generated. The combined magnetic field is helical. Except for field errors, due to the

finite numbers of coils, the magnetic geometry is axis symetric. The pitch of the field lines in Fig.1.1 is exaggerated: in a tokamak, the field lines carry out several toroidal orbits before one poloidal orbit is fulfilled. The ratio between the number of toroidal and poloidal rotations is denoted by the magnetic winding number q.

q and its derivative with respect to the minor radius, the magnetic shear $(\hat{s} = (r/q)(\partial q/\partial r))$ are continuous funtions that characterise the topology of the magnetic field. For arbitrarily small perturbations, resonant with $q = m/n$ (with m and n the integer poloidal and toroidal mode-numbers), the topology of the field changes from the ideal set of nested, perfect flux toroidal surfaces, to the generic mix of good surfaces, chains of magnetic islands and regions of chaotic field. The surfaces with simple rational winding number are the first to degenerate and form magnetic islands, the surfaces of which the winding number is 'very' irrational are the last to remain. q is associated with stability of the plasma column and therefore also often referred to as the safety factor.

1.5 Heating

Up to temperatures of $\sim 10^7\,\mathrm{K}$ (or equivalently $\approx 1\,\mathrm{keV}$), tokamak plasmas are heated by the plasma current: the plasma has a small but finite electrical resistance, leading to Ohmic dissipation. Higher temperatures are achieved with additional heating. Systems for additional heating are neutral beam injection (NBI), ion cyclotron resonant heating (ICRH), lower hybrid heating (LHH). In the experiments described in this thesis, we used electron cyclotron heating (ECH): high power microwaves, resonant with the cyclotron motion of the electrons in the magnetic field, are coupled into the plasma and absorbed by electrons. ECH enables power deposition in a small region of the plasma, referred to as localised heating. In our case in steady-state, the ECH power is typically 7 times larger than the power from Ohmic dissipation. Therefore, the power balance of the plasma is dominated by the ECH power, which unlike the Ohmic dissipation, is fully under control of the experimentalist.

1.6 Transport

One of the principal problems in nuclear fusion research is that the experimentally determined values for the energy confinement time τ_E are unexpectedly short. This could lead to big, complicated, expensive and

therefore unattractive reactors.

Neo-classical transport theory describes transport phenomena that stem from Coulomb collisions in systems with toroidal symmetry. Neo-classical transport is considered to be the concrete floor of transport in tokamak plasmas: values for the heat conductivity will always be larger or equal to the neo-classical predictions. Experiments show that the energy losses via the electrons exceed neo-classical predictions by one to two orders of magnitude, while the losses via the ions are reported to be less than one order of magnitude larger that the neo-classical predictions. Turbulent mechanisms, not taken into account in the neo-classical theory, are held responsible for the enhanced heat transport. Much effort has been put into the study of anomalous transport. The ultimate goal of this effort is to understand turbulent transport, to control turbulent transport and thus to achieve important reductions in the dimensions of the magnetic vessel of next generation reactor size tokamaks.

The research of anomalous transport covers many aspects. Statistical analysis on discharges of present-day tokamaks is done to find an emperical relationship in scaling laws between τ_E and 'engineering' parameters such as plasma current, plasma shape, volume and B_ϕ. These studies are carried out to predict the performance of next generation tokamaks. Experimental studies are carried out to pin-point the values of the heat and particle diffusion coefficients. Much attention is paid to experimental scenarios in which the turbulent transport is importantly reduced. Theoretical efforts aim at identifying and describing processes driving turbulent transport.

In various tokamaks conditions have been reached in which the ion thermal conductivity is reduced, at least transiently, to the neo-classical level in part of or even the entire plasma. This reduction appears to be associated with a strong shear of the plasma velocity and a reduction of the density fluctuation levels.

The electron thermal transport behaves differently from that of the ions. Electron transport barriers may form, but not necessarily at the same time, or the same place as the ion transport barriers, and there is neither a clear relation to the velocity shear, nor to the level of density fluctuations. Thus, electron and ion thermal transport appear to be driven by different mechanisms.

When the ion transport is reduced to the neo-classical level, the heat losses via the electrons are the dominant energy leak. The fact that reductions in the electron channel have been observed motivates further research into the conductivity of heat via electrons.

1.7 This thesis

This thesis is about barriers in the electron channel. We will try to answer the questions:

- Do barriers for the electrons exist?

- On which parameters do they depend?

- How can they be influenced?

As a starting point in our research, we note that in the vicinity of the $q = 1$ surface, a barrier for the electron thermal transport has been measured on several tokamaks [5, 6, 7]. This suggests a relation between the magnetic topology and these barriers, and we are specifically going to investigate the role of the q-profile in electron thermal barrier formation.

The experiments were carried in the Rijnhuizen Tokamak Project (RTP). RTP is equiped with a high power system for ECRH. The EC-power is typically 7 times the power that stems form the Ohmic dissipation. The EC power deposition can be concentrated in small region of the plasma. RTP features high resolution diagnostics for T_e and n_e. These specific features make RTP well suited to study the mechanisms that drive the heat transport via the electrons: The powerful ECRH enables the production of a wide variaty of T_e profiles, current density (j) profiles and q-profiles. The high resolution diagnostics for measuring T_e and n_e enable the study of small-scale structures. The coupling between ions and electrons is small, as a consequence of which electron thermal transport can studied independently of ion thermal transport.

RTP is a small tokamak ($R_0 = 0.72\,\text{m}$, $a = 0.164\,\text{m}$ with $B_\phi < 2.4\,\text{T}$ and $I_p < 150\,\text{kA}$. Maximum values for T_e in low density RTP discharges are roughly $4\,\text{keV}$. The plasma volume in JET is approximately 100 times larger than in RTP. Despite these modest parameters, transport studies at RTP are relevant for big tokamaks with hot plasmas, because it has been observed that the character of turbulence is independent of the size of the tokamak. Large and small tokamaks can be desribed by the same scaling laws.

This thesis is composed of the following elements. Neo-classical transport, anomalous transport and the mechanisms that can create transport barriers are introduced. The two standard experimental approaches to anomalous transport via the electrons are local power balance analysis and heat pulse propagation analysis (see chapter 2). It is pointed out that, even

with the high spatial resolution diagnostics of RTP (see chapter 3), these approaches break down when thin transport barriers exist in the plasma.

We carried out a detailed scan of the normalised ECH deposition radius $\rho_{dep} = r_{dep}/a$ around $\rho_{dep} = 0.5$. Two distinct confinement states were discovered. These states are separated by a difference in ρ_{dep} of approximately 2 mm. The difference comes about through the presence of a barrier in the state with the best confinement. Interestingly, the state with best confinement features $m = 3$ magnetohydrodynamic activity, off-axis sawtooth-like instabilities, which enabled us to associate the barrier with the $q = 3$ surface. The sharpness of the transition (< 2 mm, much sharper than the ECH-deposition of approximately 1 cm) is interpreted in terms of the loss of the $q = 3$ surface. These results were published in Phys.Rev.Let, and have been incorporated in this thesis as chapter 4.

The above mentioned observations motivated a detailed scan of ρ_{dep} from the magnetic axis of the tokamak to $\rho_{dep} \approx 0.6$. With this scan, a fine structure of electron thermal transport is uncovered. We discovered sharp transitions between plateaux of confinement. The plateaux are associated with the existence of a barrier, the transitions with the loss of a barrier. Again we observed, off-axis sawtooth-like instabilities, relating the barriers to specific values of q. These observations lead to the hypothesis that electron thermal barriers exist in the vicinity of specific values of q. The phenomenology can be reproduced with a model featuring a heat diffusivity profile with transport barriers near integer and half integer values of q. This model reproduces salient details of the experimental data, such as the sharpness of the transitions and the formation of pronounced off-axis temperature maxima for power deposition on top of a barrier. These results have been submitted for publication to Nucl. Fusion, and have been incorporated in this thesis as chapter 5.

An intriguing observation is the co-existence of distinct confinement states in the post-ECH regime. These states form after switch-off of the ECH system and remain stable until the end of the discharge. One state is the 'standard' Ohmic state at RTP with triangular density and electron temperature profiles. The other state features a flat electron temperature profile but a localised steep gradient in the density profile. The observations are at variance with the turbulent modes that are commonly proposed for tokamak plasmas without additional heating. The observations and the discussion in relation to the commonly proposed turbulent modes have been accepted for publication in Phys.Rev.Let, and have been incorporated in this thesis as Sec. 6.1. We argue that the two bifurcated

17

states can be interpreted in terms of the heat diffusivity model featuring transport barriers near integer and half integer values of q (Sec. 6.2).

We learned how the tokamak plasma organises itself in regions of high and low electron thermal transport. The crucial question is: 'Can we influence the plasma such that we improve the electron thermal confinement?' From our understanding it is clear that a low shear region has to be formed at barrier relevant q-values. Several experimental strategies were tried to form such an optimised q-profile. Transiently, it appears possible to improve the confinement, but we did not succeed in sustaining this improvement. Simulations indicate that this effect is due to self-organisation of the plasma: if a state with improved confinement is achieved, the inductively driven current density profile peaks such that the flat shear region is expelled from the barrier relevant q values. This comes about due to the strong dependence of electrical resistivity on temperature. Steady-state improvement of the electron thermal confinement is only possible in tokamak plasmas with a dominance of non-inductively driven current. The data, the first simulations and conclusions are presented in chapter 7.

1.8 Publications

1.8.1 Journals

Below a list of publications related to this thesis is presented. The publications marked with ♠ are included in the thesis (see chapters 4, 5, 6).

- ♠ *Tokamak plasmas with dominant Electron cyclotron heating; evidence for electron thermal transport barriers* M.R. de Baar, M.N.A. Beurskens, G.M.D. Hogeweij and N.J. Lopes Cardozo, submitted to Nucl.Fusion

- *A model for electron transport barriers in tokamaks, tested against data from RTP*
  G.M.D. Hogeweij, N.J. Lopes Cardozo, M.R. de Baar and A.M.R. Schilham, accepted for publication in Nucl.Fusion

- ♠ *Bifurcated states of Ohmically heated Tokamak plasmas*
  M.R. de Baar, G.M.D. Hogeweij and N.J. Lopes Cardozo, accepted for publication in Phys. Rev. Lett

- *Steady state off-axis sawtoothing near $q = 3/2$, 2 and 3 in a Tokamak*
  R.F.G. Meulenbroeks, M.R. de Baar, M.N.A. Beurskens, H.J. de Blank, B.H. Deng, G.M.D. Hogeweij, N.J. Lopes Cardozo, A. Montvai, Th. Oyevaar and the RTP team, submitted to Phys. Rev. Lett

- *Does a tokamak plasma know about the topology of the magnetic field? An experimentalist's view*
  N.J. Lopes Cardozo, G.M.D. Hogeweij and M.R. de Baar,. Physicalia Magazine, **20** PART II 1998

- *Electron thermal transport in RTP: filaments, barriers and bifurcations*
  N.J. Lopes Cardozo et al,. among them M.R. de Baar, Plasma Phys. Control. Fusion **39** (1997) B303-B316

♠ *Electron thermal transport barrier and magnetohydrodynamic activity observed in tokamak plasmas with negative central shear*
  M.R. de Baar, G.M.D. Hogeweij, N.J. Lopes Cardozo, A.A.M. Oomens and F.C. Schüller, Phys. Rev. Lett **78** (1997) 4573-4576

- *The effect of mode scrambling on pulsed radar reflectometry applied to high shear devices*
  A.J.H. Donné, M.R. de Baar and R. Cavazzana, 10th topical conference on high temperature plasma diagnostics, Rev. Sci. Instrum. **68** PART II 1997

- *Density perturbation studies by means of pulsed radar reflectometry*
  S.H. Heijnen, M.R. de Baar, A.J.H. Donné, M.J. van de Pol and C.A.J. Hugenholtz , 10th topical conference on high temperature plasma diagnostics, Rev. Sci. Instrum. **66** 1995

1.8.2 Conferences

- *Progress in EC Heating and current drive physics and technology* 17th International conference on plasma physics and controlled nuclear fusion research, Yokohama, Japan (1998) A.A.M. Oomens *et al.*, among them M.R. de Baar

- *Electron transport studies in the Rijnhuizen tokamak RTP* 17th International conference on plasma physics and controlled nuclear fusion research, Yokohama, Japan (1998) N.J. Lopes Cardozo *et al.*, among them M.R. de Baar

- *Demonstration and Control of Electron Transport barriers in RTP,* Frascati workshop, November '98, the RTP-team, among them M.R. de Baar

- *Possible experiments on electron transport barriers in JET,* Frascati workshop, November '98, the RTP-team, among them M.R. de Baar

19

- *Feedback control of ECH in RTP*, Frascati workshop, November '98, the RTP-team, among them M.R. de Baar

- *Modelling of bifurcations and barriers in RTP*
  EU-US transport task force workshop, Göteborg, september 1998,
  G.M.D. Hogeweij, M.R. de Baar, M.N.A. Beurskens, F.A. Karelse,
  N.J. Lopes Cardozo, A.M.R. Schilham and the RTP team

- *Transport barriers in RTP: dependence on I_p and n_e*
  EU-US transport task force workshop, Göteborg, september 1998,
  A.M.R. Schilham, M.R. de Baar, M.N.A. Beurskens, G.M.D. Hogeweij,
  F.A. Karelse, N.J. Lopes Cardozo and the RTP team

- *Experimental evidence for electron thermal transport barriers in RTP*
  EU-US transport task force workshop, Göteborg, september 1998,
  N.J. Lopes Cardozo, M.R. de Baar, M.N.A. Beurskens, G.M.D. Hogeweij,
  F.A. Karelse, A.M.R. Schilham and the RTP team

- *Bifurcated states within linear Ohmic confinement*
  1998 ICPP combined with the 25th EPS conference on controlled fusion
  and plasma physics, Prague, Czech republic (1998),
  M.R. de Baar, B.H. Deng, G.M.D. Hogeweij, N.J. Lopes Cardozo and
  the RTP team

- *Transport barriers and the q-profile*
  Satellite conference of the 1998 EPS, 'Role of electric fields in plasma
  confinement and exhaust', Prague, Czech republic (1998),
  G.M.D. Hogeweij *et al.*, among them M.R. de Baar

- *Transport barriers and the q-profile*
  1998 ICPP combined with the 25th EPS conference on controlled fusion
  and plasma physics, Prague, Czech republic (1998), A.M.R. Schilham,
  M.R. de Baar, N.J. Lopes Cardozo, G.M.D. Hogeweij

- *Off-axis sawtooth-like instabilities at $q = 3/2, 2$, and 3 in the Rijnhuizen tokamak*
  1998 ICPP combined with the 25th EPS conference on controlled fusion and plasma physics, Prague, Czech republic (1998), R.F.G. Meulenbroeks *et al.*, among them M.R. de Baar

- *Transport barriers and bifurcations in off-axis ECR heated discharges in RTP*
  24th EPS conference on controlled fusion and plasma physics, Berchtesgaden, Germany (1997), M.R. de Baar, P. Galli, G.M.D. Hogeweij,

N.J. Lopes Cardozo, P. Mantica, A.A.M. Oomens, F.C. Schüller and
the RTP-team

- *Non-local plasma response induced by peripheral perturbations in the
  RTP tokamak*
  24th EPS conference on controlled fusion and plasma physics, Bercht-
  esgaden, Germany (1997), P. Mantica, M.R. de Baar, J. de Kloe,
  F. de Luca, P. Galli, G. Gorini, G.M.D. Hogeweij, A. Jachia,
  N.J. Lopes Cardozo, A.A.M. Oomens and the RTP-team

- *Futher evidence of a transport barrier near the $q = 1$ rational surface
  in the RTP tokamak*
  10th Joint workshop on Electron Cyclotron Emission and Electron
  Cyclotron Reasonance Heating (EC-10), Ameland, The Netherlands
  (1997)
  P. Galli, G. Gorini, P. Mantica, F. de Luca, A. Jachia, M.R. de Baar,
  G.M.D. Hogeweij, N.J. Lopes-Cardozo

- *Electron thermal transport barriers and bifurcation of confinement in
  discharges with off-axis Electron Cyclotron Heating in RTP*
  10th Joint workshop on Electron Cyclotron Emission and Electron
  Cyclotron Reasonance Heating (EC-10), Ameland, The Netherlands
  (1997) M.R. de Baar, , G.M.D. Hogeweij, N.J. Lopes Cardozo,
  A.A.M. Oomens, F.C. Schüller and the RTP-team

- *Heat transport in the RTP tokamak* 16th International conference on
  plasma physics and controlled nuclear fusion research, Montréal, Canada
  (1996) G.M.D. Hogeweij *et al.*, among them M.R. de Baar

- *Recent results on ECCD and MHD activity in RTP* 16th International
  conference on plasma physics and controlled nuclear fusion research,
  Montréal, Canada (1996) A.A.M. Oomens *et al.*, among them
  M.R. de Baar

- *Development of double double-tearing modes in reversed shear tokamak
  plasmas*
  23th EPS conference on controlled fusion and plasma physics, Kiev,
  Ukraine (1996), M.R. de Baar, G.M.D. Hogeweij, N.J. Lopes Cardozo,
  A. Montvai, A.A.M. Oomens, F.C. Schüller and the RTP-team

- *First results on ECCD in RTP*
  22th EPS conference on controlled fusion and plasma physics, Bournemouth,
  England (1995), E. Westerhof, R.W. Polman, J. Lok, M.R. de Baar and
  the RTP-team

- *The RTP pulsed radar system*
  International symposium on physics and engeneering of millimeter and submillimeter waves, Kharkov, Ukraine (1995) S.H. Heijnen, M.R. de Baar, A.J.H. Donné, M.J. van de Pol, C.A.J. Hugenholtz and the RTP-team

Bibliography

[1] Y. Miyamoto, Plasma physics for nuclear fusion, MIT press, Cambridge (1980)

[2] R.J. Goldston, Introduction to plasma physics, Institute of physics publication, Bristol (1995)

[3] B.B. Kadomtsev, Tokamak plasma: a complex system, Institute of physics publication, Bristol (1992)

[4] J. Wesson, Tokamaks, second edition, Clarendon press, Oxford (1997)

[5] G.M.D. Hogeweij *et al.*, Nucl.Fusion **36**, (1996) 535

[6] TFR Group, Nucl.Fusion **27**, (1987) 1975

[7] R. Gianella *et al.*, Plasma Phys. Control Fusion **34**, 1992 687

Chapter 2

Electron thermal transport

2.1 Classical and neo-classical transport

Classical [1] and neo-classical [2] transport theory describe those transport phenomena in plasmas that are caused by Coulomb collisions of the particles. While classical theory is valid in cylindrical geometries, neo-classical theory also takes effects into account that stem from the toroidal symmetry of the tokamak. Neo-classical theory is the rock-bottom level of transport in a tokamak. The schematics of the magnetic field in the toroidal plasma are indicated in Fig. 2.1. The toroidal magnetic field (B_ϕ) is combined with a smaller poloidal component B_θ. The resulting helical field lines lie on nested tori, which are characterised by their minor radius r, or $\rho = r/a$, where a is the radius of the outermost magnetic surface. The direction parallel to the surfaces is referred to as parallel ($\parallel$), the direction perpendicular to the surfaces is referred to as perpendicular ($\perp$) or cross-field. When resistivity is not taken into account, thermodynamic quantities such as pressure, temperature and density are constant on a magnetic surface. Neo-classical theory breaks-down if, due to finite resistivity, magnetic surfaces reconnect and the toroidal symetry is broken.

The main difference between classical and neo-classical theory is due to 'banana' orbits of electrons in toroidal geometry: since the magnetic field is necessarily higher at the inboard side of the torus than on the outboard side, electrons can be trapped in the magnetic well on the outboard side. Such electrons carry out a banana-shaped orbit.

In neo-classical theory, both the thermo-dynamic forces and the fluxes are averaged over a magnetic surface. This means that neo-classical transport reduces to a one-dimensional problem, the fluxes being a function of the radius r only. These fluxes can be perpendicular (as for heat diffusion) or parallel to the surfaces (as for the current density).

The aim of transport studies is to find the relation between the fluxes
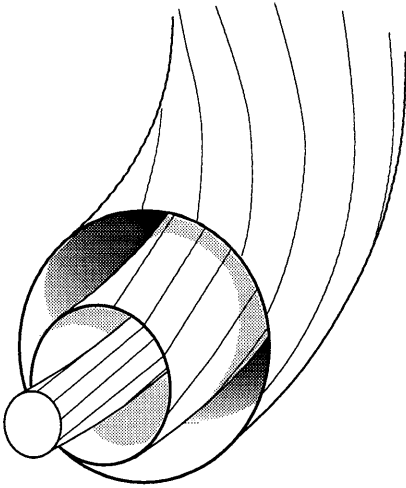
Figure 2.1: *Magnetic field lines and surfaces in a tokamak plasma. To good approximation, the helical magnetic field lines (the combination of B_ϕ and B_θ) form a set of nested tori. These tori can labeled by the normalised minor radius ($\rho = r/a$) of the system. In neo-classical theory, both the thermo-dynamic forces and the fluxes are averaged over a magnetic surface.*

(particle flux Γ, ion thermal flux q_i electron thermal flux q_e, current density j) and the thermodynamic forces (∇n_e, ∇T_i, ∇T_e and E_ϕ). Often these relationships are writen in matrix notation

$$\begin{pmatrix} \Gamma \\ q_\mathrm{e} \\ q_\mathrm{i} \\ j \end{pmatrix} = \begin{pmatrix} D & a_{12} & a_{13} & W \\ a_{21} & \chi_\mathrm{e} & a_{23} & a_{24} \\ a_{31} & a_{32} & \chi_\mathrm{i} & a_{33} \\ B & a_{12} & a_{13} & \sigma \end{pmatrix} \begin{pmatrix} \nabla n_\mathrm{e} \\ \nabla T_\mathrm{e} \\ \nabla T_\mathrm{i} \\ E_\phi \end{pmatrix} \qquad (2.1)$$

The fluxes are due to both diagonal and off-diagonal matrix elements. The fluxes due to the diagonal elements are often referred to as diffusive. In equation 2.1 we recognize particle diffusion, electron thermal diffusion, ion thermal diffusion and the inductive current density. The fluxes due to the off-diagonal components are often referred to as convective. Neo-classical estimates for all collisional fluxes (convective and diffusive) can be given. The best known examples of fluxes due to the off-diagonal components are the Ware-pinch (associated with W in equation 2.1) and the Bootstrap-current (associated with B in equation 2.1). B and W are the only off diagonal elements in the transport matrix that have been investigated experimentally. The others (the a_{ij}) are very difficult to access

experimentally, but are non-zero in neo-classical theory.

Considering the radial electron diffusion as a random walk process with a typical step length of the Larmor radius for electrons ρ_e and at a typical time scale of the collision time τ_e, the classical diffusion coefficient for electrons is

$$D_{\text{class}} \propto \frac{\rho_e^2}{\tau_e}. \qquad (2.2)$$

In a system with toroidal symmetry, the appropriate step length is the width of the banana orbit, which is an order of magnitude larger than ρ_e. Three distinct regimes exist. In the first regime, $\tau_e > Rq/\epsilon^{3/2}v_T$, in which v_T is the thermal velocity, R the major radius, $\epsilon = r/R$ with r the minor radius and q the safety factor. This means that electrons are free to carry out banana-orbits. This is the banana regime with diffusion coefficient $D_B = D_{\text{class}}q^2(R/r)^{3/2}$ in which q is the safety factor. For $\tau_e < Rq/v_T$, the particles cannot carry out banana-orbits. This is the Pfirsch-Schlüter regime, with diffusion coefficient $D_{PS} = D_{\text{class}}(1 + q^2)$. The regime for which $Rq/v_T < \tau_e < Rq/\epsilon^{3/2}v_T$ is referred to as the plateau regime.

According to neo-classical theory, the electron thermal diffusivity χ_e and the particle diffusion coefficient D are of the same order of magnitude. The ion thermal diffusivity exceeds the electron thermal diffusivity by the square root of the ratio of the electron and ion masses,

$$D \approx \chi_e \approx \chi_i\sqrt{m_e/m_i} \approx 0.01\,\text{m}^2/\text{s}, \qquad (2.3)$$

for typical tokamak plasmas.

2.2   Anomalous transport

The transport parallel to the magnetic surfaces proves to be well discribed by neo-classical transport theory and the estimates for both B and $\sigma_\parallel$ agree with experimental observations. The neo-classical cross-field diffusivities $\chi_{i,e}$ and D however do not agree with experimental observations. χ_i exceeds neo-classical predictions up to one order of magnitude. χ_e exceeds neo-classical predictions by up to two orders of magnitude. Experiments showed that typically

$$\chi_i \approx \chi_e \approx (3 - 5)D \approx 1\,\text{m}^2/\text{s}. \qquad (2.4)$$

Moreover, the scaling of transport coefficients with experimental conditions and machine parameters is not understood. Fluctuations are assumed responsible for these anomalies in heat conductivity and particle transport.

Two pictures exist: First, it can be assumed that the magnetic surfaces are perfect, but that fluctuating electric fields drive particle fluxes and turbulent transport via fluctuating $E \times B$ drifts. This picture is referred to as 'electrostatic turbulence'. Second, fluctuations in the magnetic fields can break the toroidal symmetry and destroy the set of nested flux surfaces. Field lines in such a system show radial excursions, and particles moving along the field lines cause the enhanced radial transport. This picture is referred to as 'magnetic turbulence'. It is remarked that any physical fluctuation has both electric and magnetic components, but the classication is nonetheless a useful one.

2.3 Barriers for thermal transport

With the discovery of the H-mode [3] a new era of tokamak physics started. In the H-mode, a transport barrier, a region in which the thermal transport is reduced dramatically, forms in the edge region of the plasma. Sixteen years after the discovery of the H-mode, many regimes have been reported in which transport barriers, at various positions in the plasma, form. The formation of barriers is often associated with bifurcations in confinement. Barriers can occur both in the edge and core region of the plasma (e.g. in tokamak plasmas featuring an off-axis maximum in current density).

2.4 Mechanisms for barrier formation

2.4.1 Electrostatic turbulence quenching

The best established theory for barrier formation is the $E \times B$ sheared flow supression of turbulence. $E \times B$ sheared velocity can influence a wide variety of modes through nonlinear decorrelation of turbulence [4]. For any plasma species ξ, the radial electric field can be evaluated from the radial force balance equation,

$$E_{\mathrm{r}} = \frac{\nabla p_\xi}{n_\xi Z e} + v_{\phi\xi} B_\theta - v_{\theta\xi} B_\phi \,, \tag{2.5}$$

in which p_ξ is its partial pressure, n_ξ is the species density, Z is the charge number, e is the electron charge, $v_{\xi\theta}$ is its poloidal flow velocity, $v_{\xi\phi}$ is its toroidal flow velocity, B_θ is the poloidal and B_ϕ toroidal magnetic field. The total electric field E_r influences the $E \times B$ velocity and its shear. Any one of the righthand side terms in eq. 2.5 can affect $E \times B$ flow velocities.

Assuming isotropy of turbulence in the plane perpendicular to the magnetic field leads to the formulation of a characteristic rate for turbulence decorrelation

$$\gamma_{\mathrm{E \times B}} = \frac{E_{\mathrm{r}}}{B} \left[\frac{1}{E_{\mathrm{r}}} \frac{\partial E_{\mathrm{r}}}{\partial R} - \frac{1}{B_{\theta}} \frac{\partial B_{\theta}}{\partial R} - \frac{1}{R} \right] , \qquad (2.6)$$

valid on the outer midplane of the tokamak. In eq. 2.6 R is the major radius. Decorrelation of turbulence occurs when the characteristic rate for turbulence decorrelation is larger than the maximum linear growth-rate of the dominant turbulent mode,

$$\gamma_{\mathrm{E \times B}} > \gamma_{\mathrm{lin}}^{\mathrm{max}} . \qquad (2.7)$$

$E \times B$ sheared flow suppression of turbulence has been identified as a mechanism to form thermal barriers in the ion channel [5, 6]. It has been shown that the ion thermal barrier formation is associated with damping of density fluctuations below the detection limit [7] after which the ion thermal diffusivity reaches neo-classical estimates. A striking observation is that the damping of density fluctuations does not lead to neo-classical electron transport, and that barriers in the electron channel only form 'sometimes.'

In addition to the $E \times B$ sheared flow supression of turbulence, a few alternative mechanisms for barrier formation have been put forward in the literature. In case of pure ion temperature gradient (ITG or η_{i}) modes and electron temperature gradient (ETG or η_{e}) modes, a threshold gradient scaling with n_{e} exists. In principle, this could lead to particle source-driven bifurcations in thermal confinement [8]. In practice however, density gradients destabilize other instabilities such as the dissipative trapped ion mode (DTIM) and the dissipative trapped electron mode (DTEM) and density-gradient driven bifurcations are only expected in the vicinity of the magnetic axis or in the highly collisional edge region (due to the absence of trapped particles).

2.4.2 Magnetic turbulence quenching

The two abovementioned mechanisms are based on the local quenching of electrostatic turbulent modes. However, also in tokamak plasmas that are prone to magnetic turbulence, transport barriers can form.

It has been proposed that so-called KAM-surfaces (see below) may form in the magnetic topology: It can be shown that the time independent magnetic field in a tokamak can be described in terms of a Hamiltonian, in which the toriodal coordinate ϕ replaces the time-coordinate [9]. If the

Hamilitonian is unperturbed, the magnetic field organises itself in magnetic surfaces, that are labeled by the radial coordinate only. Small perturbations of the magnetic field lead to the destruction of the magnetic surfaces. Such perturbations can be expected in a tokamak plasma, due to both imperfections of the externally applied field and small asymmetries of the current density distribution. However, there is no 'first principles' theory that gives a quantitative prediction of the perturbations of the magnetic field in a tokamak.

For arbitrarily small perturbations, the topology of the field changes from the ideal set of nested, perfect flux toroidal surfaces, to the generic mix of good surfaces, chains of magnetic islands and regions of chaotic field. The surfaces with simple rational winding number are the first to degenerate and form magnetic islands, the surfaces of which the winding number is 'very' irrational are the last to remain. The well-known KAM-theorem garantees that for sufficiently small perturbations there are always good surfaces left, the KAM-surfaces.

This mathematical theory makes clear that the topology of ideal nested surfaces which is commonly assumed in tokamak theory, must be an idealisation. However, as said before, there is no theoretical prediction of the measure in which the topology is broken up. How big are the magnetic islands, do they overlap, are there regions of chaotic field? are questions that must be answered by the experiment. However, the difficulty here is that it can be shown that magnetic fluctuations of the level $\tilde{B}/B \sim 10^{-4}$ are sufficient to significantly enhance transport. Such fluctuations (or magnetic islands with a size of a few millimeter) are difficult to diagnose.

However, measurements that can be interpreted as fingerprints of magnetic perturbations have been put forward in the literature. Big magnetic islands have been observed near $q = 1/1$ and $q = 2/1$, and have been associated with MHD-instabilities such as the sawtooth instability and the disruption. Small islands have been routiniously been observed with high resolution Thomson scattering [10, 11, 12]. Analysis alows the identification of an $m/n = 3/2$-mode [11, 12], but also smaller islands have been observed in RTP. The formation of small islands is under debate, however. The parameter for linear tearing stability, Δ', indicates stability of tearing modes with high values for m and n [13]. In spite of this apparent problem, chains of small islands (with higher values for m and n) are likely to exist, due to non-linear tearing evolution. As an example, directly after the sawtooth crash, high harmonics of the $m = n = 1$ perturbation are excited giving rise to growing, saturating and shrinking islands at $m > 1$, $n > 1$. Also

filamentation of the plasma current [14, 15] breaks the symmetry of the magnetic surfaces. Spatial fluctuations in T_e and p_e have been observed in RTP under various conditions and interpreted as filaments [16]. Even so-called electrostatic fluctuations may give rise to magnetic perturbations.

There is a further difficulty in relating the theory of the toplogy of perturbed magnetic fields to measured quantities in a tokamak. This is the fact that the theory of transport in the mixed topology is not fully developed. In the first place, field line 'trajectories' are very complicated: field lines certainly do not make a random walk, but can stick to magnetic islands for a long time, only to make unpredictable large excursions later. Secondly, the transport of particles in such a system is an unresolved problem. Thus, there remains a large gap to bridge between theory and experiment. The experiments described in this thesis aim at building part of that bridge, from the side of the experiment.

Another mechanism for barrier formation by quenching of magnetic turbulence has been put forward by Drake [17] who evaluates the Shavranov-shift induced magnetic shear $\tilde{s}$. $\tilde{s}$ is negative on the low field side of the tokamak and positive on the high field side. $\tilde{s} \propto \alpha = a\epsilon d\beta_p/dx$ in which β_p is the normalised pressure, $\epsilon = a/R$ and x is the coordinate in direction of the density gradient. The standard flux average magnetic shear $\hat{s}$, combined with $\tilde{s}$ can become less than zero on the low field side of the torus if α is large enough. In this regime, MHD ballooning modes have access to the so-called second stability regime and high pressure gradients can be achieved. Moreover, transport driven by resistive ballooning modes is also decreased, such that a confinement bifurcation can occur. Resistive ballooning modes are likely candidates for anomalous transport in the edge region of the plasma [18, 19] .

2.5 Experimental approaches to anomalous electron heat diffusivity

In this thesis we restrict the discussion to the electron heat diffusivity χ_e. There are essentially two ways to determine χ_e experimentally, i) by carrying out a power balance analysis (a static, equilibrium method) and ii) by perturbing the T_e-profile and analysing the relaxation process (a dynamic method). The two methods yield two different quatities: $\chi^{pb} = q/n\nabla T_e$ and $\chi^{pert} = \partial q/\partial n\nabla T_e$.

2.5.1 Power balance analysis

From conservation of energy it follows directly that the local changes in energy content of the plasma are the consequence of the interplay between power sources and sinks and the divergence of the heat flux. In power balance analysis, the power sources and sinks in the plasma are evaluated locally. Assuming a system with toroidal symmetry, electron cross-field transport depends on the radial coordinate r only. In steady state, the changes $\frac{\partial}{\partial t} = 0$, the heat flux $q_e(r)$ follows from

$$q_e(r) = \frac{\Pi_e^{\text{in}}(r) - \Pi_e^{\text{out}}(r)}{4\pi^2 r R_0}, \qquad (2.8)$$

in which $\Pi_e^{\text{in}}(r)$ represents the sources integrated from the axis up to r, $\Pi_e^{\text{out}}(r)$ the sinks integrated from the axis up to r.

Examples of sources are the Ohmic dissipation (P_Ω) and the ECH input power (P_{ECH}). Examples of sinks in the electron channel are the electron-ion exchange (P_{ei}) and the energy losses due to radiation (P_{rad}). From the radial profiles for n_e, $T_{\text{i,e}}$, Z_{eff}, P_Ω, P_{ECH} and P_{rad}, the heat flow in the plasma is deduced. In the absence of information on off-diagonal components to the heat flux, a quantity χ_e^{pb} (pb from power balance) is defined by

$$\chi_e^{\text{pb}} = \frac{q_e(r)}{n_e \nabla T_e}. \qquad (2.9)$$

χ_e^{pb} can be subject to large errors, due to the uncertainty in both $\Pi_e^{\text{in}}(r) - \Pi_e^{\text{out}}(r)$ and the errors in the evaluation of ∇T_e. Moreover, in the analysis, it is tacitly assumed that $\chi_e(r)$ is smooth, and that the radial profiles are sampled at sufficient radial resolution. As will be shown in this thesis, this criterion proves hard to meet.

2.5.2 Perturbative transport analysis

An alternative experimental approach to χ_e is heat pulse propagation analysis [20]. In a plasma that is otherwise in stable equilibrium, small perturbations are induced, e.g. by application of modulated local heating. Local measurements of $T_e(t, r)$ yield the radial phase velocity and amplitude decay of the heat pulse. These are used to deduce the the incremental heat diffusivity,

$$\chi_e^{\text{pert}} = \frac{\partial q_e(r)}{\partial n_e \nabla T_e}. \qquad (2.10)$$

State-of-the-art hardware for power-modulation experiments are radiometers for $T_e(t,r)$-measurements and gyrotrons for localised modulation of $P_{\text{ECH}}(r)$. It has been observed on various tokamaks [20] that $\chi_e^{\text{hp}} \approx (2 - 5)\chi_e^{\text{pb}}$. This difference is partly ascribed to a possible non-linear relation of q_e as a function of $n\nabla T q_e$, in which case χ^{pb} and χ^{pert} are simply different quantities as given by their definitions. Further systematic differences can be due to a part of the flux driven by off-diagonal elements of the transport matrix.

2.6   Transport barriers and RTP

In general, the mechanisms leading to transport barriers are hard to isolate: The $E \times B$ sheared velocity and Shavranov shift are not independent of each other. The Shavranov shift increases with density and $E \times B$ sheared velocity can either increase or decrease with density. Barrier formation in the ion channel can influence T_e and j, provoking the formation of a KAM barrier. The formation of steep gradients in the density profile (as in the TFTR Enhanced Reversed Shear type I discharges [21]) affects the j-profile via the bootstrap current. On the other hand the temperature gradient affects both $E \times B$ and the Shavranov shift.

In RTP, due to the low pressure gradients in the edge regions, ballooning-modes are unimportant. Consequently, transport bifurcations due to shear induced stabilisation of ballooning modes are unlikely. The interplay between ∇p and the rotational shear is expected in all machines, but as the coupling between electrons and ions is weak, barrier formation in the ion channel is not expected to affect the current-density profile via P_{ei} and T_e. Up to high densities, discharges with central ECH are in the banana regime (the normalised collisionality $\nu^* < 1$). For discharges with power deposition at half radius $\nu^* \approx 1$ over an important part of the minor radius. This means that also density gradient driven bifurcations are not expected in centrally heated discharges in RTP, but may play a role in the off-axis heated cases. These features make RTP well suited for investigations in the field of electron transport barriers, and their possible influence on the electron temperature profiles.

Bibliography

[1]   R. Balescu, Transport processes in plasmas, Part 1, Classical transport, North-Holland, Amsterdam (1988)

[2] R. Balescu, Transport processes in plasmas, Part 2, Neoclassical transport, North-Holland, Amsterdam (1988)

[3] F. Wagner *et al.*, Phys. Rev. Lett. **49** (1982) 1408

[4] P.H. Diamond *et al.*, Phys. Rev. Lett. **72** (1994) 2565

[5] E.J. Synakowski, *et al.*, Nucl. Fusion **40** (1998) 581

[6] R.E. Bell *et al.*, Nucl. Fusion **40** (1998) 609

[7] E. Mazucato *et al.*, Phys. Rev. Lett. **77** (1996) 3145

[8] G.M. Staebler, Density gradient driven transport bifurcation, in preparation

[9] A.H. Boozer, Phys. Fluids **26** (1987) 1288

[10] M.F.F. Nave *et al.*, Nucl. Fusion **32** (1992) 825

[11] M.N.A. Beurs *et al*, 'Double pulse multiposition Thomson scattering and dynamics of small scale T_e and n_e structures in RTP', submitted to Nucl. Fusion

[12] F.Salzedas *et al.*, Proc. 24th EPSC on Contr.Fusion and plasma physics, Berchtesgaden (1997) P2.026

[13] J. Wesson, Tokamaks, second edition, Clarendon press, Oxford (1997)

[14] R. Kinney *et al.* Phys. Plasma **1** (1994) 260

[15] S.V. Mirnov, Plasma Physics Reports, **24** (1998) 813

[16] N.J. Lopes Cardozo *et al*, Phys. Rev. Lett. **73** (1994) 256

[17] J.F. Drake, Phys. Rev. Lett. **77** (1996) 494

[18] P.N. Guzdar *et al.*, Phys. Fluids B **3** (1993) 3712

[19] A. Zeiler *et al.*, Phys. Plasmas (to be published)

[20] N.J. Lopes Cardozo *et al* Phys. Plasmas **2** (1995) 4230

[21] F.M. Levinton *et al*, Phys. Rev. Lett. **75** (1995) 4417

Chapter 3

RTP, ECH and diagnostics

The Rijnhuizen Tokamak Project (RTP) is a tokamak dedicated to the study of electron thermal transport. For this specific task, the tokamak is equiped with high resolution (both spatial and temporal) diagnostics [1] for n_e and T_e. Moreover, RTP features a system for local electron heating at a level significantly exceeding the Ohmic dissipation, using ECH. In this section, RTP, the 110 GHz ECH system and the diagnostics relevant for this thesis are discussed.

3.1 RTP

RTP ($R_0 = 0.72\,\mathrm{m}$, $a = 0.164\,\mathrm{m}$) has a circular cross section, a toroidal magnetic field $B_\phi < 2.4\,\mathrm{T}$ and a plasma current $I_p < 150\,\mathrm{kA}$. Baking, glow discharge cleaning and boronisation are applied to give values of the effective ion charge $Z_{\mathrm{eff}} < 2$. For all data in this thesis, hydrogen is used as a filling gas. The discharge duration is typically 0.5 s. Without additional heating, the Ohmic dissipation typically results in a central electron temperature of 700 eV. With application of ECH, this can be increased up to 4 keV.

3.2 Gyrotron for 110 GHz ECH

The discharges presented in this thesis are either Ohmic or heated with 110 GHz microwaves, injected from the low field side in X-mode, and absorbed at the 2nd harmonic of the electron cyclotron frequency. The microwave source is a GYCOM gyrotron (pulse duration < 200 ms, nominal output power 500 kW, but effective maximum output power 300-500 kW at the time of these experiments). For current drive purposes (ECCD), the system features a tiltable mirror so that co and counter (with respect to the plasma current) drive can be applied. Moreover, the mirror can be used to vary the

deposition in vertical direction. In horizontal direction, the deposition can be tuned by changing B_ϕ. The microwave beam has a waist of $\approx 1.5\,\mathrm{cm}$, the radial localization of the deposition is $\sim 1\,\mathrm{cm} < a/10$. The ratio between EC power and Ohmic input power $P_{\mathrm{ECH}}/P_\Omega$ varies between 4 and 7 during the ECH phase of the discharge, depending on the location of power deposition.

3.3 Diagnostics

3.3.1 Magnetics

The basic diagnostic system is a set of coils measuring the magnetic fluxes. RTP features 12 coils for poloidal magnetic field (B_θ) component measurements and 12 saddle coils for radial magnetic field component (B_{r}) measurements. Both the horizontal and vertical plasma position are determined by combined measurements of two B_θ-coils and six B_{r}-coils. The combined signal is used for feed-back control of the plasma-position. I_{p} is measured with the coils for B_θ. The current through the plasma column and the vessel is measured by a Rogowski-coil.

3.3.2 Interferometry

Two interferometers are mounted on RTP [2, 3]. First, a single chord interferometer at a wavelength of 2 mm is used in combination with a gas-feed system for density feed-back. The 2 mm interferometer is also used for absolute calibration of the density profiles as measured with Thomson scattering (see below). Second, a 19 channel interferometer is available for measurement of the temporal evolution of the density profile $n_{\mathrm{e}}(r,t)$. A slab beam at a wavelength of $432\,\mu\mathrm{m}$ is injected vertically into the plasma. Phase delays are measured at 19 positions. Abel inversion can be applied to retrieve the local density from the phase profile. During the inversion, refraction of the probing-beam is taken into account, relevant for high density studies as in chapter 6. After Abel-inversion the estimated error on the local n_{e} is 5%.

3.3.3 Thomson scattering

More than 100 years after the proof of the existence of the electron by lord Thomson, the most sophisticated diagnostic in the world for Thomson scattering is used at RTP [4, 5]. This instrument enables the study of small structures in T_{e} and $n_{\mathrm{e}}(r)$ (small meaning a few times the ion larmor

radius). These small scale structures are important in this thesis. The abovementioned (see chapter 1 and 2) transport barriers are in some cases only a few points in the Thomson scattering profiles, and the ultra-high resolution was an absolute requirement to identify them.

Thomson scattering is the scattering of photons by free electrons. The Thomson scattering diagnostic employs a laser pulse to scatter photons of the electrons in the plasma. The number of collected photons is a measure for the density. From the Doppler broadening of the scattered light, the temperature of the electron population can be derived.

The RTP set-up (see also chapter 5 for more information) features a ruby-laser that can be pulsed twice (max $2 \times 12.5\,$J, $40\,$ns pulse). The two measurements are obtained in rapid succession, separated 20 to $800\,\mu$s in time. The measurements are carried out simultaneously at 350 spatial points along a vertical chord of $300\,$mm with a resolution of $3\,$mm FWHM. T_e can be measured with an accuracy of $\leq 3\,\%$ in the range $50\,$eV to $6\,$keV for $n_e = 5 \times 10^{19}\,m^{-3}$.

3.3.4 Heterodyne radiometer for ECE-measurements

In a tokamak, B_ϕ decreases with radius: $B_\phi = R_0 B_{\phi,0}/R$, with $B_{\phi,0}$ the magnitude of the toroidal magnetic field at R_0. This leads to a variation of the electron cyclotron frequency f_{ce} with R and thus the possibility of local measurements of I_{ce}, the intensity of electron cyclotron emission. As I_{ce} is associated with T_e, ECE measurements can be interpreted as measurements of $T_e(r,t)$.

In RTP a 20 channel system for 2nd-harmonic X-mode ECE with a spatial resolution of $\approx 1.5\,$cm is installed. Measurements are obtained from the so-called low field side of the tokamak. The ECE-radiation is collected in a high gain antenna, and fed into a broad-band detector. In two steps, the original frequency band of 86 - 146 GHz is down-converted to 0 - 1.5 GHz, at which it can be processed. Around the high-gain antenna absorbing Macor is mounted, to damp spurious reflections.

In this set-up,

$$I_{ce} = \frac{\kappa e B_0 R_0}{m_e R} T_e(R)(1 - e^{-\tau}), \qquad (3.1)$$

where e is the electron charge, m_e is the electron mass and τ is the optical thickness. κ is a constant for calibration. The optical thickness τ in 2nd-harmonic X-mode is proportional to the electron pressure.

35

Bibliography

[1] A.J.H. Donné *et al.*, Plasma Physics Reports **20**, (1994) 192

[2] C.A.J. Hugenholtz, Microwave Interferometer and Reflectometer Techniques, Thesis ' Technische Universiteit Eindhoven', (1990)

[3] J.H. Rommers, Faraday rotation measurements in the RTP tokamak, Thesis 'Rijks Universiteit Utrecht', (1996)

[4] C.J. Barth *et al*, Rev. Sci. Instrum **68**, (1997) 3380

[5] M.N.A. Beurskens *et al*, submitted to Nucl. Fusion

[6] J.F.M. van Gelder, Electron Cyclotron Wave Absorbtion Experiments in Tokamak Plasmas, Thesis 'Rijks Universiteit Utrecht', (1996)

Chapter 4

Electron thermal transport barrier and magnetohydrodynamic activity observed in tokamak plasmas with negative central shear

This chapter is a reproduction of the paper 'Electron thermal transport barrier and magnetohydrodynamic activity observed in tokamak plasmas with negative central shear' by M.R. de Baar, G.M.D. Hogeweij, N.J. Lopes Cardozo, A.A.M. Oomens and F.C. Schüller, Phys. Rev. Lett. **78** (1997) 4573 and is reproduced with kind permission of Phys. Rev. Lett.

4.1 Abstract

In the Rijnhuizen Tokamak Project (RTP) plasmas with steady-state negative central shear (NCS) are made with off-axis electron cyclotron heating. Shifting the power deposition by 2 mm results in a sharp transition of confinement. The good confinement branch features a transport barrier at the off-axis minimum of the safety factor (q), where $q \leq 3$ and two magnetohydrodynamic (MHD) instabilities, one localized at the off-axis minimum of q, and one covering the entire NCS region. The low confinement branch has $q > 3$ everywhere, no transport barrier and no MHD activity.

4.2 Introduction

Tokamaks [1] are toroidal devices in which hot plasmas are confined by means of magnetic fields. The plasma is characterised by the major radius of the torus (R_0) and the minor radius (a). External coils generate the dominant toroidal magnetic field (B_ϕ). A toroidal electric current in the plasma (I_p) adds a smaller poloidal component. The resulting helical field lines lie (to good approximation) on nested tori, which are characterised by their minor radius r, or $\rho = r/a$. The safety factor, q, is a function of ρ. q and its derivative with respect to ρ, the magnetic shear $\hat{s} = (\rho/q)(\partial q/\partial \rho)$ play an important role in plasma stability. In standard tokamak operation the current density (j) is peaked on axis, leading to a q-profile $q(\rho)$ with $\hat{s} > 0$ everywhere. Recently, tokamak plasmas with an induced off-axis minimum in q and a region of NCS have gained much attention in view of their good plasma confinement. Strong peaking of the ion temperature (T_i) and the electron density (n_e) profiles leading to record values of the fusion performance have been reported from several devices [2-8]. RTP plasmas with steady-state NCS showed that the net energy transport was nearly zero in the core, which was shown to be caused by the cancelling of diffusive and convective components of the heat flux [9].

The present paper concentrates on the observation of an electron thermal transport barrier and reports specific instabilities that can develop as a result of the NCS. Theoretical analyses have shown that the negative shear can stabilise the high-n ballooning mode, allowing higher values of the ratio of kinetic and magnetic pressure (β) [10]. However, other MHD modes can be destabilised, such as the infernal mode [11, 12], an ideal pressure-driven MHD mode which requires $\hat{s} \approx 0$, or the double tearing mode [13, 14]. Chu *et al.* [15] report the observation of the resistive interchange mode in NCS
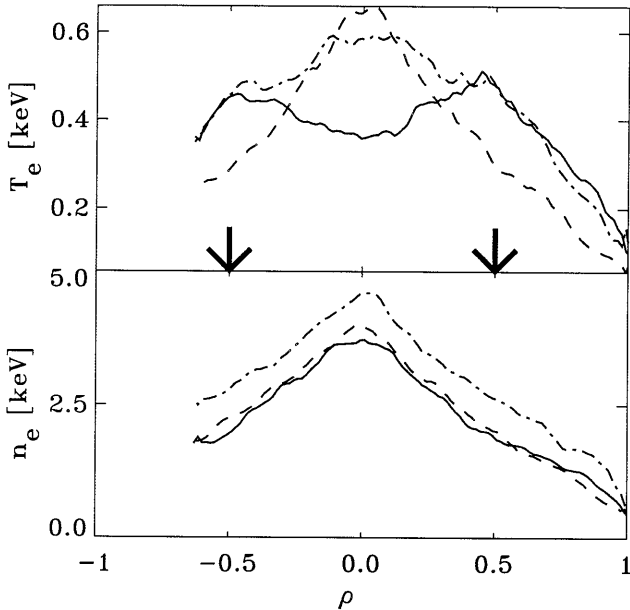
Figure 4.1: *Evolution of the T_e and n_e-profile as measured with Thomson scattering in a series of nearly identical discharges with $q_a = 5.2$. ECH is switched on at $t = 150$ ms. The arrows indicate ρ_{dep}. Shown are profiles measured at $t= 149$ ms (dashed line), $t=155$ ms (dash-dotted line), and $t=230$ ms (full line). The shape of the n_e profile is hardly affected by the off-axis heating. The differences in top density are due to shot to shot variations, which are smaller than 10%.*

discharges with peaked pressure profiles.

In RTP [9] NCS can be made reproducibly by off-axis electron cyclotron heating (ECH) in discharges with $n_e > 3 \times 10^{19}$ m^{-3}, and $I_p < 80$ kA. Power from a 110 GHz gyrotron (2nd harmonic, X-mode) is injected in the horizontal midplane, from the low field side. The ECH pulse length is 150 ms. In the experiments described here the power deposition was at $\rho_{dep} \approx 0.5$. The 350 kW absorbed ECH power exceeds the ohmic input power by a factor 5 in the ECH phase. The off-axis heating leads to a steady-state hollow T_e-profile with a corresponding hollow j-profile and NCS. Measurements have been done with a multi-channel radiometer and a 118-point single shot Thomson scattering system.

Figure 4.1 shows a series of Thomson scattering n_e and T_e-profiles. The first T_e-profile (t=149 ms) is obtained with Ohmic dissipation only. ECH is switched on at t=150 ms. After 5 ms, a rapid increase of $T_e(\rho > 0.5)$
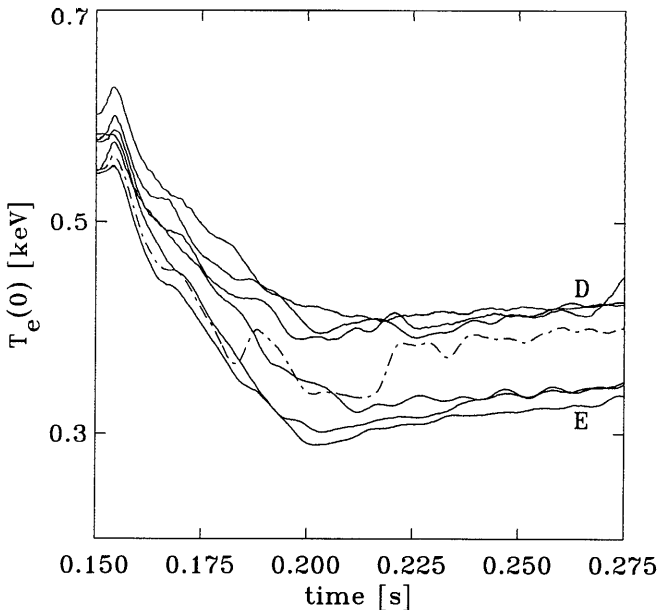
Figure 4.2: *Evolution of $T_e(0)$ as measured by ECE in 7 nearly identical discharges after switch on of ECH at $t = 150$ ms, showing the two levels of confinement. The subtlety of the distinction between these levels is illustrated by one discharge (dash-dotted) that crosses over from the low to the high branch.*

is observed. As a consequence the current diffuses outwards. The central current density decreases, and with it, the Ohmic power density in the centre of the plasma. For sufficiently high n_e, the electron-ion energy exchange can now beat the Ohmic input, leading to a hollow T_e-profile. The peakedness of the density profiles (see fig. 4.1) is favourable for this process. Typically after 50 ms a new equilibrium is reached.

The final equilibrium can be in one of two classes with different confinement. In Fig. 4.2, the evolution of $T_e(0)$ as measured by the radiometer, is presented for 7 discharges. Although the discharges all start from nearly the same state, they split into two branches after ≈ 30 ms . There is no correlation between the initial T_e and the final state of the discharge. The subtlety of the branching is illustrated by one discharge (dash-dotted), which hesitates and then crosses over from the low to the high branch.

The current diffusion time is ≈ 20 ms, full current diffusion is established 50 ms after switch on of ECH. After this time the q-profiles can be computed from $T_e(\rho)$ assuming neoclassical resistivity with a uniform
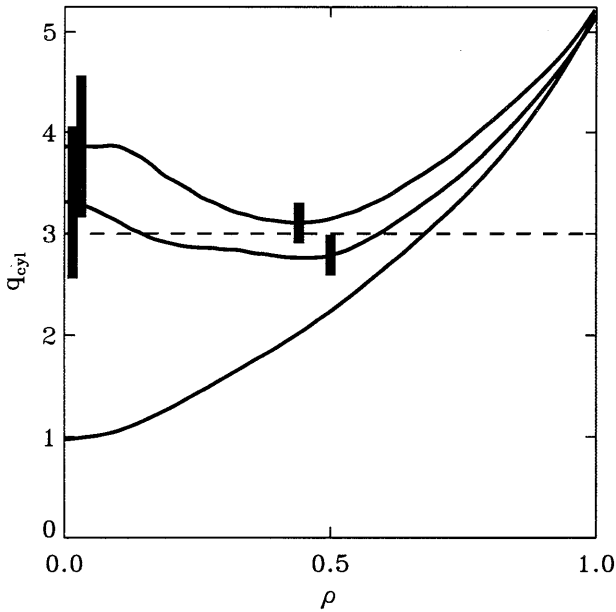
Figure 4.3: *Safety factor of high confinement discharge (dotted line). Note that $q(\rho_{\mathrm{dep}}) < 3$. The q profile of a discharge of the low confinement branch is shown (dash-dotted line) for comparison. The minimal value of q in this case is 3.1. In full line the q-profile in the Ohmic phase of the discharge is shown. The error bars are presented for q_0 and the region around q_{min}.*

distribution of the effective ion charge Z_{eff}. In these discharges $Z_{\mathrm{eff}} \approx 2$. In Fig. 4.3, $q(\rho)$ is plotted for an Ohmic discharge, and for discharges in the low and high branch of confinement. In the high branch, a minimum of q goes just under 3, whereas in the low branch, $q = 3$ is not reached. The error bars are obtained by allowing the Z_{eff}-profile to vary by 20 % over the cross-section, in accordance with previous measurements [17]. The shown q-profiles are consistent with polarimeter data.

Figure 4.4 shows the electron pressure (p_{e}) profiles of two discharges in the different branches. Clearly visible is the steep gradient in p_{e} at $\rho = .5$ of the high branch; this region will be referred to as the transport barrier. It has a width of $\approx 1.5\,\mathrm{cm}$. Apart from the barrier, the gradients in p_{e} are similar, and the difference in confinement is fully determined by the presence or absence of the barrier. The energy confinement time in the low and in the high branch are $\tau_{\mathrm{E}}^{\mathrm{L}} = 1.4\,\mathrm{ms}$ and $\tau_{\mathrm{E}}^{\mathrm{H}} = 1.7\,\mathrm{ms}$, respectively.

Corroborating evidence for the existence of a transport barrier is obtained with the ECH system in modulation mode heating a plasma that
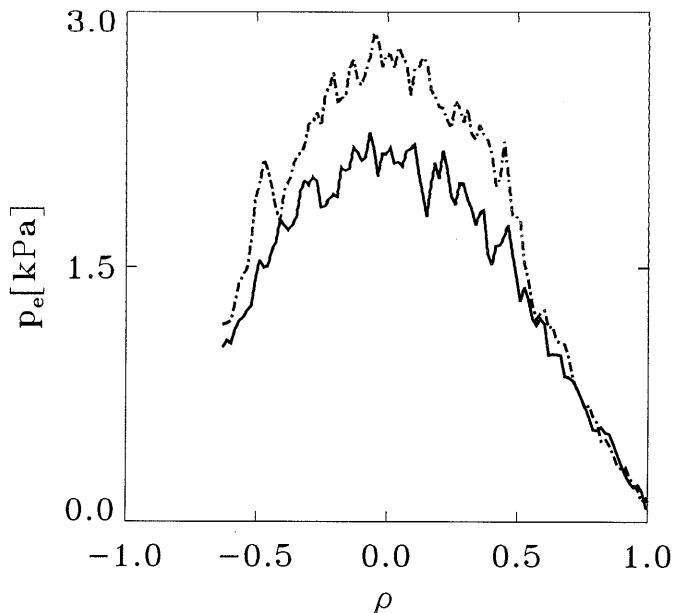
Figure 4.4: *Pressure profiles of a discharge in the low branch (full line) and a discharge in the high branch (dash-dotted line). Note that both profiles have the same gradients, except for the region around $\rho = 0.5$. Here a transport barrier has formed in the high branch.*

crosses over from the low to the high branch of confinement. Heat pulses propagate through the plasma and their amplitude and phase relative to the ECH pulses can be related to the electron heat transport. In Fig. 4.5, the dashed line depicts the modulation of the ECH power and trace (a) $T_e(0)$. Between $t = 165$ms and 170ms, the discharge crosses over to the high branch. Trace (b) and (c) represent $T_e(\rho_{dep})$ and $T_e(\rho > \rho_{bar})$, respectively, in which ρ_{bar} is the position of the barrier. The ampitude of the modulated $T_e(\rho_{dep})$ increases significantly when the transition from the low to the high branch occurs. The T_e-modulation outside ρ_{bar} slightly decreases. These observations are consistent with the formation of a transport barrier just outside ρ_{dep}.

While none of the discharges in the low branch of confinement show MHD activity, many in the high branch do. In Fig. 4.6a $T_e(t)$ at ρ_{dep} is shown. An oscillation with a period of 1 ms is observed. This oscillation has a constant amplitude over 30 periods. During this time, the central T_e shows no activity. The rise-time of the oscillation is typically $800\,\mu$s and the rapid decrease occurs in $200\,\mu$s. We shall refer to this fast decrease
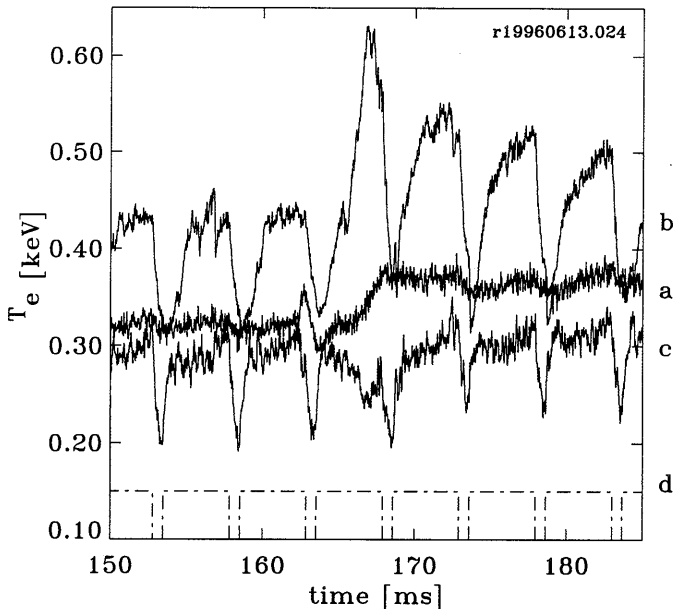
Figure 4.5: *ECH modulation sequence (dashed) and $T_e(0)$ (a), $T_e(\rho_{\mathrm{dep}})$ (b) and $T_e(\rho > \rho_{\mathrm{bar}})$ (c). The ECH was switched on at $t = 110$ ms. Between $t = 165$ ms and 170 ms, the discharge crosses over to the high branch. The formation of the barrier is evidenced by the fact that inside ρ_{dep} the amplitude of the modulation in T_e significantly increases, whereas outside the barrier the amplitude of the modulation in T_e decreases.*

as a minor crash. Figure 4.7a shows the T_e profiles just before and right after the minor crash. Note that the minor crash is a phenomenon that is localised near ρ_{dep} where q reaches an off-axis minimum with $q < 3$.

The period of oscillations with constant amplitude ends when at t = 252 ms the amplitude of the oscillation at ρ_{dep} starts to grow. It reaches its maximum value at t = 254 ms, when a sudden increase in central T_e is observed (see Fig. 4.6b). Then the amplitude of the oscillation at ρ_{dep} decreases again. The central T_e decreases in 5 ms, after which the sequence repeats itself. The sudden increase of the central T_e will be referred to as the major crash. Figure 4.7b shows the T_e profiles just before and just after the major crash. In this event, the entire central part ($\rho < \rho_{\mathrm{dep}}$) of the plasma column is affected, while the outer region ($\rho > \rho_{\mathrm{dep}}$) is not affected.

The high branch q-profile plotted in Fig. 4.3 was measured 1 ms before the major crash and between two minor crashes. A double tearing mode involving the two $q = 3$ surfaces is a likely candidate for the cause of this
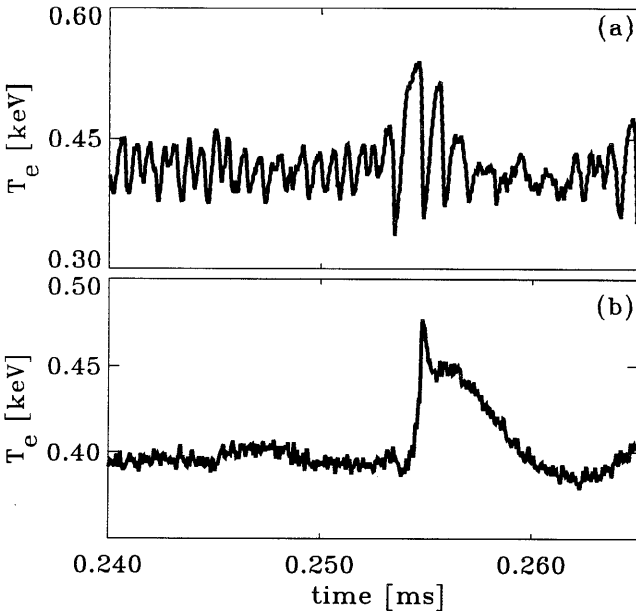
Figure 4.6: $T_e(\rho_{dep})$ *(a) and* $T_e(0)$ *(b) showing many minor crashes and one major crash (see text).*

crash, but the conditions are also favourable for the resistive interchange mode. On the basis of the present data we cannot decide between these two. The infernal mode is less likely because at $\beta_{pol} \approx 0.5$, the pressure is insufficient to drive this mode unstable. The explanation of the major crash remains open until more detailed knowledge on the evolution of the plasma parameters is available. Note that while in the minor crash the energy of the off-axis T_e maximum is mainly transported out, to larger ρ, in the major crash the energy is transported inward leaving the plasma outside ρ_{dep} unaffected. It should be noted that in both cases, the Mirnov-coils do not show any signal in relation to the modes observed, nor could they be expected to do so. The coils are positioned rather far from the plasma and the magnetic perturbations under observation have a high mode number ($m \geq 3$) and are localised within r= 8 cm. The 5 camera soft X-ray tomography system did clearly observe the activity, but could not resolve the mode structure.

The difference in confinement between the two branches is due to the presence or absence of the transport barrier near ρ_{dep}. Two pertinent questions are 1) why does the transition occur, and 2) is the transport barrier associated with the deposition radius or rather with the position of the

44
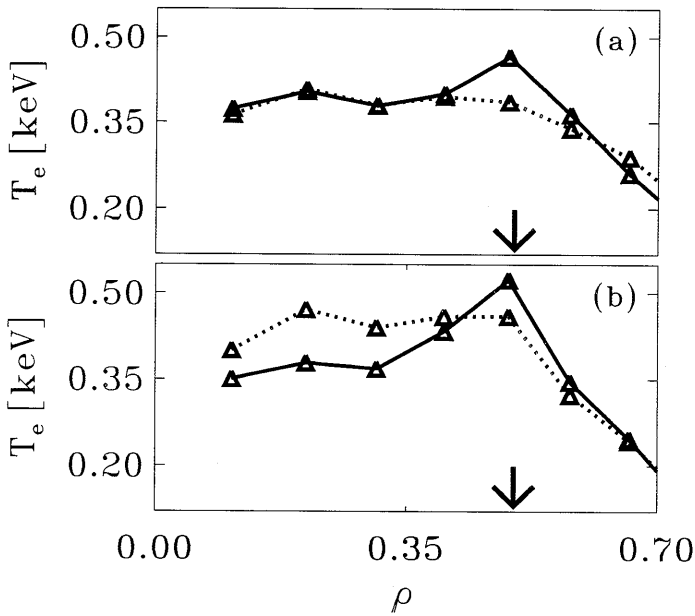
Figure 4.7: $T_e(r)$ *just before (solid line) and after (dotted line) a minor crash (a) and a major crash (b). The minor crash only affects the region around ρ_{dep}, whereas the major crash affects the whole central ($\rho < \rho_{dep}$) plasma.*

$q = 3$ surface? There is a single experimental answer to both questions. The one macroscopic plasma parameter that appears to be decisive for the sharp transition is the precise location of the power deposition, here defined as the radius of cold resonance: in the discharges in the high confinement branch, ρ_{dep} is marginally smaller than in those with low confinement (see Fig. 4.8). The transition occurs sharply for a variation of ρ_{dep} by 0.01 (i.e. 0.2 cm in the plasma). Note that this is much less than the width of either the barrier or the power deposition, which rules out the possibility that the barrier is present in both confinement modes. The discrete step in confinement brought about by this small change of ρ_{dep} indicates that the transport barrier is associated with an intrinsic plasma property, rather than the power deposition itself. The only plasma property that has such a discrete localization is the position of the $q = 3$ surface. Corroboration of this interpretation was obtained in later experiments, in which ρ_{dep} was kept constant while I_p was varied. In these experiments a similarly sharp step of confinement was observed for a variation of I_p of $< 2\%$.

The answer to the question why there are two discrete levels of confine-
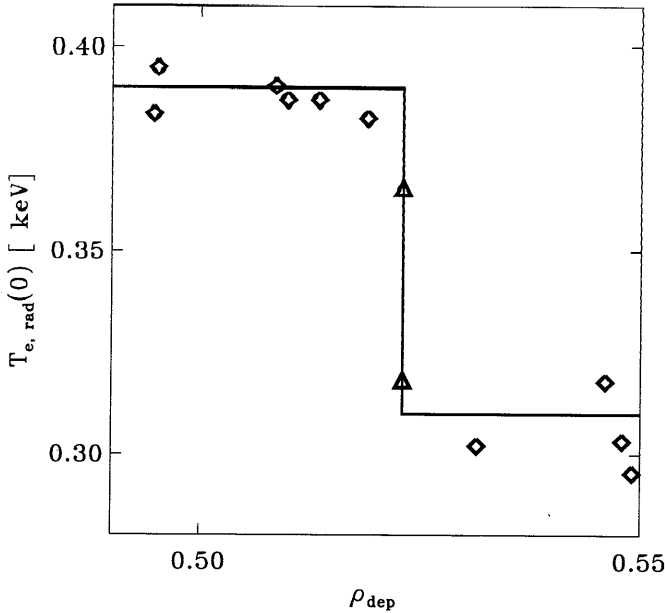
Figure 4.8: *Discharges in the high ($T_e(0) \approx .4$ keV) and low ($T_e(0) \approx .3$ keV) branch of confinement are separated by ρ_{dep}. The sharp transition corresponds to a difference of ρ_{dep} of 0.01. The discharge that crosses over sits exactly at this transition (squares).*

ment in the equilibrium situation is then that deposition just inside the barrier leads to a more pronounced off-axis maximum in T_e, which prevents the minimum of q from going above 3. Conversely, deposition a little further out allows the minimum of q to rise above 3, in which case the transport barrier disappears altogether, with a further rise of q as a consequence. Hence, the paradoxical situation presents itself, that the MHD activity develops only in the high confinement branch precisely because of the better confinement. The MHD activity does not destroy the good confinement, but it does prevent the T_e and j-profiles from developing more strongly pronounced off-axis maxima.

In conclusion, the shape of the q-profile with an off-axis minimum close to $q = 3$ is the cause of the oberved phenomena. The question remains when this situation is reached. At the start of the ECH the deposition is well inside the $q = 3$ surface. In the first few ms all discharges develop in the same way. In the experiments shown in Fig. 4.2 there are some trivial differences due to the small differences in ρ_{dep}, in the experiments in which ρ_{dep} was fixed while I_p was varied, these differences do not occur. At

$t \approx 165\,\mathrm{ms}$ there is a hitch in the evolution. According to current diffusion calculations, at this moment the q-profile is flat inside ρ_{dep}. The high and low branch separate some time after this hitch. A detailed analysis of this phase, which should reveal when the transport barrier is formed, will be given in a forthcoming paper.

Bibliography

[1]   J.A. Wesson, Tokamaks, The Oxford engineering science series, (1997) 12-13

[2]   E.J. Straight *et al*, Phys.Rev.Lett. **75**, (1995) 4421

[3]   B.W. Rice *et al*, Plasma Phys. Control. Fusion **38**, (1996) 869-881

[4]   F.M. Levinton *et al*, Phys.Rev.Lett. **75**, (1995) 4417

[5]   P. Smeulders *et al*, Nucl. Fusion **35**, (1995) 225-242

[6]   M. Hugon *et al*, Nucl. Fusion **32**, (1992) 33

[7]   X. Litaudon *et al*, (1996), EUR-CEA-FC 1565

[8]   Y. Neyatani *et al*, Proc. 23rd EPS conference on Con. Fus. Pl. Phys., Kiev (1996), to be published

[9]   G.M.D. Hogeweij *et al*, Phys.Rev.Lett. **76** (1996) 632

[10]   C. Kessel *et al*, Phys.Rev.Lett **72**, (1994) 1212

[11]   T. Ozeki *et al*, Nucl. Fusion, **33**, (1993) 1025

[12]   L.A. Charlton *et al*, Nucl. Fusion, **31**, (1991) 1835

[13]   T.H. Stix, Phys.Rev.Lett. **36** (1976) 521.

[14]   D. Biskamp, Nonlinear Magnetohydrodynamics, Cambridge University Pres (1993)

[15]   M.S. Chu *et al*, Phys.Rev.Lett. **77**, (1996) 2710

[17]   D.F. da Cruz,"Soft X-ray emission from tokamak plasmas", Ph.D. thesis, Rijksuniversiteit Utrecht, 1993

Chapter 5

Tokamak plasmas with dominant Electron Cyclotron Heating; evidence for electron thermal transport barriers

This paper is a reproduction of the paper 'Tokamak plasmas with dominant Electron Cyclotron Heating; evidence for electron thermal transport barriers', by M.R. de Baar, M.N.A. Beurskens, G.M.D. Hogeweij, and N.J. Lopes Cardozo, submitted for publication to Nucl. Fusion 1998

5.1 Abstract

In the Dutch Tokamak RTP, experiments have been carried out with Electron Cyclotron Heating (ECH) at a power of 4-7 times the Ohmic dissipation, with a deposition profile width < 10 % of the minor radius. Central deposition gives rise to sharp gradients near the $q = 1$ surface, and hot filaments in the plasma centre. Off-axis deposition leads to (steady state) flat or hollow electron temperature profiles, with accordingly flat or inverted q-profiles. A radial scan of the ECH deposition, with steps of < 1% of the minor radius, reveals a discretised response of the electron temperature. The central electron temperature shows sharp transitions between plateaux as a function of the ECH deposition radius. The transitions occur for a displacement of the deposition by less than 1 mm, and are much sharper than the power deposition profile. The transitions are associated with the crossing of the minimum value of q through integer and half-integer numbers.

The phenomenology can be modelled with a heat diffusivity profile featuring transport barriers near integer and half integer values of q. This model reproduces salient details of the experimental data, such as the sharpness of the transtions and the formation of pronounced off-axis temperature maxima for power deposition on top of a barrier. It is pointed out that the topology of the magnetic field of a tokamak under slight perturbation naturally has characteristics similar to this model.

5.2 Introduction

5.2.1 Transport in tokamaks

One of the outstanding problems in fusion research is the anomalous transport of heat in a tokamak plasma. In particular, the measured electron heat diffusivity χ_e exceeds neo-classical predictions by one to two orders of magnitude. Turbulence is commonly invoked to explain this anomaly, but there is no consensus on the exact type of turbulence [1, 2, 3]. A crude classification distinguishes 'magnetic' an 'electrostatic' turbulence. In the former case, radial excursions of the magnetic field lines lead to enhanced transport, while in the latter case $E \times B$ drifts due to a fluctuating electric field are the cause.

In recent years, experimental conditions have been identified in which regions of improved confinement can develop. These regions are often referred to as transport barriers, albeit that they can expand to cover the

entire plasma.

DIII-D

In DIII-D, in discharges where the central confinement was determined by negative central magnetic shear (NCS) and the transport in the edge region was determined by the VH-mode, the transport barrier extends to the whole plasma column, bringing ion thermal transport below neoclassical estimates. The fluctuation level is below the detection limits for these discharges. Yet, the electron themal transport remains anomalous [4]. Rice [5] describes a discharge in DIII-D in which the ion temperature profile $T_i(\rho)$, the toroidal rotation profile $f_\phi(\rho)$ and the electron density profile n_e peak dramatically 50 ms after switch-on of neutral beam-power. Here, ρ denotes the normalised flux surface radius. Only 300 ms after switch-on of the neutral beams, the $T_e(\rho)$ profile shows a 'slight' increase in the gradient. This increased gradient appears at a position (*viz.* $\rho \approx 0.5$) different from the position at which the ion thermal barrier forms (*viz.* $\rho \approx 0.3$). Moreover, the peak value of T_e is only 10 to 20 % higher than in standard L-mode discharges with a monotonic q-profile while the peak ion temperature, rotation velocity and density are typically 2 times higher.

JT-60

Fujita *et al* [6] report the observation of a narrow region in JT-60U reversed shear discharges, in which steep gradients in the T_e- and n_e-profiles form, whereas the gradients in T_i-profile show a smooth variation. Koide [7] *et al* report on the correlation of the position of the $q = 3$ surface and the position of a barrier for the ion thermal transport in high β_p JT-60U discharges.

TFTR

The TFTR-team distinguishes between Reversed Shear (RS) and Enhanced Reversed Shear (ERS) discharges [8]. It has been shown that in ERS-discharges the electrostatic turbulence is quenched [9]. McGuire et al [10] report that for ERS discharges, steep gradients in the T_e-profile have only been observed in the region of the ion transport barrier, and only in some conditions. ERS discharges can be subdivided into ERS type I and ERS type II discharges [11]. Although these two types share the same improvements in particle, ion thermal and momentum confinement, they differ

51

significantly in NBI power threshold. Type I transitions show a sudden increase of $\partial n_e / \partial t$ within the core and are consistent with $E \times B$ shear flow suppression of turbulence as a triggering mechanism. Type II transitions are marked by an abrubt increase in T_i and T_e and at the moment that the slowly decreasing q_{min} approaches 2. A link with the evolving q-profile has been suggested.

JET

In JET optimised shear discharges [12, 13] barriers for the electrons and the ions form when the $q = 2$ surface is in the plasma.

Summarizing, in various tokamaks conditions have been reached in which the ion thermal conductivity is reduced to the neo-classical level over part of or even the entire plasma. This reduction appears to be associated with a strong velocity shear and a reduction of the density fluctuation level. The electron thermal transport behaves differently from that of the ions. Electron transport barriers may form, but not necessarily at the same time, or the same place as the ion transport barriers, and there is neither a clear relation to the velocity shear, nor to the level of density fluctuations. Thus, electron and ion thermal transport appear to be driven by different mechanisms. The present paper concentrates on electron thermal transport and investigates the possible existence of electron thermal transport barriers.

In the interpretation of experimental transport studies, the profile of the electron thermal diffusivity $\chi_e(\rho)$ is commonly (tacitly) assumed to be smooth. At the available measuring resolution, there was no reason to do otherwise. However, structures in T_e have been observed with high resolution Thomson scattering [14, 15, 16]. This, and the fact that with modulated ECH-experiments a strong inhomogeneity of the heat diffusivity $\chi_e(\rho)$ has been demonstrated, [17] lead to the idea that electron thermal transport might be determined by alternating layers of good and bad confinement [18]. This theoretical concept was earlier considered in [19, 20, 21, 22, 23] in different physics contexts.

The Rijnhuizen Tokamak Project (RTP) has a system for well localised, dominant electron heating (Electron Cyclotron Heating, ECH), and a very high spatial resolution ($< 2\%$ of the minor radius) measurement of the T_e-profile. This combination allows a new investigation into the homogeneity of electron heat transport in tokamak plasmas, down to scale lengths of a few percent of the minor radius. The main technique used in this paper is the scanning, either dynamically during a single discharge, or on a shot-
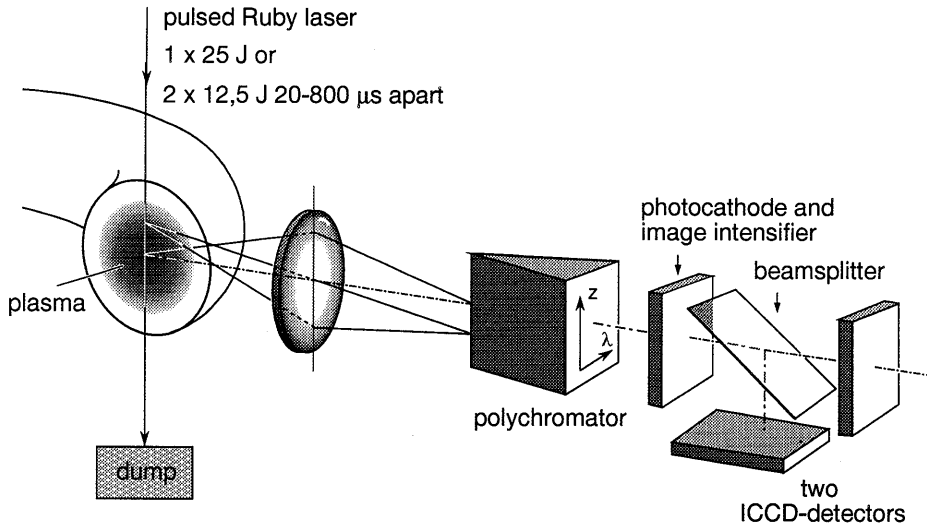
Figure 5.1: *Set-up of the RTP system for Thomson scattering.*

to-shot basis, of the ECH power through the plasma and measuring the response of the T_e-profile.

The paper is organised as follows: In section 3, the experimental set-up is presented. In section 4, experiments with strong on- or off-axis ECH are described. In particular, the results of scans of the power deposition radius (ρ_{dep}) are reported, showing that the central electron temperature varies in discrete steps for a continuous variation of ρ_{dep}. In section 5, it is shown that this result can be described with a transport model $\chi(q)$, in which the thermal diffusivity is low near simple rational values of q, and high elsewhere. Unresolved questions and possible new insights with this model are discussed. The parallels between this transport model and the generic topological properties of the magnetic field in a tokamak are briefly pointed out. We discuss the implications of the presence of internal transport barriers (ITB) on the interpretation of transport measurements.

5.3 Experimental set-up

5.3.1 The Rijnhuizen Tokamak Project RTP

The Rijnhuizen Tokamak Project (RTP) [24] is dedicated to the study of heat transport via the electrons. The RTP tokamak has the following parameters: major radius $R_0 = 0.72$ m, minor radius $a = 0.164$ m, toroidal magnetic field $B_\phi(\rho = 0) \leq 2.45$ T, plasma current $I_p \leq 140$ kA. The
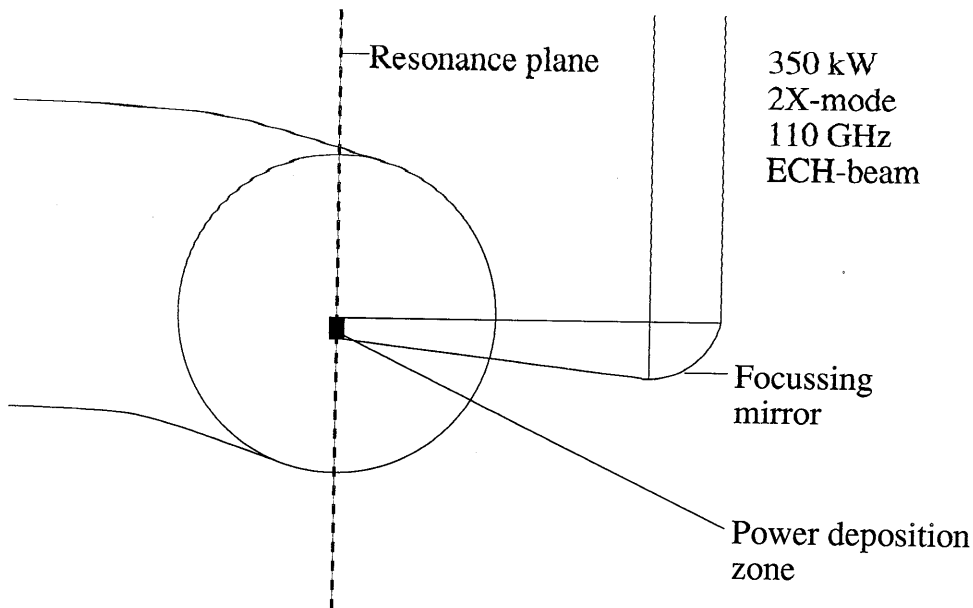
Figure 5.2: *Schematic of the beam of the 110 GHz Gyrotron for plasma heating and non-inductive current drive.*

central density can be varied between $n_e = 0.5 \times 10^{19}$ and $1.5 \times 10^{20}\,\mathrm{m}^{-3}$.

RTP is equipped with a comprehensive set of diagnostics for n_e and T_e. A multi-position Thomson scattering diagnostic (see Fig. 1) measures T_e, n_e and p_e profiles. Two measurements can be obtained in rapid succession, separated 20 to $800\,\mu s$ in time. The measurements are carried out simultaneously at 350 spatial points along a vertical chord of $300\,\mathrm{mm}$ with a resolution of $3\,\mathrm{mm}$ FWHM. The vertical chord is imaged on the entrance slit of a polychromator for spectral decomposition. The spectra for the 350 positions are intensified and measured by the two ICCD-detectors. Both wings of the measured spectrum are used in the determination of T_e. T_e can be measured with an accuracy of $\leq 3\%$ in the range $50\,\mathrm{eV}$ to $6\,\mathrm{keV}$ for $n_e \approx 5 \times 10^{19}\,m^{-3}$ [25]. The ruby laser can be pulsed twice (max $2 \times 12.5\,\mathrm{J}$, $40\,\mathrm{ns}$ pulse). In single pulse mode, the maximum energy is $25\,\mathrm{J}$ in a 15 ns pulse.

Furthermore the diagnostic park comprises a 5 camera, 80 channel system for SXR tomography [26], a 19 channel interferometer [27] and a 20 channel heterodyne radiometer for ECE and ECA measurements [28].

$T_e(\rho)$ can be manipulated with a 110 GHz., 500 kW system for second harmonic X-mode heating (see Fig. 5.2). For current drive purposes
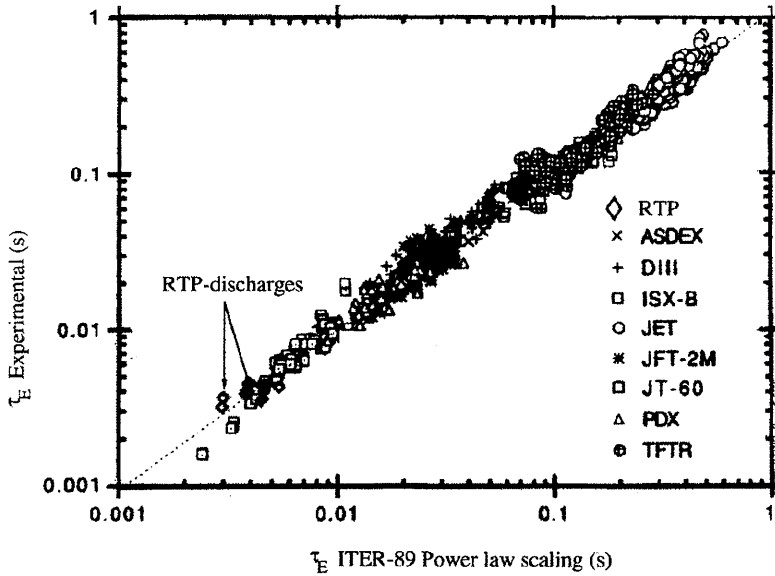
Figure 5.3: *Measured energy confinement time (τ_E Experimental) vs. ITER89-P scaling law predictions (τ_E ITER-89 Power law scaling). To the original dataset (Data taken from [29]) comprising data from Alcator C-mod, Asdex, DIII, DIII-D, JFT-2M, JT-60, PBX-M, PDX,T-10, TEXTOR, TFTR and ToreSupra), representative RTP discharges have been added. The RTP confinement agrees with the scaling law.*

(ECCD), the system features a tiltable mirror so that co and counter drive can be applied. Moreover, the mirror can be used to scan the deposition in vertical direction. In horizontal direction, the deposition can be varied by changing B_ϕ. The waist of the beam has a diameter of $\sim 1.5\,\mathrm{cm}$ and the radial localization is $\sim 1\,\mathrm{cm} < a/10$. In a standard $80\,\mathrm{kA}$ discharge ($q_a \approx 5$), the Ohmic dissipation is typically $P_\Omega = 140\,\mathrm{kW}$. During ECH this reduces to $50\,\mathrm{kW}$ for centrally heated discharges and $100\,\mathrm{kW}$ for off-axis heated discharges at $\rho_{\mathrm{dep}} = 0.5$. The ratio between EC power and Ohmic input power $P_{\mathrm{ECH}}/P_\Omega$ varies between 4 and 7 during the ECH-phase of the discharge depending on the location of power deposition.

5.4 Experimental results

5.4.1 On axis ECH

Global confinement

For a representative set of RTP discharges with central ECH the energy confinement time (τ_E) has been determined. The set contains a significant spread in q_a, line averaged density ($\bar{n}_e$) and EC-power (P_{ECH}), viz. $3.2 < q_a < 6.4$, $2.2 \times 10^{19} < \bar{n}_e < 4.1 \times 10^{19} m^{-3}$ and $110\,\mathrm{kW} < P_{ECH} < 350\,\mathrm{kW}$. τ_E was derived from the measured electron energy confinement time ($\tau_{E,e}$) and the estimated $T_i(0) \approx 400$ eV, based on previous measurements. Taking into account that $Z_{eff} \approx 2$ for the presented discharges, typically $\tau_E \simeq 1.25 \times \tau_{E,e}$, and the error induced on τ_E by the uncertainty on T_i is $\leq 10\%$. In Fig. 5.3 the thus derived τ_E is compared with results from other tokamaks and, with the ITER89-P L-mode scaling $\tau_E^{ITER89-P}$ [29]. For RTP discharges with on-axis ECH, $\tau_e \simeq 2 - 5$ ms, close to the ITER89-P scaling law. Thus, it appears that the confinement of RTP discharges with dominant central ECH is comparable to that of other tokamaks with various other additional heating methods.

Internal transport barrier near $q = 1$

Figure 5.4 shows a typical T_e-profile as measured with the high resolution Thomson scattering system for a centrally EC heated low density, low q_a discharge. Several features can be identified. First of all, in the central region ($\rho < 0.2$) T_e shows a pronounced spatial structure with several peaks with a typical dimension of 5-10 mm. These peaks can be > 1 keV above the surrounding temperature and are thought to be hot $m = 1, n = 1$ filaments, with relatively good confinement [30]. The filaments are also evident on the electron pressure p_e, but are much less pronounced on n_e.

Just outside the filamented region, very steep gradients in $T_e(\rho)$ are found, up to $200\,\mathrm{keVm^{-1}}$. The next question to be answered is, where this transport barrier (TB) is located in relation to e.g. the $q = 1$ surface. For this purpose, Fig. 5.5 shows a typical example of a double pulse Thomson scattering measurement, obtained just before (line) and after the sawtooth crash (symbols). During the sawtooth crash the filaments are wiped out; however, the steep gradient region remains intact. This places the sawtooth inversion radius (r_{inv}) near the inner margin of the TB.

The fact that the TB is coupled to the q-profile, was demonstrated in an experiment in which the q-profile was modified with ECCD. Figure 5.6a
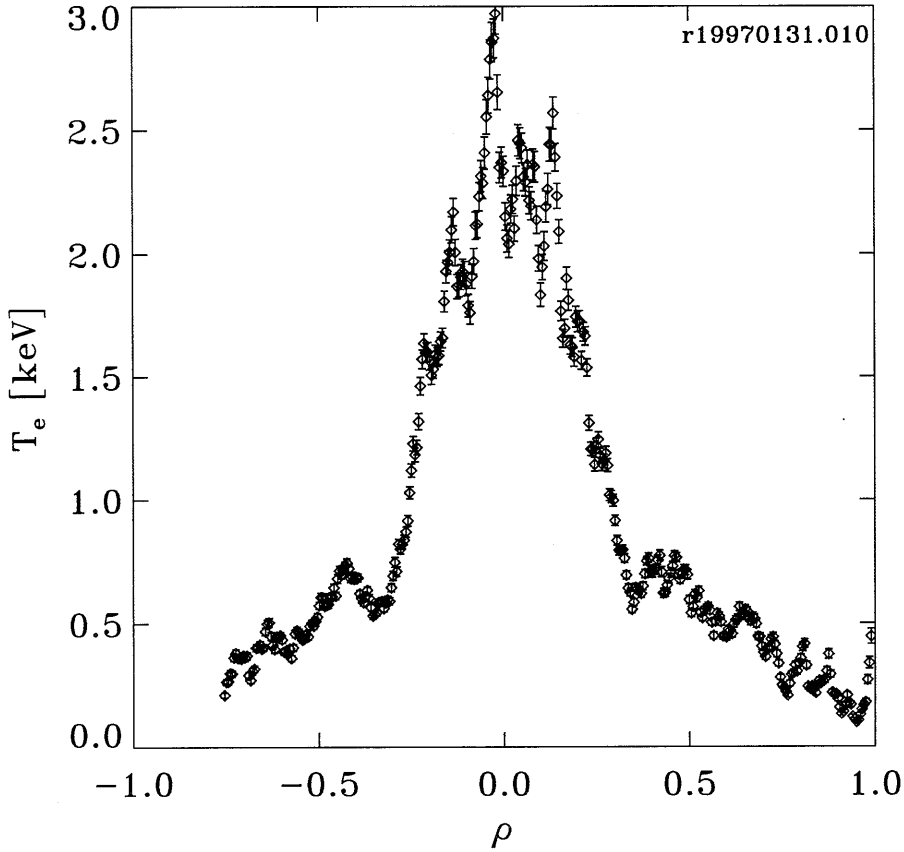
Figure 5.4: Typical T_e profile for a centrally EC heated $\bar{n}_e = 1.0 \cdot 10^{19}\,\mathrm{m}^{-3}$, $q_a = 6$ discharge, as measured with Thomson scattering. Note the central region with the filaments, the barrier region in which steep gradients in $T_e(\rho)$ are present and the outer region with relatively poor confinement where the gradient of T_e is small.
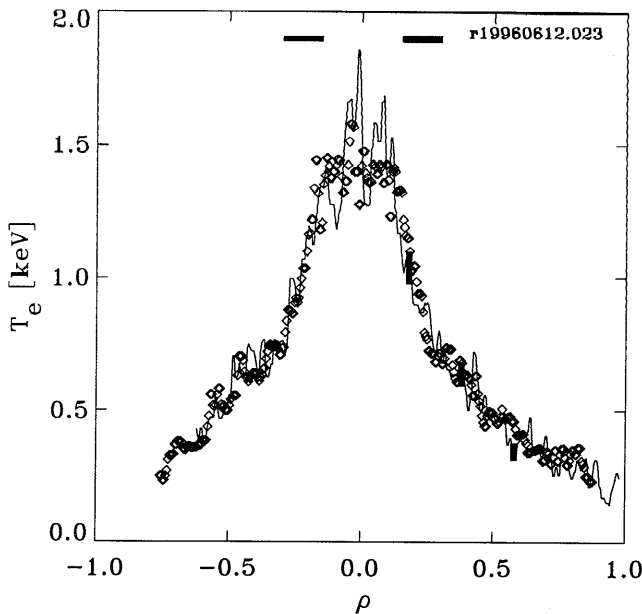
Figure 5.5: *Typical example ($q_a = 7.2$, $\bar{n}_e = 1.1 \cdot 10^{19}\,\text{m}^{-3}$) of double pulse Thomson scattering measurement of $T_e(\rho)$ just before (line) and after the sawtooth crash (symbols); the error bars are indicated at three typical positions in the profiles. The sawtooth inversion radius (r_{inv}) was determined from ECE and indicated by the horizontal bars in the figure. Note that r_{inv} coincides with the inner margin of the transport barrier.*

gives the T_e profiles of two discharges, in which approximately 15 kA was driven non-inductively, either in co or counter direction. Although ρ_{dep}, P_{ECH}, I_p, B_ϕ and n_e are the same for both discharges, the position of the barrier changed with co and counter drive. Also by changing q_a, the position of the barrier (ρ_{bar}) can be changed, as is shown in Fig. 5.6b. We present the two electron pressure (p_e) profiles instead of the T_e-profiles, because there was a 25 % varaiation in $\bar{n}_e$, which led to different values for $T_e(0)$. Note that the structures in the steep gradient region move together with the region, which excludes the possibility that they are due to instrumental artifacts.

We conclude from these experiments that the TB is located just outside the $q = 1$ surface.

One might ask whether the TB near $q = 1$ is generated by the EC heating itself, or is a generic feature of the plasma, emphasized by the localized heating of the plasma with ECH. The answer to this is given by Modu-

lated ECH (MECH) experiments with low net power (low duty cycle) in Ohmic target plasmas [31]. In these experiments the EC power was deposited either just inside or just outside r_{inv} in low q_a discharges. When the modulated power was deposited just inside the sawtooth inversion radius (r_{inv}), the outward propagating perturbation was strongly delayed and attenuated, indicating that a region of low diffusivity had to be passed; the amplitude in the central plasma was large. If the modulated power was deposited just outside r_{inv}, the opposite was observed, viz. large outward propagating heat pulses and weak heat pulses towards the centre, i.e. in this case the region of low diffusivity was inside ρ_{dep}. This experiment shows that a region of low diffusivity, i.e. a TB, near r_{inv}, is also present in Ohmic plasmas.

In summary, we have demonstrated the pressure of an electron thermal transport barrier in centrally EC heated discharges. The sawtooth crash occurs just within the region of steep gradient, placing the barrier just outside $q = 1$. Corroborating evidence that the TB is linked to the $q = 1$ surface, is the fact that it shifts inward with counter- and outward with co- current drive and also follows the $q = 1$ surface under variation of q_a. Modulation experiments with low power, low duty cycle ECH show that the barrier is also present in Ohmic plasmas, and is therefore not ECH induced.

5.4.2 Off-axis heating

In order to examine the effect of off-axis heating, two kinds of experiments have been carried out. First, a sequence of similar discharges has been performed in which the ECH deposition radius (ρ_{dep}) was scanned through the plasma in steps of $\approx 1\,\text{mm}$, by changing B_ϕ from shot to shot. Second, in a number of discharges ρ_{dep} has been ramped during the EC heating, by sweeping B_ϕ. For the interpretation of experiments with off-axis ECH, it is important to have an accurate relation between the experimental parameter B_ϕ and ρ_{dep}

5.4.3 Determination of the ECH deposition radius

To good approximation ρ_{dep} is lineary dependent on the measured quantity B_ϕ. The precise relationship $\rho_{dep}(B_\phi)$ was obtained experimentally. For the experiments in this paper ($\bar{n}_e$ between 2.4 and $3.0 \times 10^{19}\,m^{-3}$, and $I_p = 80\,\text{kA}$), it is found that
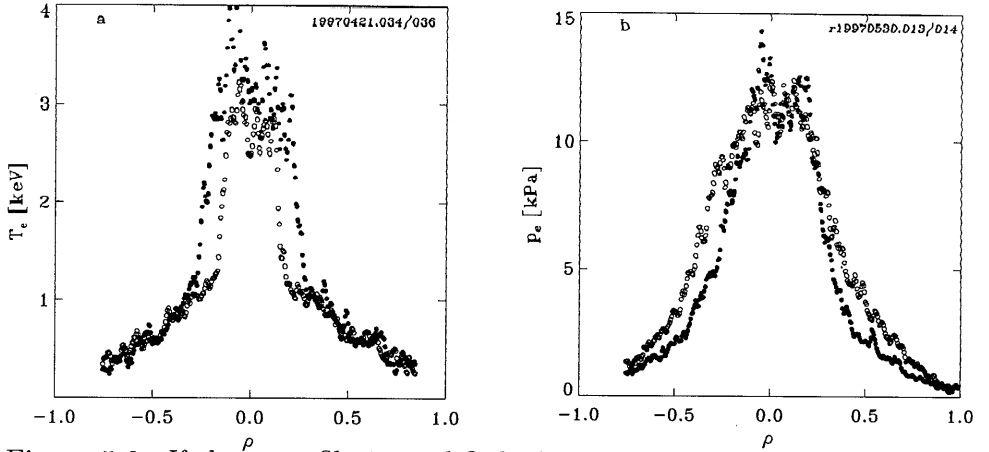
Figure 5.6: *If the q profile is modified, the position of the TB moves with it. In this plot examples of T_e profiles measured with Thomson scattering in discharges with central EC heating; the error bars are indicated at three typical positions in the profiles.* **a:** *Two identical discharges with co (q_a = 6.1; $\bar{n}_e \approx 0.54 \cdot 10^{19} \text{m}^{-3}$) and counter ($q_a$ = 6.0; $\bar{n}_e \approx 0.69 \cdot 10^{19} \text{m}^{-3}$) current drive (closed and open symbols, respectively).* **b:** *Pressure profiles (p_e) of two discharges with q_a = 6 and q_a = 3.6 (closed and open symbols, respectively).*

$$\rho_{\text{dep}} = 2.290 B_\phi - 4.646$$

for LFS deposition and

$$\rho_{\text{dep}} = -2.125 B_\phi + 4.314$$

for HFS deposition.

A detailed discussion on the determination of the ECH deposition radius is given in the appendix of this chapter.

Shot-to-shot scan of ρ_{dep}

We now turn to the results of the shot-to-shot scan of ρ_{dep}. In this scan $\bar{n}_e$ was kept in the range 2.4 to $3.0 \times 10^{19} \, m^{-3}$, while I_p was fixed at 80 kA. B_ϕ was varied from 2.10 to 2.29 T. In steady state (*viz.* 125 ms after switch-on of ECH, > 4 current diffusion times or > 30 energy confinement times), the Thomson scattering $T_e(\rho)$ was obtained. $T_e(0)$ (averaged over $\rho = [-0.03, 0.03]$) is plotted vs. ρ_{dep} in Fig. 5.7. If χ_e were a smooth function of radius one would expect a gradual decrease of $T_e(0)$ for increasing ρ_{dep}. In contrast, we observe sharp transitions, separating five plateaux (A-E).
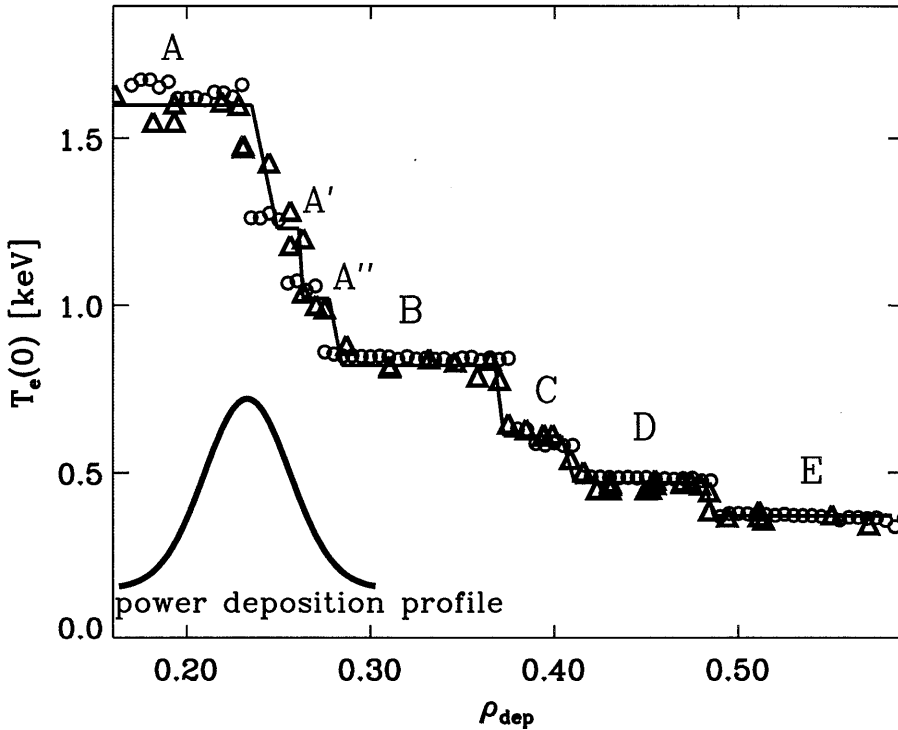
Figure 5.7: $T_e(0)$ *as measured with Thomson scattering (triangles) in a series of similar discharges in which* ρ_{dep} *was varied* ($\bar{n}_e \simeq 2.7 \times 10^{19} m^{-3}$, $q_a \simeq 5$). *Pronounced plateaux (labeled A..E) and sharp transitions are observed. Most transitions are much sharper than* σ_{ECH} *(indicated by the Gaussian). The results of simulations with a transport model featuring transport barriers at low rational q-surfacesare are plotted as well (circles); see Sec.5.5.*

Surprisingly, the transitions occur through differences in $\rho_{dep} < 1\%$, much sharper than the width of the ECH deposition profile.

The T_e-profiles of typical discharges from the plateaux A-E are shown in Fig. 5.8. Interestingly, outside the EC-power deposition radius, the profiles are similar. Many of the profiles presented are hollow (*viz.* $T_e(0) < T_e^{max}$). Steady-state hollow T_e profiles for low Z_{eff} are a unique observation on RTP [32, 33]. Typically after 50 ms a new equilibrium is reached.

The fact that hollow T_e-profiles are measured, suggests that, once a part of the current density has diffused outward due to the strong off-axis heating, the Ohmic input in the centre becomes lower than the combination of several loss mechanisms, thus causing a net energy sink in the centre,
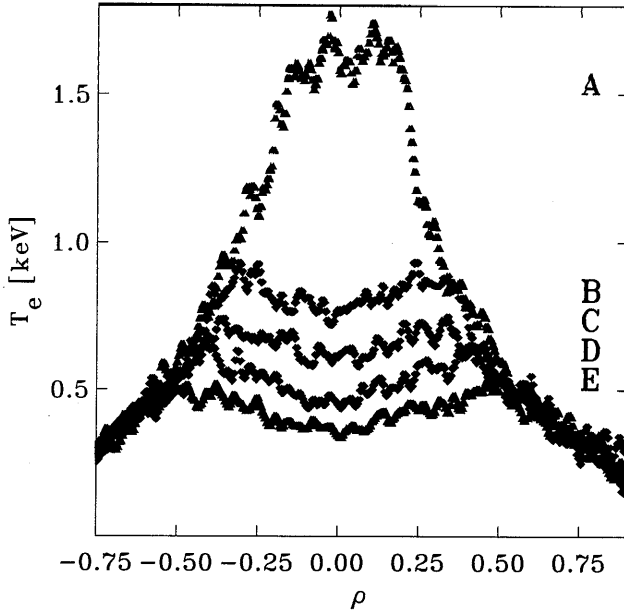
Figure 5.8: *Examples of T_e profiles for discharges at the plateaux A..E (See Fig.5.7). Note that the outer part of the profiles almost coincide.*

and concomittant a hollow T_e-profile. These central loss mechanisms for the electron will now be discussed. A local electron power balance analysis in the region inside ρ_{dep} shows that there is still a net heat source in this region [32]. For a typical discharge at level D or E, the Ohmic input power generated inside ρ_{dep} is ~ 40 kW; the loss to the ions inside ρ_{dep} (assuming the coefficient for thermal diffusivity via the ions $\chi_i = 3\chi_{i,nc}$, in which $\chi_{i,nc}$ is the neo-classical estimate for χ) is $P_{ie} \sim 20$ kW. The total radiation loss, as measured by a bolometer, is ~ 30 kW; however, this radiation is mainly emitted at the edge of the plasma. Therefore, an outward heat flux, not driven by ∇T_e, must be present inside ρ_{dep}.

The n_e-profiles for the plateaux A-E are shown in Fig. 5.9. For the A-plateau, the n_e-profiles show a flat region. For the B, C, D and E plateaux the profiles gets increasingly peaked. For the D and E plateaux profiles, a jump in ∇n_e is observed. This suggests that within ρ_{dep}, and inward particle pinch is active. Note that this inward particle convection occurs in the same region where the outward heat convection is needed to explain the hollow T_e profiles. The convective particle velocity can be estimated to be $v_p(\rho) = 3 \cdot D/a \cdot \rho$.

62
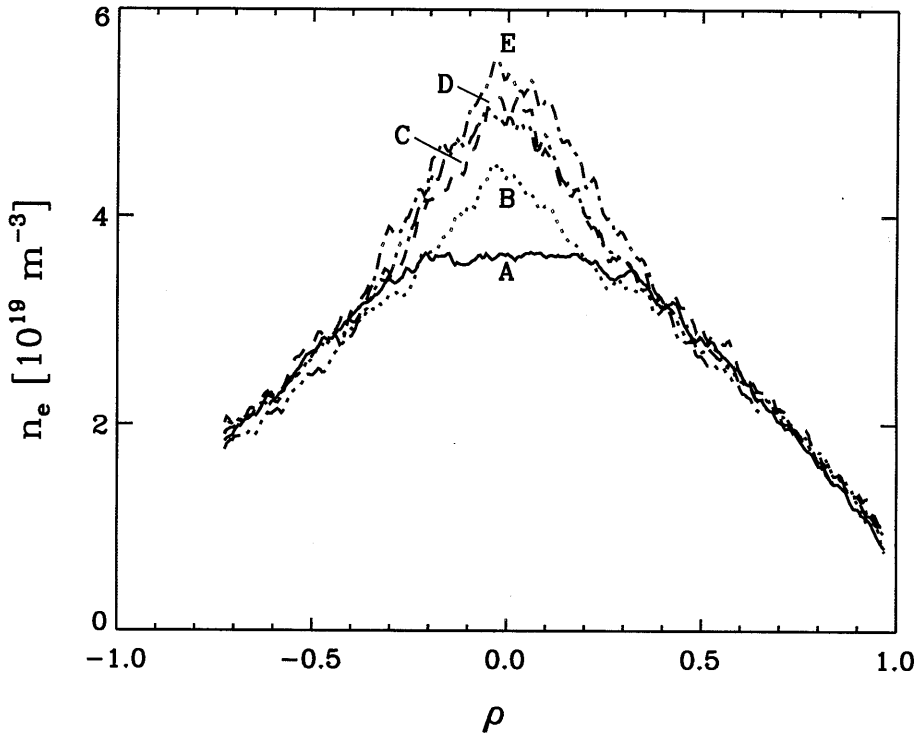
Figure 5.9: *Examples of n_e profiles for discharges at the plateaux A..E (See Fig.5.7). The boxes show the profiles with ρ_{dep} just inside (line) and outside a transition (symbols). The transitions to lower plateaux in T_e are associated with extra density profile peaking.*

Dynamic scan of ρ_{dep}.

An example of the second type of experiments, i.e. discharges with ramped ρ_{dep}, is presented in Fig. 5.10, showing $n_e(0)$ and $n_e(0.5)$ obtained from interferometry, the SXR signal along a central chord and $T_e(\rho = 0)$ as obtained from ECE are as a function of time. Although the position observed by the radiometer channels shifts with B_ϕ, $T_e(0, t)$ can be obtained by spline interpolation of a few channels. As in the shot-to-shot scan, plateaux are alternated by sharp transitions. These sharp transitions are also clearly visible in the SXR-data and are correspond to sudden changes in n_e. The SXR-intensity increases during the B-plateau phase (the time window between 208 and 280 ms). Interferometer measurements show that during this phase, $n_e(0)$ increases while $n_e(0.5)$ does not increase. This peaking of $n_e(\rho)$ leads to the increased SXR-intensity. The SXR-data

63
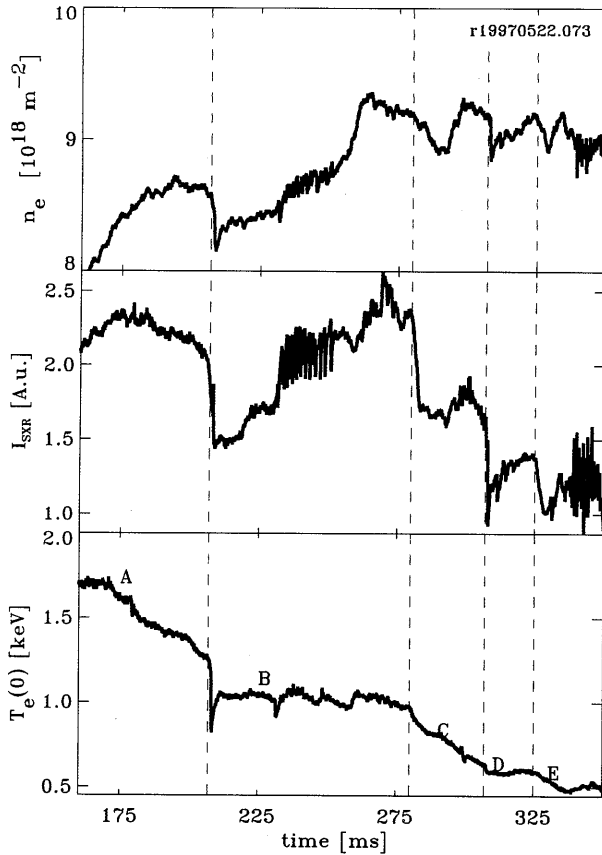
Figure 5.10: $n_e(0,t)$ (top panel), Soft X-ray intensity along a central chord (central panel) and $T_e(0)$ (bottom panel) for an EC heated discharge ($\bar{n}_e \approx 3.0 \times 10^{19} m^{-3}$, $I_p = 80kA$) in which ρ_{dep} was swept through the plasma from 0.2 at t=150 ms to 0.6 at t=350 ms. Note that the adaptation of the T_e profile occurs within small intervals of ρ_{dep}. The SXR time trace shows instabilities between 225 and 275 ms and between 337 and 350 ms. During the B-plateau phase, the density profile peaks. ECH is switched off outside the presented time window.
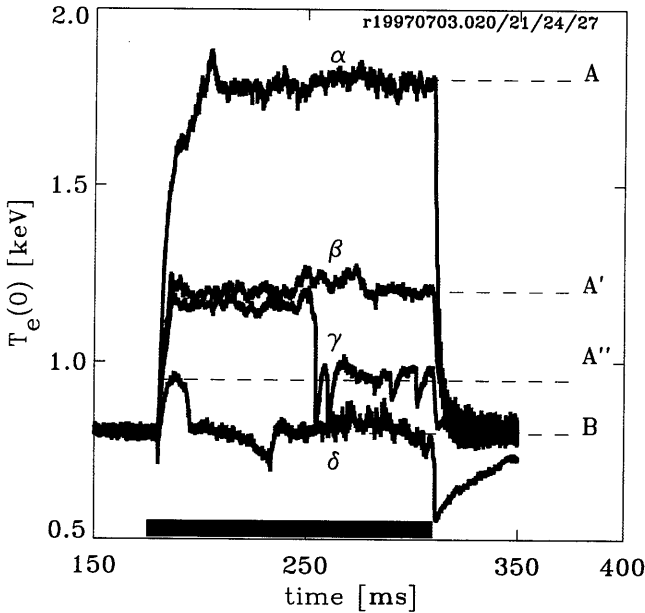
Figure 5.11: $T_e(0)$ *vs. time for four discharges, evidencing intermediate levels between levels A and B. Note that discharges β and γ, after switch on of the ECH initially reach the level A', after which γ suddenly changes to A''. Trace δ starts at A'', diving down to level B. Also note the different behaviour of trace δ after switch-off of the EC-power.*

shows the occurence of MHD-instabilities in the time windows [225,275] ms and [337,350] ms. These instabilities are off-axis sawtooth-like phenomena. They are also found in the shot-to-shot scan of ρ_{dep}, in which case they typically occur at the end of a plateau, near the transition. Their importance will be explained below.

In a dynamic ρ_{dep} sweep, the discharge makes the transitions at a larger ρ_{dep} than in the shot-to-shot scan. Comparison of Figures 5.7 and 5.10 shows that the ρ_{crit} are larger by 0.03-0.05 in the latter case, corresponding to a time delay of 15-20 ms. This delay agrees well with the current diffusion time (τ_η) in RTP.

Sub-levels in the A-B transition

The large transition from level A to level B needs closer inspection. In Fig. 5.11 four time traces of $T_e(0)$ are shown for shots with $\rho_{dep} \simeq 0.29$, i.e. near the transition between the A and B levels. Trace α shows the

65
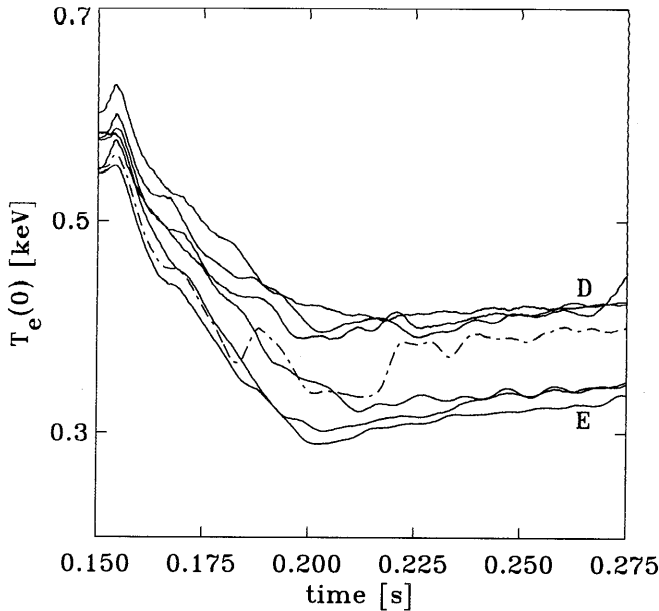
Figure 5.12: *Evolution of $T_e(0)$ as measured by ECE in 7 nearly identical discharges after switch-on of off-axis ($\rho_{\mathrm{dep}} \approx 0.5$, $q_a \approx 5.2$ and $\bar{n}_e = 2.7 \cdot 10^{19}\,\mathrm{m}^{-3}$) ECH at $t = 150\,\mathrm{ms}$, showing two levels of confinement (D and E). The subtlety of the transition is illustrated by one discharge (dash-dotted) that crosses over from E to D.*

typical case for central heating (level A), with $T_e(0) = 1.8$ keV. Trace β and γ were obtained for a slightly higher setting of ρ_{dep}. After switch-on of the ECH, these traces reach the same level, after which a sharp transition to a lower level is observed for trace γ. Trace δ reaches the final level of γ and then transits to level B. Consequently, at least two sub-levels can be identified. These are denoted by A' and A"

The evolution from Ohmic to hollw T_e

Next we focus on the evolution from the Ohmic target plasma to an off-axis EC heated plasma. This will be done for discharges close to the D-E transition. Figure 5.12 shows seven ECE $T_e(0)$ time traces for discharges near this transition (see also [33]). ECH is switched on at t=150 ms. Although the discharges all start from nearly the same state, they split into two branches after ≈ 30 ms. There is no correlation between the initial T_e and the final state of the discharge. The subtlety of the bifurcation
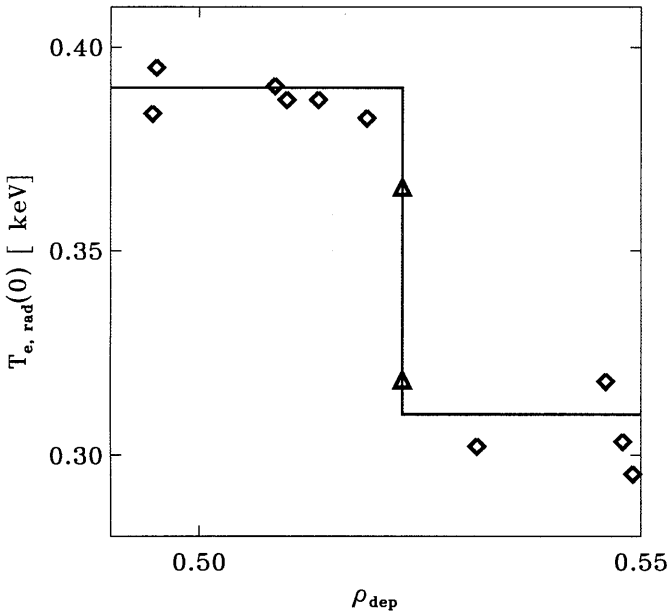
Figure 5.13: *Central radiation temperature for the discharges presented in Fig.5.12. The sharp transition corresponds to a difference of ρ_{dep} of 0.01. The discharge that crosses over sits exactly at this transition (triangles).*

is illustrated by one discharge (dash-dotted), which hesitates and then crosses over from E to D. Again, the one macroscopic plasma parameter that is decisive for the sharp transition is the precise location of the power deposition. In the discharges at level D, ρ_{dep} is marginally smaller than in those at level E, see Fig. 5.13. The transition occurs for a variation of ρ_{dep} of 0.01 (i.e. 0.2 cm in the plasma).

Similar bifurcations can be induced for fixed ρ_{dep} by varying I_{p}. In Fig. 5.14 two $T_{\text{e}}(0)$ time traces are presented for discharges in which ρ_{dep} is fixed at 0.53 and $I_{\text{p}} = 92\text{kA}$ and 94kA. Although the dataset comprises discharges with I_{p} between 80 and 101 kA (see also Fig. 5.15) only two discharges are presented for clarity. The EC heating is switched on at $t = 175\,\text{ms}$, indicated by the bar at the bottom of the graph. Again the discharges evolve into two separate regimes after switch-on. Also this transition is delicate: the traces seem to equilibrate at the level of the high I_{p} discharges, but then, 50 ms after switch-on of the heating, one of the discharges moves in two steps to a lower $T_{\text{e}}(0)$. Figure 5.15 shows $T_{\text{e}}(0)$ from ECE at t=280 ms vs. I_{p} for the whole data-set. The transition is again extremely sharp, $\delta I_{\text{p}} \leq 2\%$ separating the two regimes. The
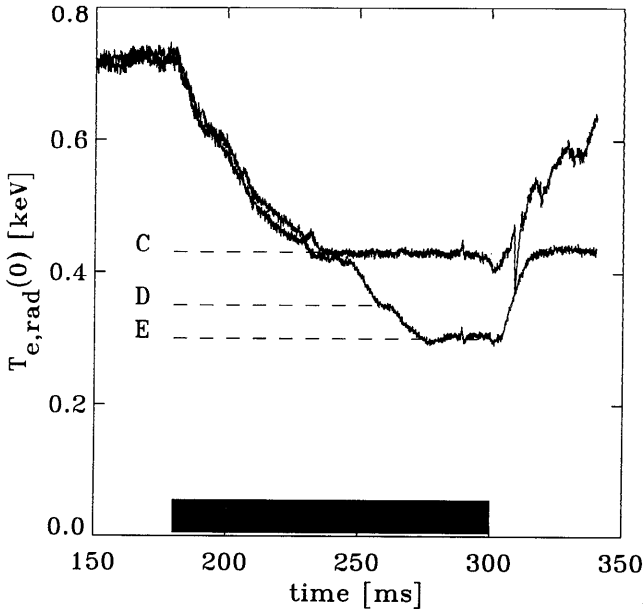
Figure 5.14: $T_e(0, t)$ as measured by ECE for two discharges with fixed ρ_{dep} and I_p was varied less than $2\,kA$. (see also Fig.5.15). ECH was switched on at $t = 175\,ms$. Note that again two levels of confinement develop and that after switch-off, the discharges in the two levels remain separated.

discharges with $I_p \leq 92\,kA$ evolve to a hollow T_e profile with low central temperature, whereas the discharges with $I_p \geq 93\,kA$ evolve to a flat T_e profile with higher $T_e(0)$. Interestingly, after switch-off, the two regimes remain separated: two Ohmic equilibria exist for the post ECH phase of the discharge. The low T_e-discharges feature a steep ∇n_e region as compared to the high T_e-discharges. This post-ECH bifurcation is described in detail in [34].

Evidence for Transport Barriers

The T_e profiles on either side of the transitions A-B, B-C, C-D and D-E are shown in Fig. 5.16. For all cases, in the region $\rho > \rho_{dep}$ the profiles are similar, and consequently the heat diffusivity χ_e is approximately the same on either side of the transition in this region. The difference between the subsequent plateaux comes about through thin layers with high ∇T_e near ρ_{dep} for the high T_e discharges: transport barriers. The width of the barrier ($\sim 1.5\,cm$) is a few times the resolution of the Thomson scattering diagnostic and consequently well resolved.
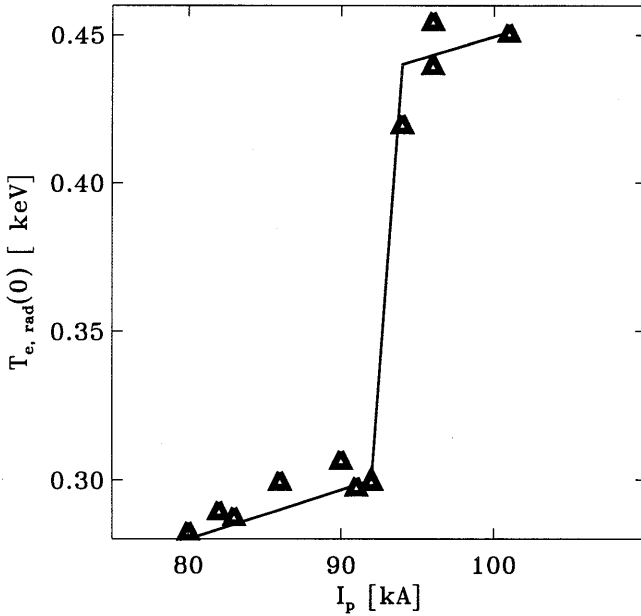
Figure 5.15: *Steady-state central radiation temperature for 11 discharges with fixed ρ_{dep}. The sharp transition corresponds to a difference of $\delta I_{\mathrm{p}} \leq 2\%$. The slow upward trend is due to an increase of Ohmic heating with I_{p}.*

When heat is deposited just on top of a barrier, i.e just before a transition, pronounced ears appear on the profiles. Figure 5.17 shows an example. These ears emphasize the improved local confinement. The ears are hot toroidal shells, $m = 0$ structures. Sawtooth like instabilities (see also Fig. 5.10) can develop in the barrier region, periodically destroying the barriers. At least four types of such instabilities have been observed. Below, the relevance of these sawtooth instabilities will be adressed.

Corroborating evidence for the existence of a transport barrier is obtained from power modulation experiments on discharges which cross over from the E level to the D level of confinement. The phase delay and amplitude decay of the propagating heat pulses are related to the electron heat transport. Figure 5.18 shows time traces of T_{e} in the centre, at ρ_{dep} and at a position $\rho_3 \sim 0.2$ outside ρ_{dep}. Between $t = 165$ ms and 170 ms, the discharge crosses over from level E to level D. At the transition the amplitude of the modulation increases significantly at ρ_{dep}, however decreases slightly at ρ_3. These observations show that a transport barrier just outside ρ_{dep} has formed.
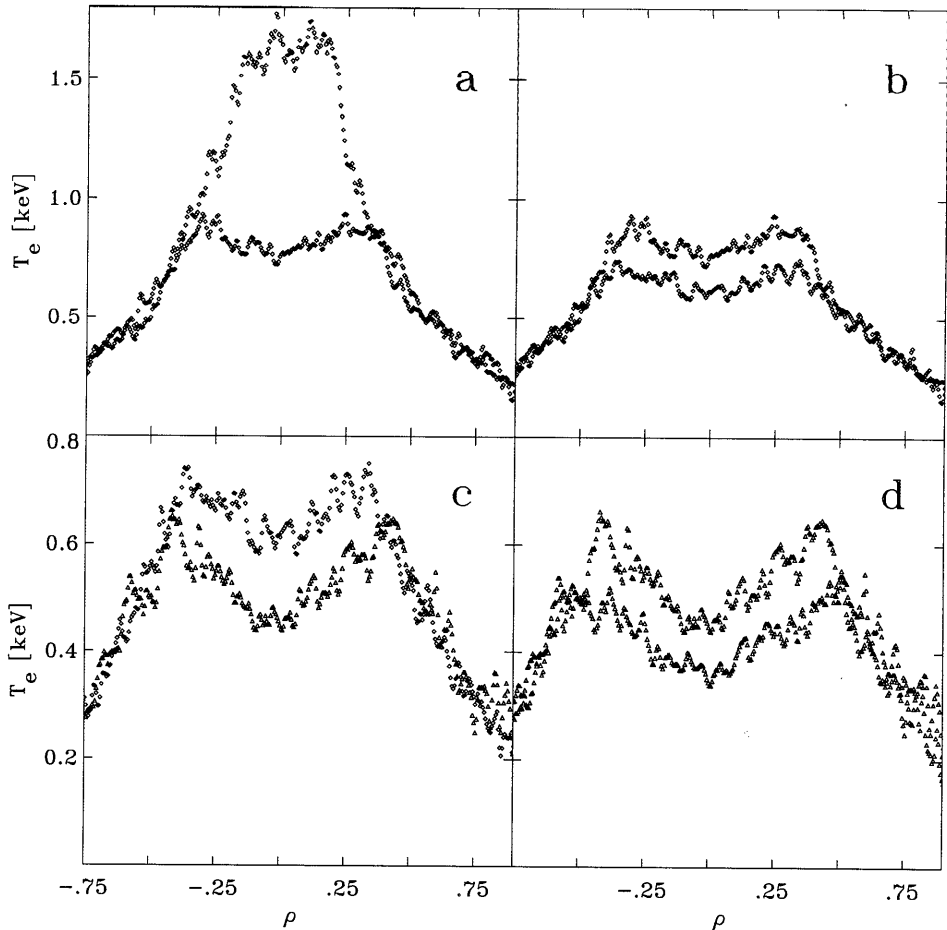
Figure 5.16: T_e-profiles for the subsequent plateaux. Presented are the profiles for the A and B plateaux (a), the B and C plateaux (b) the C and D plateaux (c) and the D and E plateaux (d). For all profiles, the differences between the subsequent plateaux come about through thin steep ∇T_e-regions, present in the plateau with the relatively high T_e.
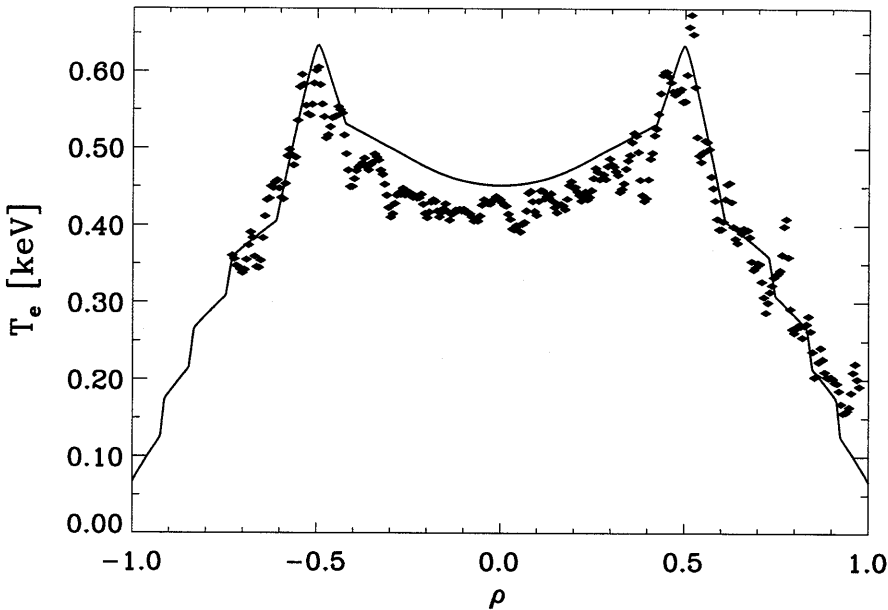
Figure 5.17: *For discharges with ρ_{dep} just inside a transition, the T_e-profile (diamonds) exhibits conspicuous ears around ρ_{dep}, footprint of a low χ_e region. These ears are very well reproduced by simulations (line), see Sec.5.5.*

Correlation with q-profile

The sharp transitions occur for a variation of ρ_{dep} by 0.01 (i.e. 0.2 cm in the plasma). Note that this is much less than the width of either the barriers as they appear in the T_e-profiles measured by Thomson scattering or the power deposition. This means that the barrier-dynamics is due to the non-linear evolution of some parameters in the plasma. As was shown in Sec. 5.4.1, the first barrier is located just outside $q = 1$. Also for off-axis deposition, the sharp transition brought about by a small change of I_p (see Figs. 5.14, 5.15) indicates that q is the critical parameter. We further note the occurence of localised MHD activity for values of ρ_{dep} just inside the transition. We shall therefore investigate the relation between the barrier and the q-profile in more detail.

We concentrate on the family of off-axis sawtooth instabilities [33, 35, 36]. These instabilities occur when EC-power is deposited in just the barrier region. Repetitive crashes, of which the mode structures have been identified, occur in the barrier region. ECE-imaging measurements in combination with standard radiometer measurements show clearly that these
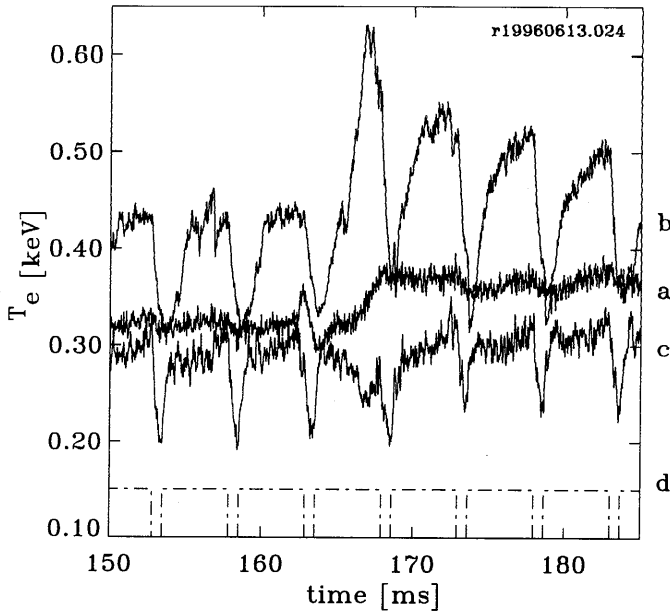
Figure 5.18: *ECH modulation sequence (dashed) and $T_e(0)$ (a), $T_e(\rho_{dep})$ (b) and $T_e(\rho_3)$ with $\rho_3 > \rho_{dep}$ (c). The ECH was switched on at $t = 110$ ms. Between $t = 165$ ms and 170 ms, the discharge crosses over to level D.*

instabilities feature a poloidal mode number $m = 3$, 2, and 3 character for the A"-B, B-C and the D-E transition respectively. The toroidal mode number for the B-C and D-E transition was shown to be $n = 1$, while for the A"-B transition $n \neq 1$ [36]. In one scan at $I_p = 60$ kA ($q_a \approx 7$) a similar mode has been observed for the C-D transition. No mode analysis could be carried out for this case since one of the ECE systems was not available. This places barriers near $q = 3/2$, $q = 2$, and $q = 3$.

This schematics is consistent with calculated (from Thomson T_e-profiles) and measured q-profiles (measured with Tangential Thomson scattering, see [37]). Figure 5.19 shows the steady-state q-profiles for the discharges in Fig. 5.8. The q-profiles were calculated from $T_e(\rho)$ and n_e assuming neo-classical resistivity, taking the bootstrap current into account. This is justified since the T_e-profiles were obtained more than 5 current equilibration times after switch-on of the ECH. For the calculations no discharges showing MHD activity were used. In the calculation, a uniform distribution of Z_{eff} is assumed, and an estimate for the uncertainty in q is obtained by allowing the Z_{eff}-profile to vary by 20 % over the cross-section, in accordance with previous measurements [38]. This leads to an uncertainty of
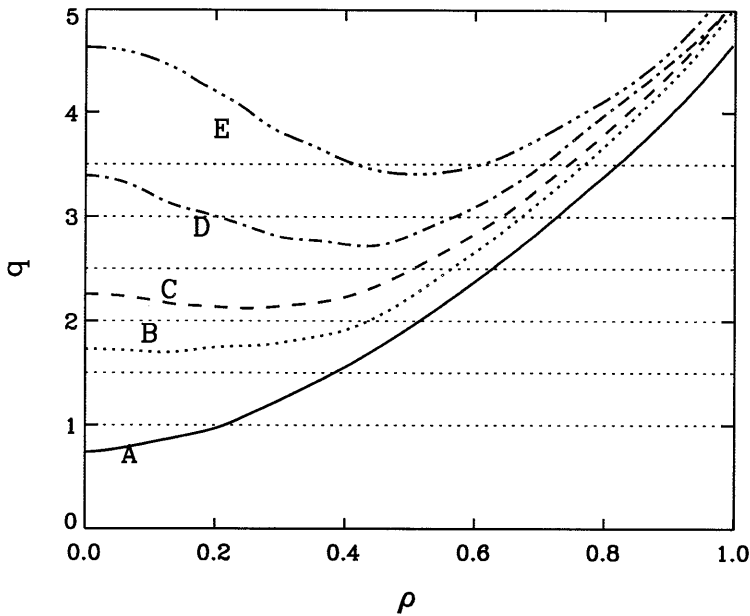
Figure 5.19: *Calculated q-profiles for the plateaux A-E. The gaps between the minimum values for q of the subsequent profiles is ~ 0.5.*

10 % in $q(0)$ and 6 % in $q(0.5)$.

In all cases, the plateaux with ρ_{dep} just inside a transition reach lower values for q than the plateaux with ρ_{dep} just outside a transition. The A-B transition is due to the loss of the steep gradient region that forms between $q = 1$ and $q = 3/2$ (see Fig. 5.8). The next transition (B-C) is due to the loss of an other steep gradient region, which is present in the B-plateau, and not present in the C-plateau. This gradient region forms in the vicinity of $q = 2$. The C-D transition is due to the loss of a steep gradient region that forms around $q = 5/2$ in the C-plateau and is not present in the D-plateau. Finally, the D-E transition is due to the loss of a steep gradient region that forms around $q = 3$ in the D-plateau and is not present in the E-plateau.

Thus, there is a systematic observation that the disappearance of the steep gradient region coincides with the loss of the indicated rational q-surfaces. Within the precision indicated above, we see that the barriers form between $q = 1$ and $3/2$ and near $q = 2$, $q = 5/2$ and $q = 3$. We also see that a transition from one plateau to the adjacent lower plateau is associated with the loss of a barrier region and the associated q-value.

As a summary:

73

- We observe transitions in T_e for variations in ρ_{dep} that are much smaller than the localisation of the ECH.

- We observe barriers in the T_e-profiles, esspecially when comparing two profiles of ajacent plateaux.

- The loss of a barrier is associated with the loss of a simple rational q-value.

- the central sawteeth place the first barrier near $q = 1$

- Mode analysis of the off-axis sawteeth indicate that also barriers exist near $q = 3/2$, $q = 2$ and $q = 3$.

- Assuming that the schematics is sustained, and based on the q-profile calculated from T_e, we position the remaining barriers near $q = 4/3$ and $5/2$.

5.5 Analysis

5.5.1 A transport model

The observations reported in the previous sections call for a transport model in which χ_e is an explicit function of q. The plateaux, in which a variation of ρ_{dep} has very little effect on the T_e-profile, call for zones with high thermal conductivity. These should be separated by insulating shells, which produce the transitions. Finally, these transport barriers should be associated with the q values $1, 4/3, 3/2, 2, 5/2$, etc. Hence we construct a model in which χ_e is low in narrow regions b_i near low rational q values q_{bi} and high elsewhere.

As we study the transition after switch-on of additional heating to a new equilibrium, the time evolution of T_e and j has to be followed. Therefore, the model has been implemented in a simulation code, which selfconsistently solves the diffusion equations for the electron heat flux (q_e) and current density (j) using a fully implicit difference scheme [39].

In the model, the radial electron heat flux density q_e, the convective radial electron particle flux density Γ_e, the resistivity σ, the parallel electric field $E_\parallel$ and the net input power density to the electrons (ohmic and ECH input power density and heat exchange to the ions) are taken into account. The measured evolution of n_e and the evolution of Γ_e that can be derived from it, is used as an input to the simulation. The edge T_e and n_e as observed in the experiment are used as boundary conditions in the simulations. For the j evolution, neoclassical resistivity (taking

the boot strap current into account) is assumed. Z_{eff} is calculated from the measured loop voltage and T_e-profile in the Ohmic phase of the discharge and is taken uniform across the plasma. q_e is assumed to consist of a diffusive component $q_{e,div} = -n_e \chi_e \nabla T_e$ and a convective component $q_{e,conv} = v_0 \rho n_e T_e$ inside ρ_{dep}. For the off-axis heated discharges in RTP, an outward $q_{e,conv}$ is needed to explain the observed hollow T_e-profiles inside ρ_{dep} (see above). In the present simulations a fixed velocity $v_0 = 100$ m/s was used.

In the previous section it was concluded that barriers must be placed near $q = 1, 4/3, 3/2, 2, 5/2$ and 3. As there is no reason to assume that the plasma behaves differently outside $q = 3$, the sequence is continued with $7/2, 4$ and $9/2$. The latter three barriers were only added for consistency. Therefore the same value for χ_e is taken for these barriers. The barrier concept implicitly assumes that the barriers are narrow compared to the inter-barrier regions. For the barrier-width w_b , that is the width expressed as a range of q, $w_b = 0.08$ was adopted for all barriers, yielding inter-barrier regions ~ 5 times wider than the barriers. The actual radial width of a barrier is then determined by w_b and the local magnetic shear $\hat{s} = (\rho/q)\,(\partial q/\partial \rho)$. It is assumed that all conducting zones feature the same value for the heat conductivity: $\chi_{e,\text{hi}} = 10\,m^2/s$. The value of $\chi_{e,\text{hi}}$ is not very critical in the simulations.

In the model, the position of the barriers, the values of χ_{hi}, v_0 and w_b are fixed. This reduces the number of free parameters to $N = 7$, equal to the number of levels (A...E, plus the two sub levels between A and B). These free parameters are the values χ_e in the barriers near $q = 1, 4/3, 3/2, 2, 5/2$ and 3 and one value for χ_e in the barriers near $7/2, 4$ and $9/2$. A thorough discussion of the model itself, and a motivation for the choices and assumptions made in the model are found in [39].

It was tried to reproduce the five $T_e(0)$ values of level A...E, plus the two sublevels between A and B. The simulations started from Ohmic T_e-profiles, then switched on the additional EC heating with the experimentally known P, ρ_{dep} and power deposition width. The χ_e values in the barriers were tuned until a good reproduction of the $T_e(0)$ levels A...E was found; see Fig. 5.7. Once the strength of the barriers has been tuned, the thus fitted χ_e is kept fixed, and it is tested how the model performs in reproducing (i) the T_e-profile shapes, (ii) the values of ρ_{dep} for which the transitions occur (ρ_{crit}), and (iii) the sharpness of the transitions? We obtain one set of $\chi_{e,\text{bi}}$ for all data. Note that only the $T_e(0)$ levels are matched, the values for ρ_{dep} for which the transitions occur follow from the model. The
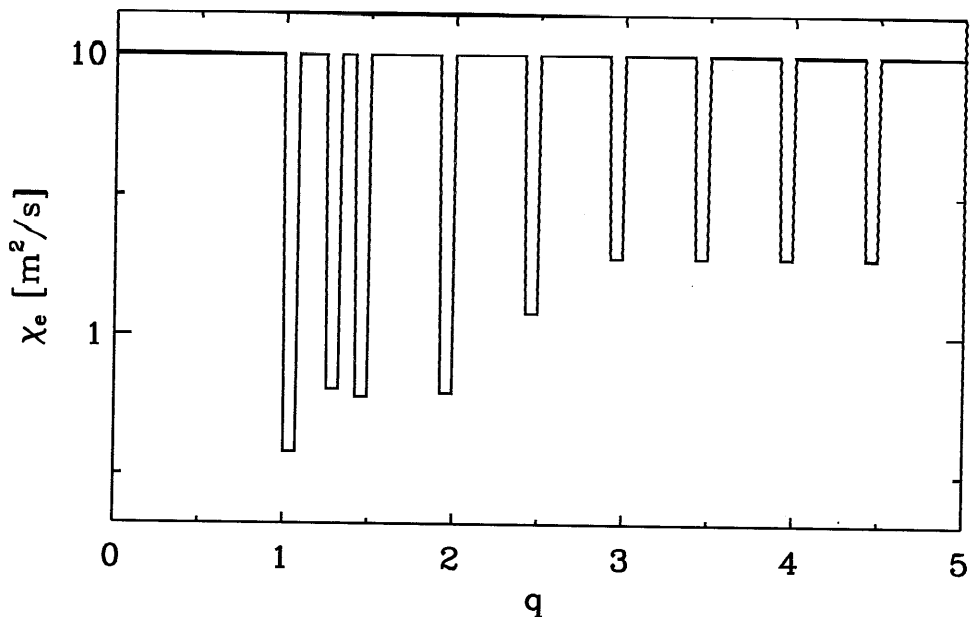
Figure 5.20: *Electron heat diffusivity* χ_e *as a function of* q. *Barriers are positioned near* $q = 1, 4/3, 3/2, 2, 5/2, 3, 7/2, 4$ *and* $9/2$. *In between the barriers* $\chi_{e,hi} = 10\,m^2/s$.

thus determined $\chi_e(q)$ is plotted in Fig. 5.20; the χ_e values in the barriers increase from $0.35\,\mathrm{m^2/s}$ near $q = 1$ till $1.8\,\mathrm{m^2/s}$ for the outer barriers. This is roughly one order of magnitude higher than the neo-classical value.

As for the first aspect: the simulated T_e-profiles are shown in Fig. 5.21. Note that the actual barrier widths depend on the magnetic shear: low magnetic shear (as in case of the A-level profile near $q = 1$) causes a relatively wide barrier; further outward the barriers are narrower due to the larger shear. Comparing the measured T_e-profiles (see Fig. 5.8) with the simulations, we observe a good correspondence. The profile shapes show good agreement in terms of barrier position and width, and the simulations even reproduce small details in the profiles. As an example, we mention the small hump around $\rho = 0.5$ in the A-type profiles, which is also reproduced by the model.

As for the second aspect: The model performs very well in reproducing the ρ_{crit} values. The first, wide, barrier is now resolved into three narrow barriers, corresponding to $q = 1, 4/3$ and $3/2$, with tiny plateaux in between.

The model was also tested in a dynamic scan of ρ_{dep} (see Fig. 5.10).
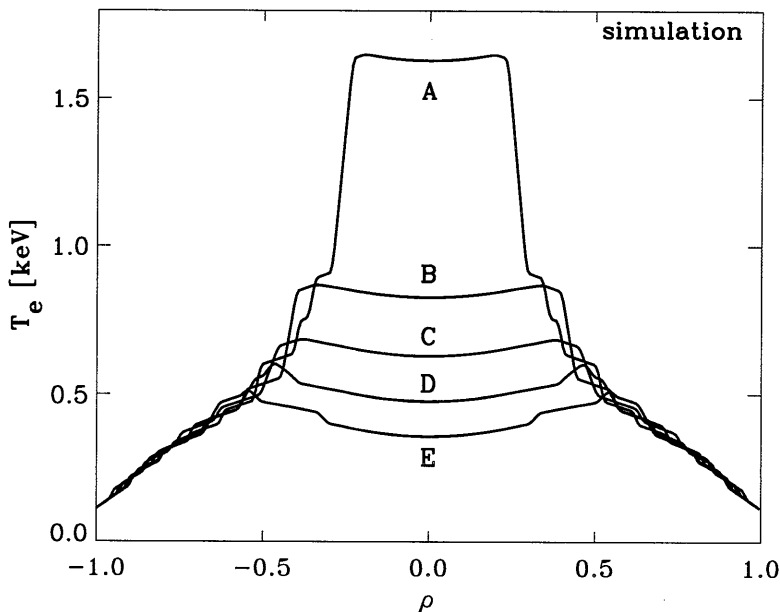
Figure 5.21: *Simulated Thomson scattering T_e-profiles for the levels A..E. No noise was added to the profile, and the steep ∇T_e can directly be appreciated from the data.*

Within a discharge ρ_{dep} was scanned dynamically from 0.2 to 0.6 by sweeping B_ϕ from 2.09 to 2.27 T in 175 ms. The same levels and transitions were observed as before, see Fig. 5.22; again the transitions were much sharper than could be expected from the width of the power deposition. Figure 5.22 shows the result of a simulation. Keeping all parameters fixed (the same as for the simulations of the static scan). The agreement with the experiment is satisfactory. The model had some difficulties predicting the exact time of the transitions of the B-C transition and the plateau C-value. Also the simulated $T_e(0)$ is lower than the experimental $T_e(0)$ for the C and D plateau. It has to be noted, however, that during a ramped B_ϕ-scan many parameters change. In particular, the changes in $n_e(\rho)$ (see Fig. 5.9) may affect $T_e(0)$ and are not taken into account in the simulations.

The third aspect, the sharpness of the transitions, is the most remarkable one: in the experimental data transition between two consecutive levels takes place over a $\delta\rho_{dep}$ much more narrow than the width of the ECH-deposition. This sharpness is very well reproduced by the simulations. The sharpness of the transitions is the result of the fact that the barriers are linked to q. An illustration and a full discussion of this effect are presented

77
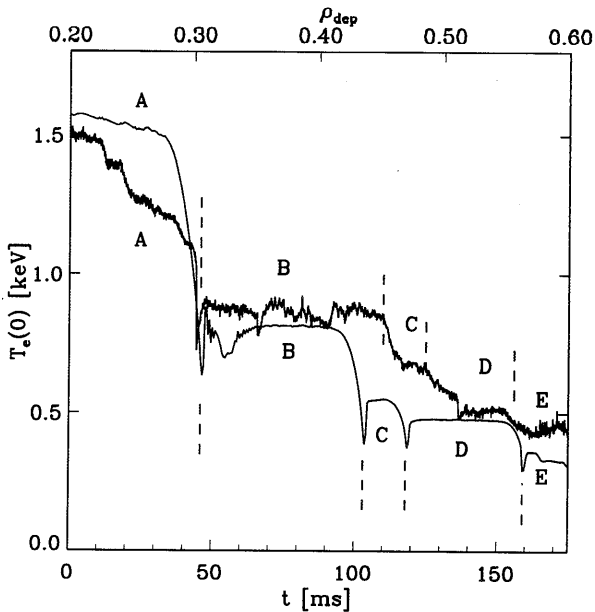
Figure 5.22: *Simulated ramped ρ_{dep}-experiment and experimental data.*

in [39].

Some other features are predicted by the model. We mention the off-axis peaks on T_e that develop just before a transition, i.e. when ρ_{dep} is just below a ρ_{crit}. An example is shown in Fig. 5.17. In the model, these 'ears' come about as follows: in such cases the low shear region, which is always present near ρ_{dep}, causes a wide thermal barrier which sits on both sides of ρ_{dep}. The wide barrier on the outside causes a rise of $T_e(\rho_{dep})$; the barrier on the inside diminishes the heat flow towards the centre; the heat loss to the ions and outward heat convection then cause a drop of $T_e(0)$ compared to $T_e(\rho_{dep})$. The 'ears' are observed only for very specific ρ_{dep} values, and the model tells why: the necessary condition is that the low shear region near ρ_{dep} falls within a barrier, i.e. has q near a (half) integer value.

5.6 Discussion

5.6.1 Data

Our observations seem to conflict with experiments on DIII-D in which an ECH deposition radius scan was applied up to radii well outside the $q = 1$ surface in which $T_e(\rho)$ remained peaked. It was concluded that for off-axis EC-heated discharges in DIII-D, an inward convective flux is present

[40, 41]. In RTP it is observed that a wide variety of profile shapes can be enforced on the plasma and that an outward convective flux is needed to model the data. It could very well be the case that the differences in experimental results are due to the difference in the ratio between Ohmic and EC- input power. The RTP-observations were done in both high n_e-, low T_e-discharges and low n_e-, high T_e-discharges. Consequently, ν^* was varied between 0.05 and 10. However, this doesnot mean that the differences in ν^* can be ruled out as the explanation for the differences in observations for the two tokamaks, because $\nu^*_{\mathrm{DIII-D}} \ll \nu^*_{\mathrm{RTP}}$ under all conditions.

5.6.2 Model

Profile stiffness

For the discharges in the A-plateau a stepped $\chi_e(q)$-profile leads to stiffness of T_e-profiles. Due to the relatively large heat diffusivity within the inversion radius ρ_{inv}, $T_e(\rho < \rho_{\mathrm{inv}})$ is flat, and is hardly affected by the exact value of ρ_{dep}. In the barrier region, the heat fluxes induce the gradient, irrespective where the heat was deposited. Quite similar T_e-profiles form for different deposition radii. In steady-state, similar T_e-profiles have similar q-profiles. A related feature is the self-organisation for the discharges in the A plateau that is possible through the shear $\hat{s}$. If $\hat{s}$ increases, the barrier tends to become thinner and less effective. As a consequence, heat is confined less effectively and $T_e(0)$ decreases and with that $j(0)$ decreases. $\hat{s}$ becomes smaller, and the barrier becomes more effective.

Width of the barrier and the value of the χ_e in the barrier

In our model, the width of the barrier in terms of q, $w_{\mathrm{bar,q}}$, and the value of the χ_e in the barrier χ_e^{bar} are defined. The actual strength of the barrier in the plasma is then determined by the local shear only. In principle, other combinations of χ_e and $w_{\mathrm{bar,q}}$ can be used, because only the insulating strength $\sim w_{\mathrm{bar,q}}/\chi_e^{\mathrm{bar}}$ of the barrier is determined from the fit. However, we note that the range in which the parameters can be varied is limited. The barriers must be narrow enough to leave room for the 'bad' regions, while too thin barriers yield 'ears' that are much more peaked than the ones that have been observed. A further lower boundary in $w_{\mathrm{bar,q}}$ is the banana width. If a barrier (in terms of ρ) becomes as thin as the banana orbit, the concept transport barrier loses its physical meaning.

In view of the discussion on the possible range of the barrier width, $w_{\mathrm{bar,q}}$ and χ_e^{bar} can be varied by a factor of two. The presented values for χ_e^{bar} are

one order of magnitude higher than neo-classical value, and this difference
is far outside the uncertainty boundaries.

Other possibilities

In the model, we assumed a sequence of barriers, of which the effectivity is
determined by the local magnetic shear. Is this choice the only possible?
The only readily visible regions improved local confinement in the exper-
imental data (the $q = 1$-barrier and the ears) form in low shear regions.
As an alternative, a model could be postulated in which a barrier only
forms when a low magnetic shear region exists in vicinity of a rational in
the q-profile. In such model, only one barrier would exist in the plasma.
Such model would be in line with the arguments put forward in [42], but
would be at variance with the stacked barriers near $q = 1$, 4/3, 3/2 and
$q = 2$. Islands have been observed in between these region [16]. We note
also that our model resembles the 'venitian blinds-model,' put forward by
Dominguez and Waltz [19], in which thermal short circuits caused by island
formation were allowed at integer values of q.

5.6.3   Relation to magnetic topology

Our model is based on experimental observations. It contains no plasma
physics, and puts forward the concept of alternating layers of good and
bad confinement. Although we did not state any physical mechanism that
causes this behaviour of χ_e, we note that the magnetic field in a tokamak
plasma resembles many of the features we discussed.

It has been proposed that KAM-surfaces (see below) may form in the
magnetic topology: It can be shown that the time independent magnetic
field in a tokamak can be described in terms of a Hamiltonian, in which the
toriodal coordinate ϕ replaces the time-coordinate [43]. If the Hamilito-
nian is unperturbed, the magnetic field organises itself in magnetic surfaces,
that are labeled by the radial coordinate only. Small perturbations of the
magnetic field lead to the destruction of the flux surfaces. Such pertur-
bations can be expected in a tokamak plasma, due to both imperfections
of the externally applied field and small asymmetries of the current den-
sity distribution. However, there is no 'first principles' theory that gives
a quantitative prediction of the perturbations of the magnetic field in a
tokamak.

For arbitrarily small perturbations, the topology of the field changes
from the ideal set of nested, perfect flux toroidal surfaces, to the generic

mix of good surfaces, chains of magnetic islands and regions of chaotic field. The surfaces with simple rational winding number are the first to degenerate and form magnetic islands, the surfaces of which the winding number is 'very' irrational are the last to remain. The well-known KAM-theorem garantees that for sufficiently small perturbations there are always good surfaces left, the so called KAM-surfaces.

This mathematical theory makes clear that the topology of ideal nested surfaces which is commonly assumed in tokamak theory, must be an idealisation. However, as said before, there is no theoretical prediction of the measure in which the topology is broken up. How big are the magnetic islands, do they overlap, are there regions of chaotic field? are questions that must be answered by the experiment. However, the difficulty here is that it can be shown that magnetic fluctuations of the level $\tilde{B}/B \sim 10^{-4}$ are sufficient to significantly enhance transport. Such fluctuations (or magnetic islands with a size of a few millimeter) are difficult to diagnose.

There is a further difficulty in relating the theory of the toplogy of perturbed magnetic fields to measured quantities in a tokamak. This is the fact that the theory of transport in the mixed topology is not fully developed. In the first place, field line 'trajectories' are very complicated: field lines certainly do not make a random walk, but can stick to magnetic islands for a long time, only to make unpredictable large excursions later. Secondly, the transport of particles in such a system is an unresolved problem.

In relation to the experimental results, we note the following problems. 1) Both from local power balance analysis and the fits for χ_e we see that even in the barrier region the electron heat diffusivity is still much larger than neo-classical predictions. This indicates that in addition to the mechanism that causes the alternating layers of high and low χ, an other turbulent transport driving mechanism is active. 2) The effect of chains of small islands that may form is also not clear.

5.6.4 Measurability

As was mentioned in Sec. 2.6, two approaches have been put forward in the literature to measure χ: Power balance analysis and heat pulse propagation analysis. From our data it appears that the barriers extend at maximum over 10% of the minor radius. With the typical resolutions at which diagnostics are operated in present-day tokamaks, both methods can only yield a harmonic average of $\chi_{\text{har}} = < \chi^{-1} >^{-1}$ which neither does reflect the value for χ_e in the barrier region nor the value for χ_e in the conducting
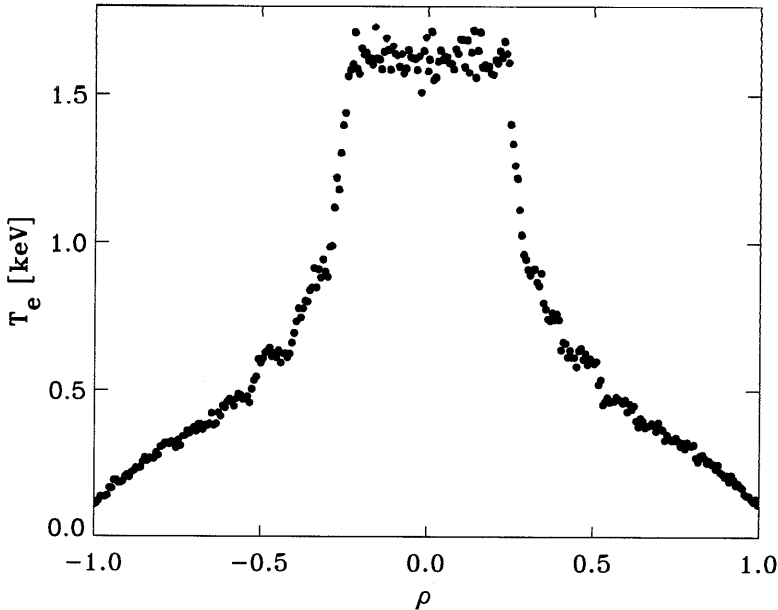
Figure 5.23: *Simulated Thomson scattering T_e-profile for the A level. Noise was added to enable a fair comparison with the measured Thomson scattering T_e-profiles.*

zone.

As an example, RTP would be perfectly suited to carry out power balance experiments: It features a strong electron heating per volume unit of $\sim 1\,MW/m^3$ (i.e. a strong electron heat flux) and a diagnostic with a radial resolution of 1.5% of the minor radius. Even local power balance analysis of the RTP Thomson scattering profiles cannot yield the desired information, because in order to resolve $\nabla\chi(\rho)$, one needs to determine $\nabla^2 T_e(\rho)$ at sufficient accuracy. The analysis is complicated due to the presence of small islands and noise (approximately 4%) in the data, resulting in an artificially wild behavior of χ_e^{PB}.

In practice, only the strong barrier near $q = 1$ is readily visible in T_e and χ_e^{PB}. Figure 5.23 shows the simulated T_e profile for a typical level A case, in which, the known experimental Thomson scattering noise of $\sim 4\%$, depending on T_e and n_e, has been added. It should be noted that this added noise makes the barriers, expect the one at $q = 1$, nearly invisible in the simulations, just like in the measured profiles.

The typical instrumentation for determining χ^{HP} are radiometers. If barriers are thin in comparison to the resolution of the EC diagnostoics, in

these experiments a mean value over regions of good and bad confinement is measured. Therefore, it is no surprise that sofar, heat-pulse propagation studies have only indicated the presence of the barrier near $q = 1$, this barrier being the most pronounced.

5.6.5 Consequences for experimental transport studies

A consequence of the observations presented here, is that a transport analysis based on an average ∇T_e yields a value of χ_e that reflects neither the value in the barriers nor the value in the conduction zones [18]. Hence, an observed parametric dependence may be caused by a change of χ_e in the barriers, outside the barriers, or might be due to a changed width of the barriers. Therefore, instead of determining averaged χ_e, electron heat transport studies should focus on the determination of position, width and strength of the barriers.

A1 Determination of the ECH deposition radius

To good approximation ρ_{dep} is lineary dependent on the measured quantity B_ϕ. The precise relationship $\rho_{dep}(B_\phi)$ was obtained experimentally. The major radius of the 'cold' 2nd harmonic resonance (R_{cr}) is given by $R_{cr} = B_0 R_0 e / \pi m_e f_{ech}$, in which B_0 is the magnetic field at R_0 ($= 0.72$ m), m_e is the electron mass and f_{ech} is the gyrotron frequency. Due to the relativistic mass increase, the actual deposition radius is shifted inward, $R_{dep} = R_{cr} - \delta R_{hot}$. To find the minor radius of power deposition, also the Shafranov-shift of the flux-surface of deposition $s(\rho_{dep})$ has to be taken into account. This leads to two expressions: one for low field side (LFS) deposition and one for high field side (HFS) deposition:

$$\rho_{dep}^{LFS} = (R_{dep} - R_0 - s(\rho_{dep}))/a.$$

$$\rho_{dep}^{HFS} = (-R_{dep} + R_0 + s(\rho_{dep}))/a.$$

Experimentally, it is possible to identify two values of B_ϕ, one for HFS (B_0^{HFS}) and one for LFS deposition (B_0^{LFS}) which give rise to the same $T_e(0)$. Assuming that in this case $\rho_{dep}^{LFS} = \rho_{dep}^{HFS}$ and that δR_{hot} is the same for LFS and HFS deposition, the relationship between ρ_{dep} and B_ϕ can be

83

found by cadding the equations for LFS and HFS deposition:

$$\rho_{\text{dep}} = \frac{(B_0^{\text{LFS}} - B_0^{\text{HFS}})R_0 e}{2\pi a m_e f_{\text{ech}}},$$

while the Shafranov shift follows from subtracting the equations

$$s(\rho_{\text{dep}}) + \delta R_{\text{hot}} = \frac{(B_0^{\text{LFS}} + B_0^{\text{HFS}})R_0 e}{2\pi m_e f_{\text{ech}}} - R_0.$$

δR_{hot} can be calculated, and consequently also $s(\rho_{\text{dep}})$ can be determined from the LFS and HFS comparison. Finally, assuming a quadratic dependence of $s(\rho) = s_0(1 - \rho^2)$, $s_0 = s(\rho_{\text{dep}})/(1 - \rho_{\text{dep}}^2)$, the Shafranov-shift of the magnetic axis can be approximated.

The above-described procedure was carried out for several conditions $(I_{\text{p}}, n_{\text{e}})$. For the experiments in this paper, $\bar{n}_e = 2.4 - 3.0 \times 10^{19} \, m^{-3}$ and $I_{\text{p}} = 80 \, \text{kA}$, the result is that

$$\rho_{\text{dep}} = 2.290 B_\phi - 4.646$$

for LFS deposition and

$$\rho_{\text{dep}} = -2.125 B_\phi + 4.314$$

for HFS deposition. Van Gelder [44] has calculated that δR_{hot} is $5 - 7 \, \text{mm}$ for the conditions at hand. A relativistic downshift of $\delta R_{\text{hot}} \approx 7 \, \text{mm}$ corresponds to electron energies of $\sim 5 \, \text{keV}$, in agreement with the rule of thumb that optimal EC absorbtion occurs at $(2 - 3) \, v_{\text{th}}$, in which v_{th} is the thermal velocity. Consequently, for the Shafranov shift at the magnetic axis we find $s_0 \approx 2 \, \text{cm}$. There are no equilibrium reconstructions available for these discharge conditions to compare this experimental determination of s_0 with; however, this value is in good agreement with the Shafronov shift calculated from the pressure profile for typical central EC heated discharges.

Bibliography

[1]   P.C. Liewer, Nucl. Fusion **25**, (1985) 543

[2]   J.W. Conner *et al*, Plasma Phys. Control. Fusion **36** (1994) 719

[3]   R.J. Bickerton *et al*, Plasma Phys. Control. Fusion **39** (1997) 339

[4]   E.J. Doyle *et al.*, Proc. 16th IAEA fusion energy conference, **1**, (1997), 547

[5]   B.W. Rice *et al*, Nucl. Fusion **36**, (1996) 1271

[6]   T. Fujita *et al*, Phys.Rev.Lett. **78** (1997) 2377

[7]   Y. Koide *et al*, Phys.Rev.Lett. **72** (1994) 3662

[8]   F.M. Levinton *et al*, Phys.Rev.Lett. **75** (1995) 4417

[9]   E. Mazzucato *et al*, Phys. Rev. Lett. **77**, (1996), 3145

[10] K.M. McGuire *et al*, Proc. 16th IAEA fusion energy conference, **1**, (1997), 19

[11] R.E. Bell *et al*, Plasma Phys. Control. Fusion **40** (1998) 609-613

[12] The JET team, Plasma Phys. Control. Fusion **39** (1997) B353-B369

[13] A.C.C. Sips *et al*, Plasma Phys. Control. Fusion **40** (1998) 647-652

[14] N.J. Lopes Cardozo *et al*, Phys.Rev.Lett. **73** (1994) 256

[15] M.F.F. Nave *et al*, Nucl. Fusion **32** (1992) 825

[16] M.N.A. Beurskens *et al*, 'Double pulse multiposition Thomson scattering and dynamics of small scale T_e and n_e structures in RTP', submitted to Nucl. Fusion

[17] G.M.D. Hogeweij *et al*, Nucl. Fusion **36** (1996) 535

[18] N.J. Lopes Cardozo *et al*, Phys. Plasmas **2** (1995) 4230

[19] R.R. Dominguez *et al*, Nucl. Fusion **27**, (1987) 65

[20] C.C. Hegna *et al*, Plasma Phys. Control. Fusion **35** (1993) 987

[21] T.A. Gianakon *et al*, Phys. Plasmas **1** (1994) 2245

[22] P.H. Rebut *et al*, Proc. 12th conf. Plasma physics and Controlled Nuclear Fusion Research bf 2 IAEA (1989)

[23] B.B. Kadomtsev *et al.*, Proc. 7th conf. Plasma physics and Controlled Nuclear Fusion Research bf 1 IAEA (1989) 649

[24] A.J.H. Donné, Plasma Phys. Reports **20** (1994) 192

[25] R. Barth *et al*, Rev.Sci.Instrum. **68** (1997) 3380

[26] D.F. da Cruz *el al* Rev.Sci.Instrum. **61** (1990) 3067

[27] J.H. Rommers *et al*, Plasma Phys. Control. Fusion **38** (1996) 1805

[28] J.F.M. van Gelder *et al*, Rev.Sci.Instrum. **66** (1995) 418

[29] P. Yushmanov *et al*, Nucl. Fusion **30** (1990) 1999

[30] N.J. Lopes Cardozo *el al*, Phys.Rev.Lett. **73** (1994) 256

[31] P. Galli *et al*, Proc. 10th Joint workshop on electron Cyclotron Emission and Electron Cyclotron Resonant Heating (EC-10), (1997) 379

[32] G.M.D. Hogeweij *et al*, Phys.Rev.Lett. **76** (1996) 632

[33] M.R. de Baar *et al*, Phys.Rev.Lett. **78** (1997) 4573

[34] M.R. de Baar *et al*, accepted for publication in Phys.Rev.Lett.

[35] N.J. Lopes Cardozo *et al*, Plasma Phys. Control. Fusion **39** (1997) B303

[36] R. Meulenbroeks *et al*, EPS-contribution 1998

[37] F.A. Karelse *et al*, EPS-contribution 1998

[38] D.F. da Cruz,"Soft X-ray emission from tokamak plasmas", Ph.D. thesis, Rijksuniversiteit Utrecht (1993)

[39] G.M.D. Hogeweij *et al*, to be submitted to Phys. Plasmas

[40] T.C. Luce *et al*, Phys.Rev.Lett. **68** (1992) 52

[41] C.C. Petty *et al*, Nucl. Fusion **34**, (1994) 121

[42] J.F. Drake, Phys. Rev. Lett. **77** (1996) 494

[43] A.H. Boozer, Phys. Fluids **26** (1987) 1288

[44] J.F.M. van Gelder, "Electron Cyclotron absorbtion experiments in Tokamak plasmas", Ph.D. thesis, Rijksuniversiteit Utrecht (1997)

Chapter 6

Bifurcated states of Ohmically heated Tokamak plasmas.

Section 6.1 is a reproduction of the paper 'Bifurcated states of Ohmically heated Tokamak plasmas,' by M.R. de Baar, G.M.D. Hogeweij and N.J. Lopes Cardozo, accepted for publication in Phys. Rev. Lett, and reproduced with kind permission of Phys. Rev. Lett. Experimental evidence is presented for bifurcated Ohmic states, that form when the ECH is switched off in discharges that are heated around half radius. These states are discussed in relation to other Ohmic confinement regimes and candidate turbulent modes for Ohmic confinement. In chapter 5 it was shown that a model featuring transport barriers in the vicinity of simple rational values of q, reproduces a wide range of phenomena observed in EC-heated discharges. In section 6.2 it is argued that for the post ECH Ohmic phase, the barriers may give rise to the distinct steady states of confinement.

6.1 Experimental observations

6.1.1 Abstract

Experiments in the Rijnhuizen Tokamak Project (RTP) are reported that show bifurcated states of plasmas in the Linear Ohmic Confinement regime. One branch is the usual Ohmic state. The second, newly discovered, state features a much broader temperature profile, while the density has a very pronounced gradient near half-radius. The bifurcated states form after off-axis electron cyclotron heating (ECH) is switched off. The new state contradicts theoretical models which predict inproved confinement for peaked density profiles or high collisionality.

6.1.2 Introduction

In tokamaks [1], hot plasmas are confined in a torus by means of an externally applied toroidal magnetic field (B_ϕ) and a much smaller poloidal field, which results from a toroidal current density j. The plasma torus is characterised by the major radius (R_0) and the minor radius (a). The helical field lines lie on nested tori, with minor radius r, or $\rho = r/a$. The safety factor (q), defined as the number of toroidal turns a field line makes to complete one poloidal turn, is a function of ρ.

For tokamak discharges without additional heating, the energy confinement time τ_E is proportional to n_e (Linear Ohmic Confinement (LOC)) at low electron density (n_e), while above a line-average density of $\bar{n}_{e,cr} = 3 - 5 \times 10^{19} m^{-3}$ confinement becomes independent of n_e (Saturated Ohmic Confinement (SOC)). It has been shown in many tokamaks [2, 3, 4, 5] that SOC is due to saturation of the electron energy content W_e. By forcing the density profile to peak it is possible to go from SOC to Improved Ohmic Confinement (IOC), where the linear scaling of τ_E with n_e is recovered. Statistical analysis indicates that IOC is a high density continuation of LOC [3]. In the three regimes the q-profile reaches just below unity in the center of the discharge.

The n_e dependence of τ_E is often brought in relation to the density-peakedness, $Q_n = n_e(0)/n_e^v$, in which n_e^v is the volume-average density. It has been observed that in LOC Q_n increases with n_e, that Q_n is constant or even slightly decreasing in SOC, and increases again in IOC. Q_n is associated to the density gradient length $L_n = n_e/\nabla n_e$ and can be increased actively by multiple pellet injection [6, 7] or reduction of the edge density by tailoring of the edge-radiation profile with low Z_{eff} impurities [8]. Several scenarios for turbulent transport have been put forward in the literature

to explain the complicated dependence of τ_E on Q_n. The candidate modes (the dissipative trapped ion mode (DTIM), the dissipative trapped electron mode (DTEM), the ion temperature gradient mode (ITGM or η_i-mode) and electron temperature gradient mode (ETGM or η_e-mode)) are either stabilised with decreasing L_n [9, 10] or increasing collisionality ν^*.

The present paper reports on RTP ($R_0 = 0.72$ m, $a = 0.16$ m, $B_\phi < 2.5$ T, pulse length typically 0.5 s) discharges which are all in the LOC regime. Two distinct Ohmic states have been observed. One is the normal Ohmic state with a peaked T_e-profile and central q touching unity. The second, newly found, state has a much broader T_e-profile, a q-profile which stays well above unity, and high Q_n n_e-profile, with strong local gradients near half radius.

The plasma was heated at half radius with 350 kW, 110 GHz ECH (2nd harmonic, X-mode, launched from the low field side) during 150 ms, corresponding to > 30 energy confinement times and > 5 current diffusion times. The ECH power exceeds the Ohmic dissipation by a factor > 5. When the ECH deposition is placed off-axis, in RTP steady state flat or hollow T_e -profiles are obtained [11]. This contrasts the finding in DIII-D, where off-axis ECH led to peaked T_e -profiles [12]. However, both experiments have in common that significant heat convection up the T_e-gradient must be invoked to explain the power balance. Importantly, in the off-axis heated RTP plasmas, the central q is increased well above q=2, and a region with small or inverted shear is created. When this state is allowed to relax by switching off the ECH, the two stable, Ohmic states can be accessed.

We consider a database of 37 RTP-discharges with very similar parameters ($B_\phi = 2.26$ T, $I_p = 80$ kA and $\bar{n}_e = 3 \times 10^{19}$ m^{-3}), with $\rho_{dep} = 0.55$. Figure 6.1 shows the evolution of $T_e(0)$ measured with Electron Cyclotron Emission spectroscopy (ECE) (top panel) and n_e as measured with an interferometer (bottom panel) in two typical discharges. Note that $T_e(0)$ decreases during off-axis ECH, when a hollow T_e-profile develops. The discharges reach almost the same steady state during the ECH, but evolve differently after ECH is switched off. State I discharges feature values for $T_e(0)$ and Q_n (dashed) that are similar to the pre-ECH phase, while state II discharges have lower $T_e(0)$ and higher Q_n (full). The two branches reach a steady state and remain separated until the end of the discharge, i.e. > 30 energy confinement times and > 5 current diffusion times. The database shows that there are indeed distinct branches, separated by a gap (Fig. 6.2).

89
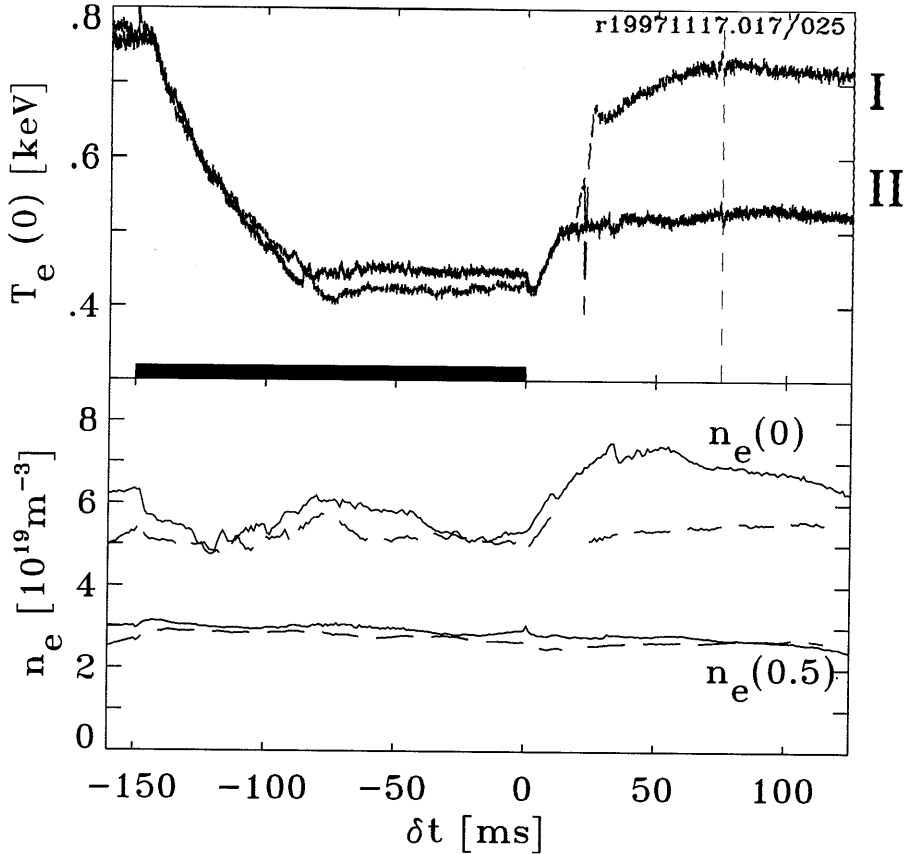
Figure 6.1: *The evolution of the central electron temperature $T_e(0)$ (top panel) a for two representative discharges, which have near identical parameters. During the off-axis ECH ($\delta t = [-150, 0]$ ms), the profiles of T_e and j become hollow, hence $T_e(0)$ decreases. After switch-off of the ECH, two distinct branches form. The state I discharge returns to a state that is very similar to the pre-ECH Ohmic plasma. The state II discharge settles at a much lower $T_e(0)$. The bottom panel shows the behaviour of the central density and the density at half radius. After switch-off of the ECH, the state II n_e-profile (full) becomes more peaked. The state I (dashed) discharge passes through a few instabilities (see Fig.6), which distort the interferometer signals for a short period. The profiles of both states, measured with Thomson scattering at $\delta t = 75$ ms (indicated by the dashed vertical line), are compared in Fig. 6.4.*

Figure 6.2: *A histogram of the steady state central electron temperature, reached 75 ms after ECH is switched off, of 37 near identical discharges. The gap between state I and II is clearly observed. Detailed analysis shows that state I may in fact consist of two distinct states, the upper one of which corresponds to the pre-ECH Ohmic state.*

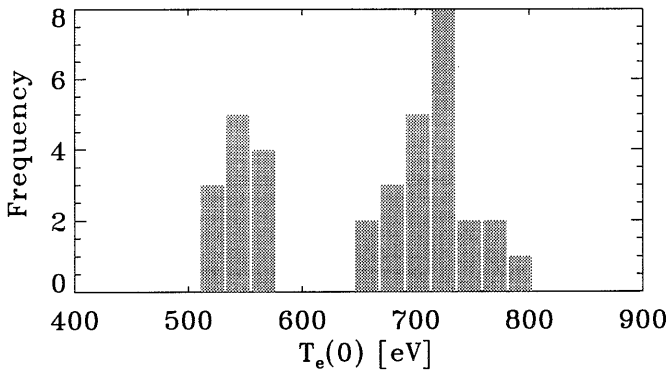Figure 6.3 compares the profiles of T_e, n_e and electron pressure (p_e) in the two branches, measured with multi-position Thomson scattering 75 ms after ECH has been switched off, i.e. well into the steady state phase. The high T_e-branch (state I, symbols) and the low T_e-branch (state II, line) profiles are similar in the outer region ($\rho > 0.4$), but diverge in the center. State I is very similar to the pre-ECH state of the discharge albeit that the central T_e is often (but not always) slightly lower. The n_e and T_e-profiles are triangular. The state II n_e-profiles develop a steep gradient at $\rho \approx 0.38$. Note that no pellet injection was applied. State II has less peaked pressure profiles than state I. The Ohmic dissipation is 130 kW and 165 kW for the state I and II discharges presented here.

The fact that both states are in LOC has been established experimentally. In Fig. 6.4 the T_e and n_e-profiles are presented for discharges with different $\bar{n}_e$. The variation in density is 13% for the state-II discharges and 20% for the state-I discharges. The T_e-profiles are very similar and show no density dependence. The density profiles are self-similar. $Q_n = 3.04$ and 3.11 for the low and high density state-II discharges respectively. $Q_n = 2.82$ and 2.78 for the low and high density state-I discharges respectively. For both states W_e and τ_E increase linearly with density. This result agrees with the density at which saturation is expected for $I_p = 80$ kA RTP-discharges, $\bar{n}_{e,cr} = 4.3 \times 10^{19} \, \text{m}^{-3}$. This is 30% higher than the highest density presented in this paper. State I discharges follow the Neo-
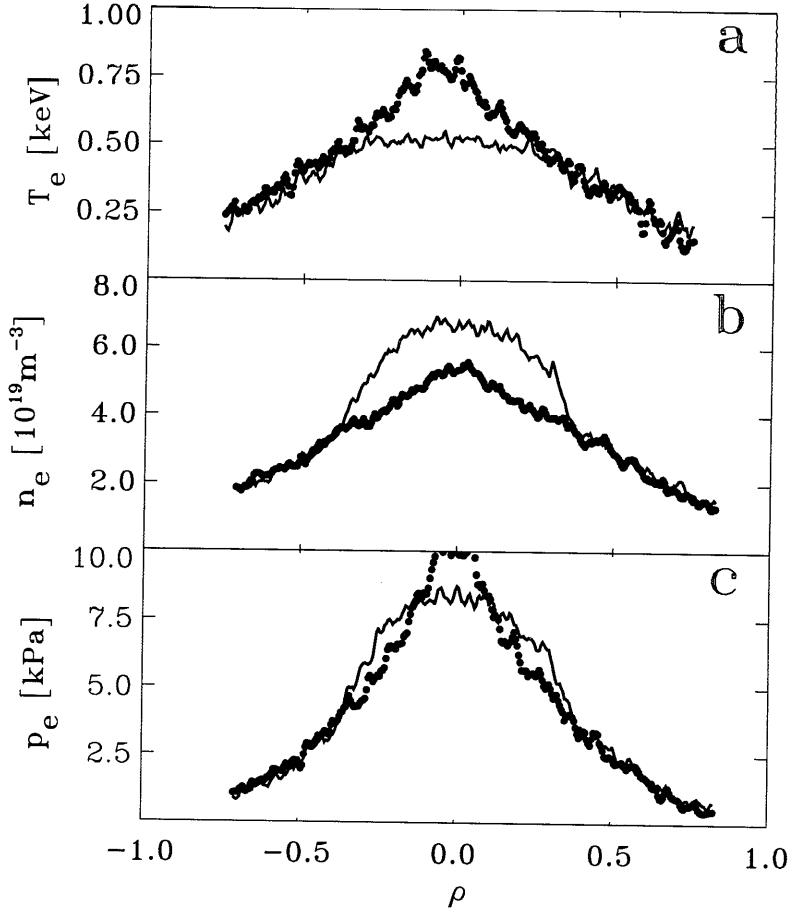
Figure 6.3: Profiles of T_e, n_e and p_e measured with Thomson scattering at 75 ms into the post-ECH phase for both states (symbols=state I, line=state II). In state II the n_e-profile develops a localized gradient near $\rho = 0.38$. The differences are very pronounced in the T_e and n_e-profiles but largely cancel in the p_e -profile, which nonetheless is more peaked in state I than in state II. For the presented discharges, $\tau_{Ee}^{I} = 4.4$ ms and $\tau_{Ee}^{II} = 4.2$ ms.
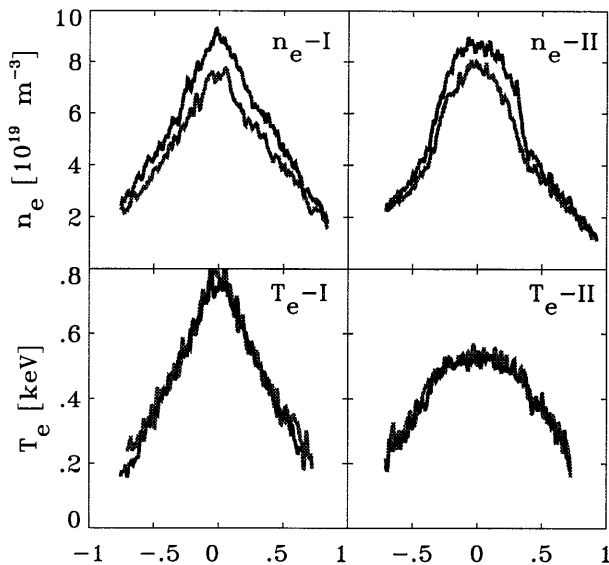
Figure 6.4: T_e and n_e profiles for the two states at different densities. For both states, the increase of the n_e is not associated with changes in T_e. The profile-shapes are constant, and $W_e \propto \bar{n}_e$.

Alcator scaling, and state II discharges do 25 % worse.

In Fig. 6.5 a sequence of T_e (a) and n_e-profiles (b) is presented for discharges which evolve to state-II. When ECH is switched off, the off-axis maximum in T_e is not sustained and $T_e(\rho > \rho_{dep})$ decreases within the first 3 ms, while $T_e(0)$ increases slightly. The sharp n_e-gradient around $\rho = 0.38$ develops on a much longer time scale. Why this local gradient forms is not clear. Influx of neutral particles can be ruled out as an explanation for the differences in the two states, because 1) the neutrals come from the edge region of the plasma where both states are similar and 2) a neutral influx can not explain such a localized increase of ∇n_e. Specific effects of ECH, such as anisotropy or deformation of the velocity distribution function should disappear much faster than the gradual build-up of the density gradient. The gradient formation must then be due to a reduction of the local particle diffusion coefficient, an increase of the inward particle convection or a combination of the two effects. So-far we are not able to distinguish between these effects, and the question why the steep n_e-gradient forms remains open.

With the high Q_n and the linear τ_E dependence on $\bar{n}_e$, state II profiles may appear to be a low density variant of IOC- discharges. However,
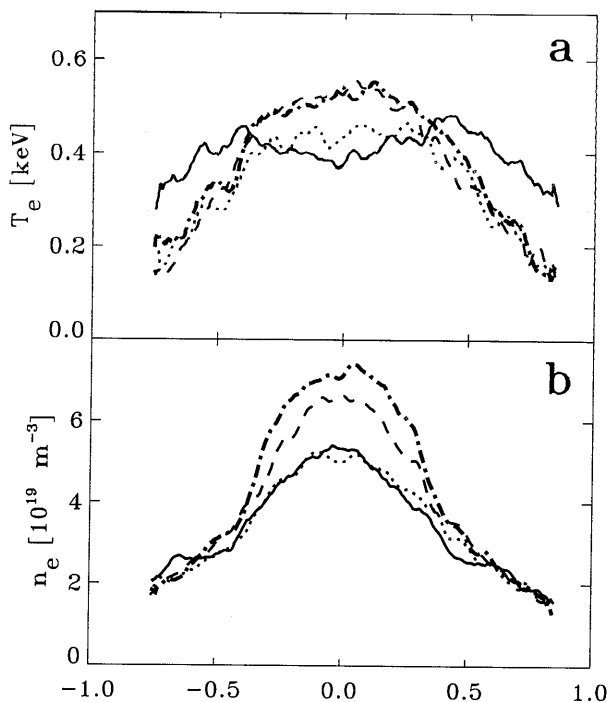
Figure 6.5: *Development of state II profiles. The profiles shown are taken 0 ms (thin line), 3 ms (dotted), 20 ms (dashed) and 35 ms (thick dash-dotted) after ECH is switched off. The T_e-profile changes rapidly after switch-off, but is at 3 ms (i.e. about one energy confinement time) already close to its final state. The changes in the n_e-profile, most notably the formation of a steep ∇n_e-region around $\rho = 0.38$ take tens of ms, or several current diffusion times*

we note the following essential differences: 1) the bifurcation of the T_e-profile is already established long before the n_e-profile peaks 2) the state II discharges have worse (rather than 'improved') confinement compared to state I. 3) the state II discharges develop a n_e-gradient, which is much more localised than the profile peaking reported for IOC discharges. Moreover, in state II discharges, the n_e peaking is not the consequence of density-profile control but evolves spontaneously. Finally, the state II is produced at much lower density than IOC.

Figure 6.6 depicts traces of T_e, measured by ECE, showing two fast relaxations that only occur in state I discharges. The first event is localized off-axis, and often displays precursor activity with an $m = 2$, $n = 1$ character as could be determined from ECE and soft X-ray measurements.
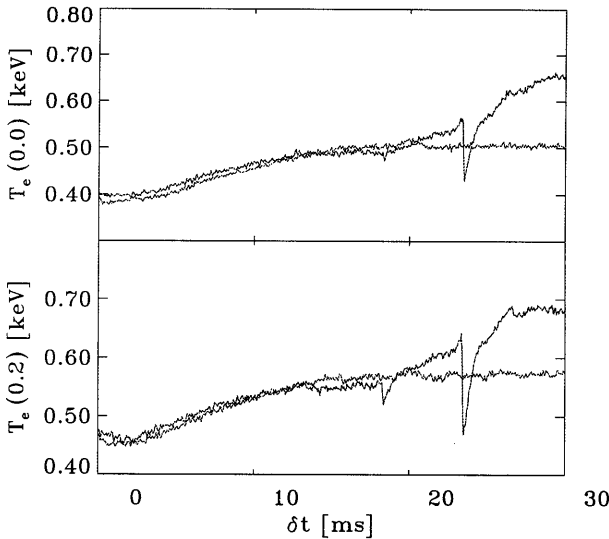
Figure 6.6: ECE measurements of the electron temperature at $\rho = 0$ and $\rho = 0.2$, showing two 'fast events' in a state I discharge. For reference, state-II traces are presented. The first event coincides with the divergence of the two states, and may be the cause of it. This event does not affect the centre, and often has an m=2 precursor. The second event is much stronger and does affect the centre.

Off-axis relaxation phenomena with $m \neq 1$ have been observed in several tokamaks [13, 14, 15] and are often associated with non-monotonical q-profiles. The second, more violent, event also affects the centre of the discharge. The steep n_e gradient near $\rho = 0.38$ disappears within 1 ms after this event. For this event precursor activity has not been observed.

In equilibrium, the current density $j(\rho)$ (see Fig. 6.7a) can be calculated from T_e and p_e assuming neo-classical resistivity. In leading order, the bootstrap current is driven by ∇n_e and the effect of the steep ∇n_e-region for state II discharges is clearly visible. The effect of the bootstrap current is that, in addition to the effect of the flat T_e region, the q-profile (see Fig. 6.7c) remains flat out to $\rho = 0.38$ for state II discharges with $q_{min} \approx$ 1.8. For state I discharges $q_{min} \approx 1$. The observation that the two branches separate when an m=2 MHD event occurs, after which the two branches have very different q-profiles, may indicate a role of the q-profile in the transport physics.

In conclusion, a new Ohmic state has been found, in which the energy confinement is proportional to the density as in normal LOC discharges.

95

Figure 6.7: *Profiles of the total current density $j(\rho)$ (a), bootstrap-current profile $j(\rho)_B$ (b) and the safety factor $q(\rho)$ (c) for both states (state I dashed, state II 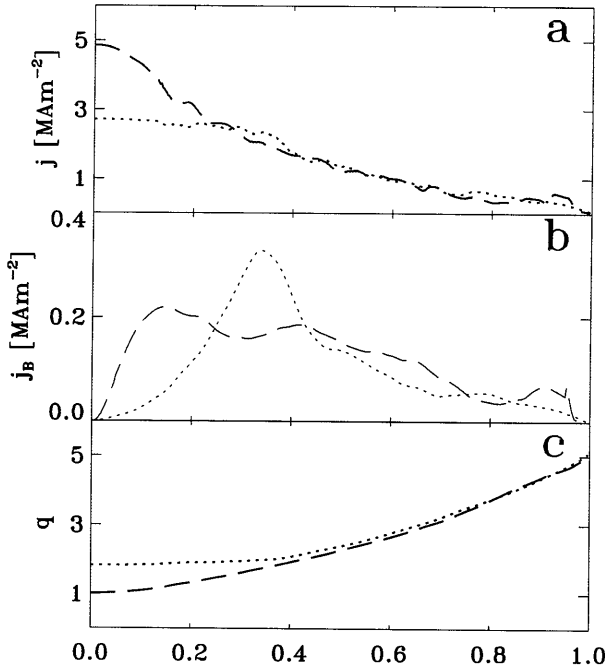dotted). The effect of the off-axis maximum of the bootstrap-current for state-II discharges is that $j(\rho)$ and $q(\rho)$ remain flat from the center up to $\rho = 0.38$.*

In this state a sharp n_e -gradient forms spontaneously near $\rho = 0.38$. In theoretical models commonly forwarded to explain the LOC - SOC and IOC regimes, it is thought that density peaking or increased collisionality leads to improved confinement. In contrast, in the present experiment the density peaking arises spontaneously, comes after the bifurcation, and does not lead to improved confinement. Since both state I and state II are in LOC regime, and state I follows the usual neo-Alcator scaling, the coexistence of both states appears to be at variance with usual picture in which turbulent modes that are sensitive to L_n or ν^* are responsible for transport. Furthermore, from the steady state profiles and the evolution of state II, it is evident that χ_e and D are decoupled, thus differing from the conclusion reached in [5] for LOC discharges.

As an alternative, the present experiments indicate a role of the q-profile determining the transport of heat and particles. This places the present results in wider class of experiments with intense additional heating or pellet injection, wheré an extreme sensitivity of confinement to initial conditions was found, which was related to the evolution of the q-profile [15, 16, 17, 18, 19, 20]. Thus, the bifurcation of Ohmic plasma states reported here, and e.g. the formation of an electron transport barrier in JET discharges with 'optimised shear' [19] may have a common physical explanation.

Bibliography

[1] J.A. Wesson, Tokamaks, Clarendon press, Oxford, (1997) 12-13

[2] X. Garbet *et al*, Nucl.Fusion **32** (1992) 2147-2155

[3] E.E. Simmet *et al*, Plasma Phys. Control. Fusion **38** (1996) 689-704

[4] F. Alladio *et al*, Plasma Phys. Control. Fusion Research **1** (1991) 153

[5] G. Becker, Nucl.Fusion **30** (1990) 2285-2193

[6] M. Kaufmann *et al*, Nucl.Fusion **28** (1988) 827-848

[7] M. Greenwald *et al*, Phys.Rev.Lett. **53**, (1984) 352

[8] M. Bessenrodt *et al*, Nucl. Fusion **31**, (1991) 155

[9] F. Romanelli *et al*, Nucl. Fusion **26**, (1986) 1515

[10] Y.C. Lee *et al*, Phys. Fluids **30**, (1987) 1331

[11] G.M.D. Hogeweij *et al*, Phys.Rev.Lett. **76** (1996) 632

[12] T.C. Luce, C.C. Petty and J.C.M. de Haas, Phys.Rev.Lett. **68** (1991) 52

[13] R.M. Meulenbroeks *et al*, 'Steady state off-axis sawtoothing near $q = 3/2$, 2, and 3 in a Tokamak,'submitted to Phys.Rev.Lett

[14] Z. Chang *et al*, Phys.Rev.Lett. **77**, (1996) 3553

[15] M.R. de Baar *et al*, Phys.Rev.Lett. **78** (1997) 4573

[16] P. Smeulders *et al*, Nucl.Fusion **35**, (1995) 225-242

[17] N.J. Lopes Cardozo *et al*, Plasma Phys. Control. Fusion **39** (1997) B303-B316

[18] Y. Koide *et al*, Phys.Rev.Lett. **72**, (1994) 3662

[19] A.C.C. Sips *et al*, Plasma Phys. Control. Fusion **40** (1998) 647-652

[20] R.E. Bell *et al*, Plasma Phys. Control. Fusion **40** (1998) 609-613

6.2 Layered χ_e-structure and the bifurcated Ohmic states

In the chapters 4 and 5, for off-axis heated RTP-discharges, it is shown that the critical dependence of the state of the discharges can be interpreted in terms of a model for the heat diffusivity featuring thermal transport barriers near simple rational values of q. Is such model also applicable for Ohmic discharges? Low duty cycle, low power modulation experiments to marginally perturb the sawtoothing Ohmic plasma proved the existence of a region of low heat diffusivity in the vicinity of $q = 1$ [1]. Also the data presented in Sec. 6.1 clearly suggests q-dependent inhomogeneities of the heat diffusivity: the fast relaxations that only occur in state I discharges (see Sec. 6.1) are followed by a direct increase of the reheat-rate. We will now discuss if the transport barriers as they were described in Chap. 5 can cause the distinct Ohmic states.

We first note that the barrier-model cannot be tested sensibly at data of Ohmic discharges. In contrast to the $\chi(q)$ for EC-heated discharges (where 7 levels for $T_e(0)$ were available) we now have only one level and no robust fitting procedure can be done. The model cannot be applied without any modification. As is well known, the global energy confinement is better in Ohmic discharges than in those with additional heating. This power degradation of confinement is not included in the model as we have not established the dependence of the barriers on plasma parameters. Application of the model as it was given in Chap. 5 leads to too low T_e-profiles in Ohmic discharges. Naturally, it is possible to fit the data of Ohmic discharges with the model, but the solution is not unique. We can however assume that the model also applies for the Ohmic phase of the discharge with barriers (of unknown strength) at the same position in terms of q and discuss the data on basis of more general qualities of the model.

The measurements presented in Sec. 6.1 indicate the following sequence of events in the evolution of the post-ECH discharge:

- The ECH is switched-off, while $q_{min} \approx 3$.

- Directly after switch-off, the off-axis maxima in T_e vanish. The T_e and j-profiles tend to peak.

- Saturation of the profile peaking occurs when 1) the j and T_e-profiles are consistent and 2) the heat flux and other losses are compensated by Ohmic dissipation.

In a system with a layered χ_e-structure, it is clear that in principle, distinct solutions may exist: If the saturation occurs before barrier related

q-values exist in the center of the plasma, relatively flat T_e and j-profiles are obtained. If however, in the process of relaxation, central barrier related q-values are touched, barriers form and the saturation can only occur for T_e and j-profiles that are more peaked. The peaked T_e-profiles (state-I) can be associated with the barrier in the vicinity of $q \approx 1$, while the flat T_e-profile (state-II) in the post-ECH phase of the discharges has $q(0) > 3/2$, i.e. lacks the barriers normally present near $q = 1, 4/3$, and $3/2$.

In the present model, the particle transport is not treated. This must clearly be included in later versions, since the density profiles observed in state I and II show very distinct differences. However, it is important to note that the steep ∇n_e-region near $\rho = 0.38$ which is characteristic for state II, develops only slowly, on the time scale of several current diffusion times.

The experimental data suggests that transition from state-II to state-I is dependent on subtleties is the q-profile. Qualitatively, it appears that q-dependent inhomogeneities in the heat diffusivity may explain the behaviour of the relaxing post-ECH discharges. An important experimental observation is the occurence of two MHD instabilities when a discharges makes the transition from state II to state I. The first instability is localised off-axis and has a $m = 2$ precursor. This points to an off-axis minimum in q reachin $q = 2$ as the probable cause. During this instability, the steep ∇n_e-region that had already formed near $\rho = 0.38$ is lost. This event could be the cause of the bifurcation in the framework of the barrier model. First it must be noted that in the state II, the q-profile, is very flat out to $\rho = 0.4$ and close to 2. The experimental accuracy is insufficient to determine whether it is just above or under 2. Given the observation that an $m = 2$ instability is the trigger for a further evolution to state I, we hypothesize that the state II q-profile is just above 2. If $q = 2$ is touched, the MHD event occurs, which leads to a slight peaking of the j-profile, primarily through the loss of the steep ∇n_e region and the associated bootstrap current. Thus a low shear region with q just below 2 is created, which according to the model provides a strong transport barrier. As a result, the T_e-profile peaks and the discharge evolves to state I.

We stress again that quanitative analysis is premature at the moment: We lack a determination of the values $\chi(q)$ in the Ohmic state and we lack modelling of the MHD-events.

Bibliography

[1] P. Galli *et al.*, Proc. 10th Joint workshop on Electron Cyclotron Emission and Electron Cyclotron Reasonance Heating (EC-10), Ameland, The Netherlands (1997), 379

Chapter 7

Active barrier manipulation

7.1 Strategies for barrier manipulation

In the previous chapters, it has been put forward that electron thermal conductivity in RTP is governed by the q-profile. Alternating regions of good and bad confinement have been associated with specific values in the q-profile. By changing $q(\rho)$, $\chi_e(\rho)$ is affected. Can, by q-profile control, the electron thermal confinement be improved or not? We note that changes of confinement due to modification/manipulation of the q-profile, are best investigated by concentrating on the $q = 1$-barrier. This barrier has the lowest value for χ_e in our model, and with modest current drive facility, the q-profile is easiest to manipulate in the center. Therefore, we concentrate on strategies to widen the $q = 1$-barrier.

The barrier is characterised by its position ρ_{bar}, width in terms of q $w_{\mathrm{bar,q}}$ and its value for the heat diffusivity χ_{bar}. The width of the barrier in terms of ρ is given by:

$$w_{\mathrm{bar},\rho} = \frac{w_{\mathrm{bar,q}}}{q'(\rho_{\mathrm{bar}})},$$

in which $q'(\rho_{\mathrm{bar}})$ is the radial derivative of q evaluated in ρ_{bar}. The heat flux q_e varies as $1/\rho$ when the heat source is concentrated on axis. Assuming that χ_e is infinite outside the barrier region and that the n_e profile is flat,

$$q_e(\rho_{\mathrm{bar}}) = \frac{P_{\mathrm{ECH}}}{4\pi^2 \rho_{\mathrm{bar}} a R_0 n_e \chi_{\mathrm{bar}}}$$

$$T_e(0) = T_e^{\mathrm{foot}} + \frac{P_{\mathrm{ECH}} w_{\mathrm{bar},\rho}}{4\pi^2 a R_0 \rho_{\mathrm{bar}} n_e \chi_{\mathrm{bar}}}$$

$$\delta W_{\mathrm{Ee}} = \frac{3ak}{2} \frac{P_{\mathrm{ECH}} \rho_{\mathrm{bar}} w_{\mathrm{bar},\rho}}{\chi_{\mathrm{bar}}}$$

in which, P_{ECH} is the centrally deposited EC-power, δW_{Ee} is the extra energy that is confined inside the barrier region and T_e^{foot} is the value for T_e at the foot point of the barrier.

In principle, T_e-profile characteristics can be affected via all three parameters. First, steeper ∇T_e regions and higher values for $T_e(0)$ can be created by shifting the barrier towards the magnetic axis of the system. This may lead to higher values of $T_e(0)$ but not necessarily to higher values of δW_{Ee}: depending on the local magnetic shear, δW_{Ee} can increase or decrease. To get a grip on the problem, we assume a parabolic q-profile, $q(\rho) = (q_0 - q_a)(1 - \rho^2) + q_a$, in which q_0 is the central value for q, and q_a is the edge value of q, and we assume that the position of the barrier (near $q = 1$) is given by $\rho_{\text{bar}} = 1/q_a$. Consequently, the shear in the $q = 1$ region is

$$q'(\rho_{\text{bar}}) = 2(1 - q_0/q_a),$$

and

$$\delta W_{\text{Ee}} = \frac{3ak}{4} \frac{P_{\text{ECH}} \rho_{\text{bar}} w_{\text{bar,q}}}{(1 - q_0/q_a)\chi_{\text{bar}}} .$$

The influence of electron cyclotron current drive (ECCD) on the position of the barrier near $q = 1$ has already been mentioned in chapter 5. Second, increasing w_{bar} leads to extended regions of steep ∇T_e. This leads to higher values for $T_e(0)$ and δW_{Ee}. Third, further reduction of χ_{bar} would yield steeper ∇T_e. This leads to higher values for $T_e(0)$ and δW_{Ee}. The values for χ_{bar} used in the model are still well above neo-classical estimates, and further reductions might be possible.

7.2 Barrier manipulation with electron cyclotron current drive

The model suggests the following strategy: modify the current-density profile such that a low magnetic shear region is formed in the vicinity of $q = 1$. We now report on experiments, in which it was tried to create low shear regions, and we discuss the effect on the barrier and the electron thermal confinement. j-profile modification can in principle be achieved with ECCD. In RTP, the launcher for the 110 GHz gyrotron has a tiltable mirror. Depending on the settings of the mirror, the system can be used for heating ($\alpha = 0$), ECCD in the direction of the inductively driven current (co-drive, $\alpha > 0$) or ECCD in the direction opposite to the inductively driven current (counter-drive, $\alpha < 0$). Here, α is an engineering parameter describing the tilt angle of the toroidal mirror. In [1] it was reported that maximum current drive efficiency was achieved for $\alpha = 6°$.
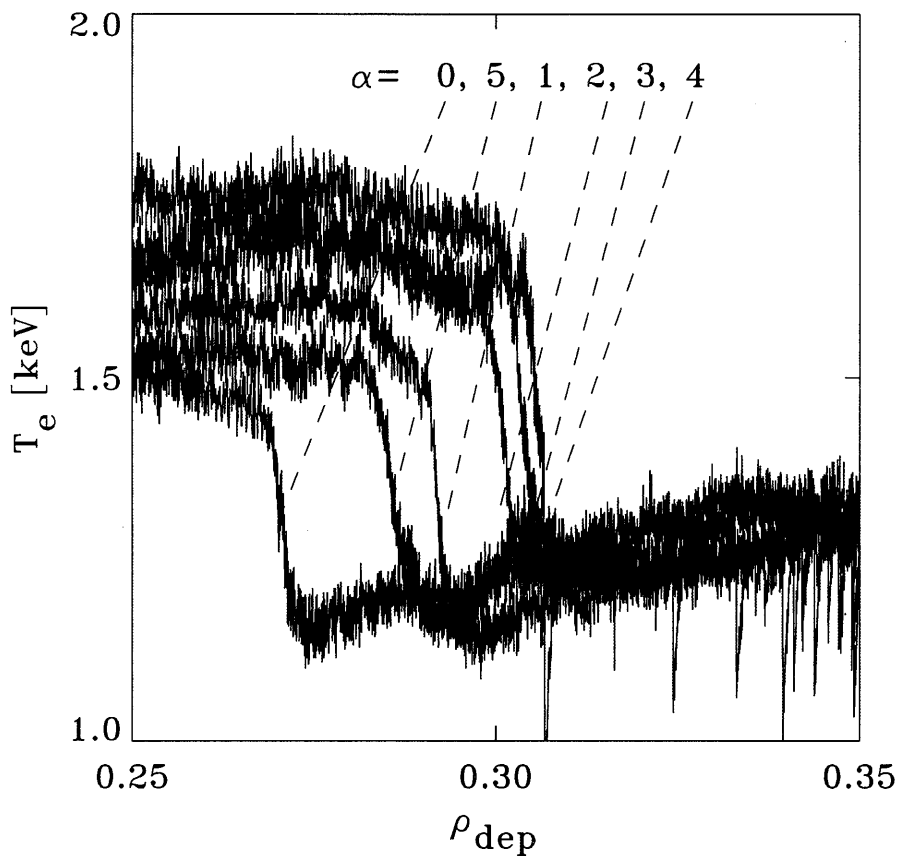
Figure 7.1: $T_e(0, t)$ *for discharges in which* ρ_{dep} *was swept through the plasma by ramping* B_ϕ. *The discharges feature very similar parameters* ($\bar{n}_e = 2.7 \cdot 10^{19} \, \text{m}^{-3}$ $Z_{\text{eff}} \approx 2$); α *and with that, the current drive efficiency were varied from shot to shot. The spontaneous transitions occur with increasing* ρ_{dep} *for* $\alpha = 0°, 5°, 1°, 2°, 3°$ *and* $4°$. *With increasing* α *(up to* $\alpha = 4°$) $T_e(0)$ *increases.*

7.2.1 Dynamic ρ_{dep}-scans

Dynamic ρ_{dep}-scans (see Chap.5) are experiments in which ρ_{dep} is ramped, within one discharge, by ramping B_ϕ. For these experiments, ρ_{dep} was ramped from 0.2 to 0.6 in $\sim 200\,\mathrm{ms}$. Figure 7.1 shows traces of $T_e(0,t)$ in dynamic scans of ρ_{dep}. The measurements were carried out in discharges with $I_p = 80\,\mathrm{kA}$, $\bar{n}_e = 2.7 \cdot 10^{19}\,\mathrm{m}^{-3}$ and $Z_{\mathrm{eff}} \approx 2$. By changing α from shot to shot from $-3°$ to $+5°$, the current drive efficiency was changed. Just as in the dynamic scan with $\alpha = 0°$ (see Chap.5), transitions occur in electron thermal confinement. It is observed that:

- The maximum value of $T_e(0)$ is reached for $\alpha = 4°$.

- The value of ρ_{dep} at which the first transition occurs, $\rho_{\mathrm{dep,crit}}$, is largest for $\alpha = 4°$.

After the first transition, the differences between the discharges become less apparent or disappear. $n_e(0)$ varies $< 4\%$ between the $\alpha = 0°$ and $\alpha = 4°$ case, while $T_e(0)$ varies 15 %. Consequently, $p_e(0)$ was increased by 10 % with co-drive, and we can conclude that with ECCD, τ_{Ee} of the tokamak plasma can transiently be influenced. An optimum setting for these experiments was $\alpha = 4°$.

We know from previous experiments (see chapter 5) that the transitions come about through the loss of a barrier. The dependency of $\rho_{\mathrm{dep,crit}}$ on α indicates that the differences between the various time traces are due to a difference in barrier conditions. Is the variation of T_e with α due to manipulation of barriers? For an answer, comparison of the T_e-profiles for the various α just before the first transition should be carried out. We know from previous measurements that the barriers can be as thin as 1 ECE-channel, and the resolution of the RTP system for Thomson scattering is an absolute requirement to indicate the difference in width of the barriers. Such Thomson scattering data is not available for the dynamic ρ_{dep}-scans. However, the measurements obtained with the radiometer can be discussed in terms of the model. First, we note that the dependence of $\rho_{\mathrm{dep,crit}}$ on α indicates that for $\alpha = 4$ ρ_{bar} achieves its maximum. If w_{bar} was constant with α, $T_e(0)$ would have decreased. We observe a maximum of $T_e(0)$ for $\alpha = 4$, which indicates that also w_{bar} increased. Not only $T_e(0)$ increased, but also the confinement has improved for these discharges with co-ECCD at $\alpha = 4$.

The above-presented data indicate a transient improvement of electron thermal confinement in dynamic ρ_{dep}-scans with co-drive. As a next step,

we will try to achieve steady-state improved confinement in static ρ_{dep}-scans. Two scenarios are tried: First we report on the static analogon of the dynamic scans: 80 kA discharges with co and counter current drive. Second, in discharges with I_{p} between 90 and 110 kA with counter ECCD, we try to increase the width of the barrier near $q = 1$, by trying to create a low shear region around it.

7.2.2 Static scan at 80 kA with co and counter current drive

In Fig. 7.2 the results of static ρ_{dep} experiments with $\alpha = -4°$ ($\square$), $\alpha = 0°$ ($\circ$), $\alpha = 1°$ ($\triangle$) and $\alpha = 3°$ ($\bullet$) are presented. The conditions were $I_{\mathrm{p}} = 80\,\mathrm{kA}$, $\bar{n}_e = 2.7 \cdot 10^{19}\,\mathrm{m}^{-3}$ and $Z_{\mathrm{eff}} \approx 2$. The positive influence of ECCD on $T_e(0)$ is **not** observed: Although the data sets are too limited to properly resolve the first transition, we can conclude that maximum values for $T_e(0)$ and ρ_{crit} are reached for $\alpha = 0$.

7.2.3 Central counter drive at 90, 95, 100, 105 and 110 kA

From the discussion on active barrier manipulation in relation to the model, it is clear that reduction of the magnetic shear in the vicinity of $q = 1$ is a strategy to achieve good confinement. In principle, such a low shear region can be created in high I_{p} (that is: sawtoothing) discharges with central counter current drive. The merits of this approach are evident. If successful, the strongest barrier in the plasma can be made thicker, while the power deposition is central.

We tried a series of discharges where both the plasma current and α were varied. The line average density was kept constant in the range $\bar{n}_e$ between $1.5 \cdot 10^{19}\,\mathrm{m}^{-3}$ and $1.7 \cdot 10^{19}\,\mathrm{m}^{-3}$. In the data base B_{ϕ} varies between 1.920 T and 1.954 T.

The discharges presented here are different from the ones presented earlier (see Chapters 4,5 and 6). First, $\alpha \neq 0$. Second, to make the laser beam path of the Thomson sattering pass as close as possible to the magnetic axis, the plasma column was shifted inward by 1 cm or $\Delta\rho \sim 0.06$. Consequently, the relation between B_{ϕ} and ρ_{dep} is different from the one derived in chapter 5. Finally, I_{p} is higher than in previous conditions while n_e is 50% lower. As will be shown below, the T_e-profiles are quite different than those presented before.

For marginally different discharge parameters, $T_e(0)$ varied between 1.8 keV ($\alpha = -3.5°$, $\bar{n}_e = 1.7 \cdot 10^{19}\,\mathrm{m}^{-3}$, $B_{\phi} = 1.945$ T and $I_{\mathrm{p}} = 89.9$) and 3.1 keV ($\alpha = -3.0°$, $\bar{n}_e = 1.7 \cdot 10^{19}\,\mathrm{m}^{-3}$, $B_{\phi} = 1.938$ T and $I_{\mathrm{p}} = 89.2\,\mathrm{kA}$). This
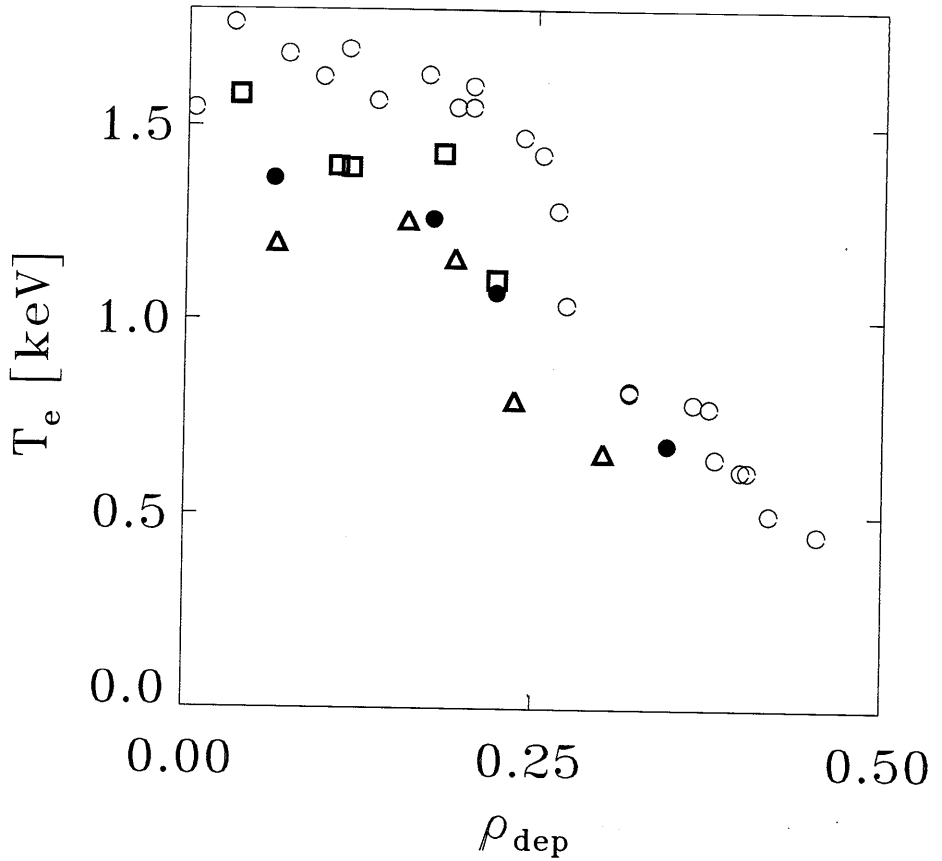
Figure 7.2: *Static scan for $\alpha = -4^\circ$ ($\square$), $\alpha = 0^\circ$ ($\circ$), $\alpha = 1^\circ$ ($\triangle$) and $\alpha = 3^\circ$ ($\bullet$). The first transition is evident in the data. Contrary to the dynamic scan, highest values for $T_e(0)$ and $\rho_{dep,crit}$ are obtained with $\alpha = 0^\circ$.*
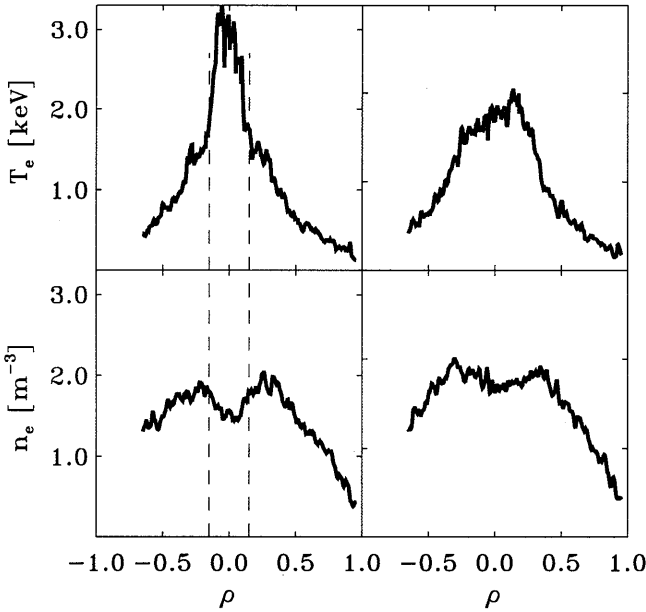
Figure 7.3: *Profiles for T_e and n_e for $I_p = 90\,kA$ and $\alpha = -3°$ and $-3.5°$. The difference between the hot (a) and cold (b) discharge comes about through a narrow hot region enclosed by steep gradients in T_e, which is present in a) and absent in b). Interestingly, the density profile for the hot discharges features a dip, bordered by steep gradients. As indicated in the figure, the steep gradients in T_e and n_e are very well aligned.*

large difference is due to a narrow region of high T_e in the latter discharge. Due to the small volume of the hot core, the changes in $T_e(0)$ are hardly reflected in τ_{Ee}.

Is the variation of 80 % in $T_e(0)$ due to barrier manipulation? In Fig. 7.3 we show the T_e and n_e-profiles for the 3.1 (a) and 1.8 (b) keV cases with $I_p \approx 90\,kA$ and $\alpha = -3°$ and $-3.5°$. It can be seen that the variation of T_e comes about through the central column which in 'the hot case' is relatively well confined, and the barrier region is again easily identified.

As an estimate for the local quality of confinement, we assume that all EC-power is deposited within the hot via power balance analysis the heat diffusivity in the barrier ($\chi_{e,pb}$) from a power balance analysis. The result is $\chi_{e,pb}^{bar} \approx 0.8\,m^2/s$, for 'the hot case.' This value for χ_e^{pb} agrees well with the values for the heat diffusivity in the model of Sec. 5.5.1 and is well above neo-classical estimates for χ_e. $\chi_{e,pb}^{bar}$ is an over-estimate of the heat diffusivity for two reasons. First, the radial dimensions of the hot core

region and the power deposition localisation are similar, and a slight miss-alignment of the power deposition and the barrier region leads to power deposition outside the barrier. Second, a striking feature for the density profile under counter drive is the inversion of ∇n_e in the hot core. A region of steep ∇n_e is formed, which region coincides with the steep ∇T_e region (see Fig 7.3). In steady-state, the net particle flux $\Gamma_{tot} = 0$. This means that in the region of ∇n_e-reversal an *outward* particle convection compensates the *inward* particle diffusion. With the particle convection, a heat sink is associated in the centre, and only part of the deposited power is transported via heat diffusion.

The aim of the experiments was the creation of a low shear region in the vicinity of $q = 1$. Did we succeed? Interestingly, the discharges in which the narrow central T_e-peak is observed, do show sawtooth like relaxations of the T_e-profile. Figure 7.4 shows $T_e(\rho)$ for a discharge just after (A) and before (B) a sawtooth collapse. Clearly during the relaxation, the barrier region remains unaffected, and the relaxation occurs off-axis. This indicates that we were not able to create the desired q-profile: It appears that, instead of low shear, we created a region of shear reversal (see Fig. 7.5). A candidate mechanism for the MHD-relaxation is the formation of two $q = 1$ surfaces that reconnect via a double tearing mode.

7.2.4 Position of barrier in terms of q

From Thomson scattering measurements of T_e just before and just after the normal sawtooth collapse, we inferred that the thermal transport barrier is located marginally above $q = 1$ (see Chap. 5). This observation is now corroborated by the off-axis MHD activity reported here. The MHD-activity indicates that we achieved negative central shear, with $q_{min} < 1$ outside the barrier region. During the proces of reconnection, the barrier region is unaffected, while a flat T_e-region forms in between the two $q = 1$ surfaces. The foot point of the barrier is located at the border of the flat T_e-region, and is located marginally above $q = 1$. It is interesting to note that the same analysis applies to the steep ∇T_e-regions outside of the flat T_e-region.

7.2.5 Conclusions ECCD experiments

In conclusion, we have shown that with ECCD, transiently, the q-profile can be manipulated such that the local electron thermal confinement is improved. In dynamic ρ_{dep}-scans with current co-drive ($\alpha = 4°$), the high-
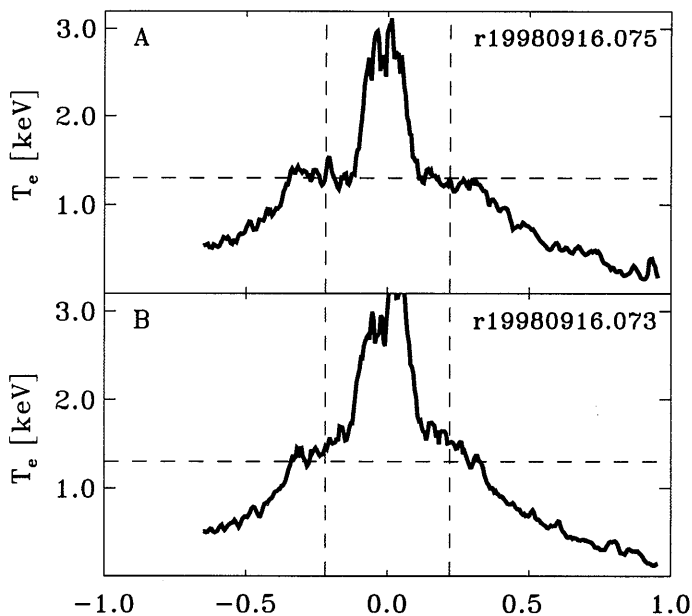
Figure 7.4: T_e-profiles just after (a) and before (b) the MHD-relaxation of high I_p-discharges under counter-drive. Note that the core is hardly affected by the relaxation (the gradients persist), and that the relaxation occurs off-axis. The foot point of the barrier is exactly at the edge of the zone that is affected·by the MHD-event. In addition to the barrier near $\rho = 0.15$, steep ∇T_e-regions form near $\rho = 0.35$, and also this barrier forms at the edge of the zone that is affected by the MHD-event. The vertical dashed lines indicate the inversion radius according to ECE, consistent with the presented Thomson scattering profiles. The dashed horizontal line is to guide the eye and indicates the decrease of T_e during the MHD-event.

Figure 7.5: Cartoon showing the q-profiles for 1) the state without ECCD (left panel) 2) the desired state and 3) the state we achieved (right panel). The range of q in which the barrier predicts a low χ_e-value is indicated by the bar at $q = 1$.

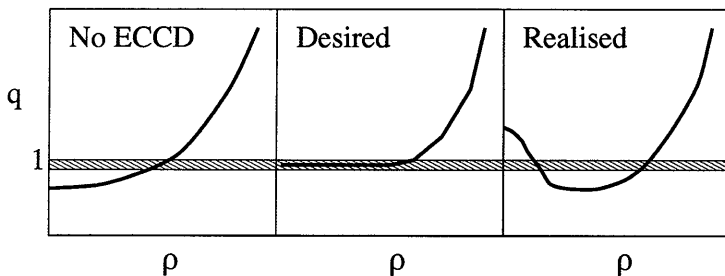est values for $T_e(0)$ and $\rho_{dep,crit}$ were measured. Although no detailed information on the profile shapes is available, the combination of these two observations indicate that the barrier is both shifted outward and widened, effectively increasing τ_{Ee}.

Different results are obtained in steady-state ρ_{dep}-scans. Here, the highest values for $T_e(0)$ and $\rho_{dep,crit}$ were measured for $\alpha = 0$. It appears that the q-profiles that are good for confinement are only accessible during transients. It has also been tried to flatten the q-profile around $q = 1$ in the central region of sawtoothing plasmas with counter ECCD. The measured T_e-profiles and MHD-activity are consistent with shear reversal and an off-axis minimum $q_{min} < 1$. Two $q = 1$ barriers are evident in the T_e-profiles, and their position in terms of ρ is consistent with a localisation in terms of q marginally above $q = 1$. Although for these discharges very hot central plasma columns have been measured, the high temperatures are neither due to barrier-widening nor to χ_e-decrease. The high $T_e(0)$-values for these discharges are due to the position of the innermost barrier very close to the axis, giving rise to high values for the heat flux, and consequently very steep ∇T_e-regions.

7.3 Pellet induced 'non-local' effect with off-axis ECH

One of the most surprising observations in Tokamak physics is the so-called non-local effect [2, 3]. By oblique pellet injection or laser blow-off experiments, the edge region the plasma is cooled. Interestingly, the core plasma often shows a reaction of opposite polarity to the edge-cooling: $T_e(0)$ increases, often on time scales an order of magnitude faster than the heat diffusion time scale. The word non-local stems from the fact that, if the increased $T_e(0)$ is due to a reduction of χ_e, this reduction occurs in the absence of changes of the local thermodynamic variables.

In RTP the non-local effect has been induced by means of oblique pellet injection over a wide range of plasma parameters, both in ohmic and in on- and off-axis EC heated plasmas [4, 5, 6]. The results can be summarized as follows (see [6]). Analysis of Thomson scattering T_e profiles after oblique pellet injection shows that the rise of the core T_e is mainly due to a steepening of the T_e profile in the region where $q < 1 < 2$; moreover, this region moves outward. The outward movement of the $q = 1$ surface is confirmed by the observation of ECE time traces crossing the inversion radius (r_{inv}). Transient local transport properties have been probed by applying modulated ECH with different values of ρ_{dep}. An example with

$\rho_{\text{dep}} = 0.15$ is shown in Fig. 7.6. A transient reduction of the amplitude of the heat pulse is observed in for central channel and for the channel at $\rho = 0.45$. Apparently, thermal transport is temporarily reduced inside the channel at $\rho = 0.14$ and between the channels at $\rho = 0.29$ and 0.45. These two regions correspond to the radius of the $q = 1$ and $q = 2$ surface, respectively. From this it can be concluded that the non-local core T_e rise is due to a transient strenghtening of the (pre-existing) transport barriers near $q = 1$ and $q = 2$. The observation of expanding r_{inv}, i.e. rapid current rearrangement, leads to the conjecture that this strenghtening may be due to a reduction of the magnetic shear, in line with the transport model precented in Ch.5.

The conjecture sketched above was further tested in experiments in which ECH was applied slightly off-axis, with ρ_{dep} just inside $\rho(q = 1)$. In this way the magnetic shear was reduced before the pellet was injected. Record values of the rise $\delta T_e(0)$ of nearly 100 % and record values of $\beta + l_{\text{i}}/2$ have been obtained in this way; see Fig. 7.7. When in a series of discharges $\rho(q = 1)$ was scanned by changing I_p and ρ_{dep} was adapted such that it was always just inside $\rho(q = 1)$, the region of positive δT_e was observed to increase with $\rho(q = 1)$, up to nearly half the plasma column. This hot core with large and rather uniform δT_e is separated from the cold outer plasma by a very sharp gradient region just outside $q = 1$.

As for the dynamic ρ_{dep} scan with co current drive, the improved confinement is transient: the effect disappears in 10 ms, approximately 2 energy confinement times and < 1 current diffusion time.

7.4   Barrier manipulation and self organisation

We observed that in transients, electron thermal confinement can significantly be improved, but that in steady state the effects are less impressive. Apparently, in time dependent situations, q-profiles can be formed that are beneficial for the confinement properties of the plasma, while relaxation processes undo the beneficial q-profiles.

To investigate what mechanisms play a role, we carried out model calculations (see chapter 5), in which the effects of a non-inductively driven component of the current are evaluated. We present 4 typical steady-state q-profiles. We start with a 90 kA plasma, with a q=1 surfaces, and we will try to improve the electron thermal confinement. Therefore, we try to widen the barrier near $q = 1$. We flatten the magnetic shear in the central region of the plasma by tuning the non-inductive counter driven current.
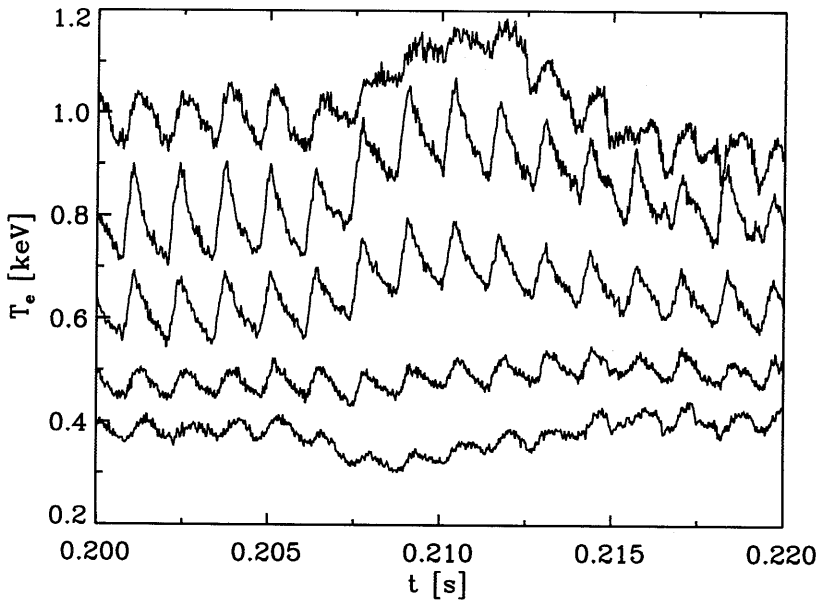
Figure 7.6: Time traces of T_e *during oblique pellet injection, in a discharge where modulated ECH was applied, with deposition at* $\rho_{dep} = 0.15$. *The time traces shown are at* $\rho = 0, 0.14, 0.29, 0.45$ *and* 0.61. *The pellet enters the plasma at* $t = 205.5$ *ms.*
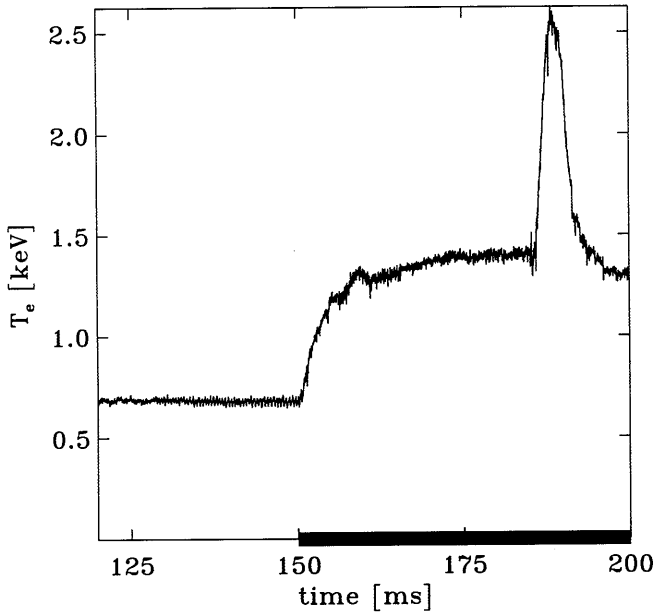
Figure 7.7: $T_e(0, t)$ *for the non-local effect, enhanced by off-axis ECH (*$q_a =$ *4.8,* $\bar{n}_e = 1.4 \cdot 10^{19}\,\mathrm{m}^{-3}$*). Off-axis ECH is applied (indicated with the bar) to reduce the magnetic shear in the core of the plasma. The injection of pellet (*$t = 185\,\mathrm{ms}$*) is associated with a strong increase of* $T_e(0)$*. Record values for* $\beta + l_i/2$ *are achieved transiently.*

We find steady-state conditions (90 kA discharge, with 7 kA counter drive) in which a wide flat shear region forms just under barrier relevant q-values (see Fig. 7.8a). By a slight decrease of the driven current to 5 kA, we try to push the low shear region into the range of barrier related q-values by increasing $q_{min}$. (Fig. 7.8b). Still, in steady-state, the low shear region forms at values just below the barrier-related q-values. By fine tuning I_p, we now try to force the low shear region into the barrier related q-values by increasing q_{min}: we decrease I_p to 85 kA and use 7 kA (Fig. 7.8c) and 5 kA (Fig. 7.8d) counter drive. Irrespective of the settings of the total current and the amount of counter driven current, in steady-state, the low shear region forms just outside the barrier-related q-values.

What is going on? In ECCD experiments and simulations, the current density is composed of a non-inductive and an inductive component $j = j_i + j_{ni}$. $T_e(\rho)$ and $j_i(\rho)$ are coupled via the resistivity. Initially we are able to create a wide barrier. Consequently, $T_e(0)$ increases. Due to the extra peaking of $T_e(0)$ the inductively driven current diffuses inward, decreasing $q(\rho)$ in the region $0 < \rho < \rho_{bar}$. This mechanism expels the low shear region to q-values outside the barrier-relevant q-values. The relaxation processes are due to the diffusion of $j_i(\rho)$. This interpretation is consistent with the observation that experimentally, transiently, significant improvements of the electron thermal confinement can be achieved.

The presented cases clearly indicate that the tokamak plasma with q-related barriers has means to undo improved electron confinement. This self organisation comes about through the coupling between j_i, q, χ_e and T_e. In order to achieve steady-state electron confinement improvement, this coupling has to be broken. This calls for discharges in which a large fraction of the total current is driven non-inductively [7, 8].
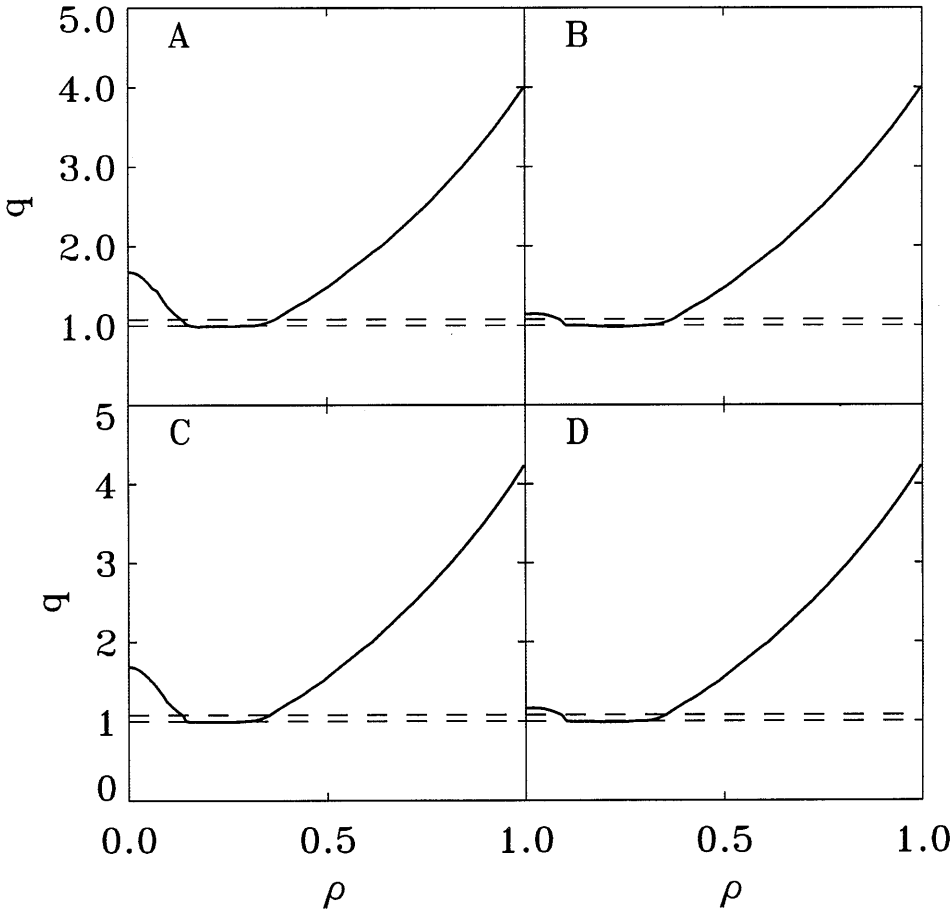
Figure 7.8: *Four simulated efforts to manipulate q to widen barriers and improve the electron thermal confinement. A: $I_\mathrm{p} = 90\,kA$, with 7 kA central counter drive. We were able to create a low shear region just below the barrier relevant q-values. B: $I_\mathrm{p} = 90\,kA$, with 5 kA central counter drive, to reach slightly higher values for q_min. The low shear region is not positioned better though. C: I_p to 85 kA with 7 kA counter drive. We decrease I_p to shift the q-profile to higher values. We observe no improvement. C: Now, we decrease the ammount of counter driven current for the same purpose. The low shear region remains fixed just below the barrier relevant q-values.*
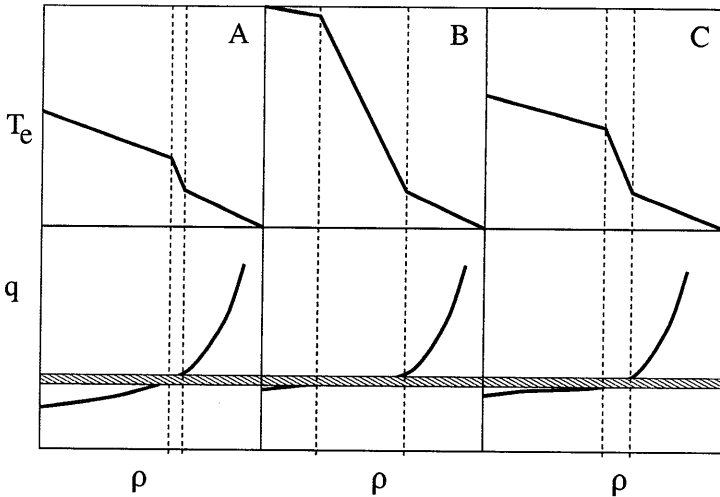
Figure 7.9: *Cartoon to elucidate the transient improvement of the thermal confinement, undone in steady-state by plasma self-organisation. Barrier relevant q-values are indicated by the bar. A: The 'normal' T_e and q-profiles. B: With non-inductive counter current drive, a low shear region is formed in the barrier relevant q-values. In the T_e-profile steep gradients are apparent over a wide range in ρ. High values for $T_e(0)$ are achieved, and the confinement is improved over the 'normal' situation. C: In reaction to the high core T_e-values, the inductive component of the current diffuses inward. q_{min} decreases such that the low shear region is expelled from the range in q-values that are associated with barriers and the confinement improvement is undone.*

Bibliography

[1] E. Westerhof *et al.*, 'Results on electron cyclotron current drive in RTP', 25th EPS conference on controlled fusion and plasma physics, Prague, Czech Republic (1998)

[2] M.W. Kissick *et al*, Nucl. Fusion **36**, (1996) 1691

[3] K.W. Gentle *et al*, Phys.Rev.Lett. **74** (1995) 3620

[4] P. Mantica *et al*, 24th EPS conference on controlled fusion and plasma physics, Berchtesgaden, Germany (1997) 1853

[5] P. Galli *et al*, 'Non-local electron heat transport effects probed by modulated ECH in the RTP tokamak', 25th EPS conference on controlled fusion and plasma physics, Prague, Czech Republic (1998)

[6] P. Mantica *et al*, submitted to Phys.Rev.Lett. (1998)

[7] A. Ekedahl *et al*, Nucl. Fusion **38**, (1998) 1397

[8] X. Litaudon *et al*, Plasma Phys Control. Fusion **38** (1996) 1603

Chapter 8

Evaluation and Discussion

This thesis is about thermal transport barriers in the electron channel in tokamak plasmas. We tried to answer the following questions: 1) if such transport barriers exist, and if they do, 2) in which conditions they occur, and on which parameters they depend and 3) how they can be influenced.

Our answers are:

- Yes, thermal transport barriers for the electrons do exist in tokamak plasmas.

- They depend on the magnetic winding number and have been observed in the RTP plasma in the vicinity of $q = 1$, $4/3$, $3/2$, 2, $5/2$ and 3.

- We have not yet established the dependence on other plasma parameters, such as density, temperature or magnetic field strength.

- The position of barriers can be influenced by means of current drive; we have no indication that the strength of the barriers can be manipulated other than by making them wider by reducing the local magnetic shear.

- A transient improvement of electron energy confinement can be achieved creating a low shear region near a barrier.

- Steady-state improvement of the electron energy confinement has not been observed.

- Model calculations indicate that for steady-state improvements of the electron confinement, dominance of the non-inductive component of the current over the inductive component is required.

Below, we summarize the main experimental findings of chapters 4, 5, 6 and 7 of this thesis, discuss unresolved issues and suggest future research.

8.1 Summary of experimental findings

The main experimental findings can be summerized as follows:

1. Both in the Ohmic and EC-heated plasma, barriers in the electron channel have been demonstrated. These barriers exist in the plasma in the vicinity of low order rational numbers in the q-profile. In EC-heated discharges, barriers near $q = 1$, $4/3$, $3/2$, 2, $5/2$ and 3 have been observed. With dominant off-axis ECH, hollow T_e profiles and corresponding inverted q-profiles can be created, of which the minimum q-value can be selected by tuning ρ_{dep} . Thus, the barriers can be peeled off one by one, giving rise to the sharp transitions in the ρ_{dep}-scans presented in chapters 4 and 5.

2. The fact that the barriers are associated with specific values of q gives rise to a non-linear coupling between the profiles of T_e, j, q and χ_e. Model calculations show that this non-linearity is responsible for many of the striking observations. We mention the sharpness of the transitions in the ρ_{dep}-scan, which occur for a variation in ρ_{dep} that corresponds to ~ 1 mm and is much sharper than the radial localisation of the ECH-deposition. Also the 'ears' that form on the T_e-profiles for specific values of ρ_{dep} are due to the non-linearity in the system.

3. To improve the confinement in a system with $\chi_e(q)$ featuring transport barriers, a region of low magnetic shear should be created around a barrier. Transiently, confinement improvements have been achieved with electron cyclotron current drive (ECCD), but in steady-state the improvements have not been observed. Model calculations indicate that due to the non-linear coupling between $T_e(\rho)$, $j(\rho)$, $q(\rho)$ and $\chi_e(\rho)$, the low shear region is expelled from q-values that are associated with barriers. This indicates that in order to achieve an important, steady-state improvement of the electron thermal confinement the coupling must be undone. Consequently, a dominant non-inductive current drive has to be applied.

4. After switch-off of far off-axis ECH, two distinct Ohmic states develop. First, we mention the state with triangular profiles for n_e and T_e (state I), which is similar to the pre-ECH state of the plasma. Second, we observe a state with a much broader T_e-profile and an n_e-profile featuring a steep ∇n_e region. These states are at variance with current models for the Ohmic confinement based on ITG, ETG, DTIM or DTEM

modes. The presented data suggests that also the confinement of the Ohmic plasma depends critically on details in the q-profile.

8.2 Barrier strength in the $\chi_e(q)$-profile

8.2.1 Width of the barrier and the value of the χ_e in the barrier

In our model, the width of the barrier in terms of q, $w_{\mathrm{bar},q}$, and the value of the χ_e in the barrier χ_e^{bar} are defined. The actual strength of the barrier in the plasma is then determined by the local shear only. In principle, other combinations of χ_e and $w_{\mathrm{bar},q}$ can be used, because only the insulating strength $\sim w_{\mathrm{bar},q}/\chi_e^{\mathrm{bar}}$ of the barrier is determined from the fit (see Chap. 5). However, we note that the range in which the parameters can be varied is limited. The barriers must be narrow enough to leave room for the 'bad' regions, while too thin barriers yield 'ears' that are much more peaked than the ones that have been observed. A further lower boundary in $w_{\mathrm{bar},q}$ is the banana width. If a barrier (in terms of ρ) becomes as thin as the banana orbit, the concept transport barrier loses its physical meaning.

In view of the discussion on the possible range of the barrier width, $w_{\mathrm{bar},q}$ and χ_e^{bar} can be varied by a factor of two. The presented values for χ_e^{bar} are one order of magnitude higher than neo-classical value, and this difference is far outside the uncertainty boundaries. This indicates that in addition to the mechanism that is responsible for the layered structure, a second turbulent mechanism is active.

8.3 The barrier model

The barrier model presented in Chapter 5, in which the thermal diffusivity is a function of the safety factor q only, should be carefully evaluated. It is important to note that the model is of a mathematical nature, it does not contain any plasma physics. It was set up as an interpretative model. Once the barriers were observed, we realised that a classical power balance analysis as a means to quantify the thermal diffusivity made little sense. The model can be seen as an alternative to the power balance analysis, i.e. a means to evaluate the strength of the barriers instead of the radial profile of χ_e. The model does contain all information on the occurrence of the transport barriers we had from the experiment, in particular their relation to specific q-values. Having said this, we did find that the model performed rather better than could be expected, given its simple form, in which no true plasma physics plays a role. Not only did it fit the data of the static

ρ_{dep} scan, including the sharpness of the transitions, it also produced good matches of the 'ears' and other peculiarities of the temperature profiles, as well as doing a fair job on the dynamic ρ_{dep} scan. So, it is fair to ask: which known aspects of electron energy transport in tokamaks is predicted by the model, and which are not? We discuss two conspicuous dependences: the scaling of confinement with plasma current and with heating power.

8.3.1 Scaling of confinement with plasma current

The energy confinement in tokamaks with strong additional heating (so called L-mode scaling) shows a rather strong dependence on the plasma current I_{p}: $\tau_{\text{E}} \propto I_{\text{p}}^{0.5}$ to $\tau_{\text{E}} \propto I_{\text{p}}$. If all parameters in the barrier model are kept fixed, it does produce a similar I_{p} scaling (τ_{E} approximately proportional to I_{p}). This comes about since the barriers at the lowest q-values are the strongest, and they shift outward with increasing I_{p} and constant B_ϕ. At this moment, however, we do not know how the strength of the barriers as determined in the experiment varies with I_{p} and B_ϕ. Preliminary analysis of ρ_{dep} scans at various values of I_{p} indicates that the I_{p} dependence is weak. We have no experimental information on a possible B_ϕ dependence.

8.3.2 Degradation of confinement with heating power

It is a common observation in tokamaks with sufficient additional heating that the energy confinement decreases with increasing input power. The barrier model does not contain any ingredient that could produce such a dependence: this calls for the introduction of plasma physical considerations. For instance, if the transport barriers are interpreted as being the result of a slightly perturbed magnetic topology, the level of perturbation could be a global parameter. In the model, this single parameter should then control the width of all barriers. On the basis of the data presented in this thesis, nothing can be said about the influence of the heating power on the width of the transport barriers. However, this is a subject that could be accessed in future experiments.

8.4 Evaluation

In this thesis, we have presented experimental evidence for the presence of electron thermal transport barriers in tokamak plasmas. Two questions need to be addressed here: 1. Since the barriers are so thin that they are hardly detectable, is it necessary at all to consider them? and 2. Does the

discovery of the barriers make any difference for the future of fusion as an energy option.

The answer to the first question is that indeed, even if the barriers are not readily visible in the temperature profile, they have a strong impact on the interpretation of transport experiments in tokamaks. A transport analysis that does not resolve the barriers, yields a spatial average of χ_e. Unfortunately, this is the harmonic average, i.e. $< \chi_e^{-1} >^{-1}$, which is dominated by the regions where χ_e is lowest. This value is not only different from both the level of χ_e in the barriers and that in the conducting zones, it may also scale differently with plasma parameters. Thus, the scaling behaviour of χ_e as determined by a power balance analysis could be a strange mix of two other scalings, obscuring the physics. A comparison of this harmonic average of χ_e with a theoretical transport model is deemed to fail, which may explain the low success rate of such comparisons (see e.g. [1]). However, if we succeed in giving reliable estimates for the thermal transport in the 'good' and 'bad' regions, specific comparisons with theoretical models which do predict such regions can be undertaken.

Concerning the impact on the development of Fusion energy, our results will not influence ITER. ITER is designed as an L c.q. H-mode tokamak without dedicated targets to manipulate the electron thermal transport barriers. Morever, in ITER, the thermal fluxes via the ions are dominant over the fluxes via the electrons. Our results may, however, be of importance in view of advanced tokamak scenarios. In advanced tokamaks, the fluxes via the ions can be reduced to neo-classical estimates, and the fluxes via the electrons have become dominant. With the dominant non-inductive current drive and q-profile control that will be available, the control of transport barriers that form in the plasma in the vicinity of specific values of the q-profile is envisaged.

8.5 Future Research

8.5.1 The role of convection

In the presented experiments, an important role is played by particle and heat convection. We already mentioned:

- The outward heat convection in the region up to ρ_{dep} during off-axis ECH (Chap. 5).

- The inward particle convection in the region up to ρ_{dep} during off-axis ECH (Chap. 5).

- The steep ∇n_e region in state II Ohmic discharges (Chap. 6).

- The sharp hole in the n_e-profile which occurs when a combination of ECH and ECCD produces a very narrow hot region in the center of the plasma.

An example of a possible role of convection that was not mentioned in this text is the following: We tacitly interpreted the barriers as regions of low heat diffusivity in comparison to the ambient plasma. Heat pulse propagation analysis of modulated ECH in the plateaux suggests that, in addition to the low heat diffusivity, an inward heat convection is active in the barrier region [2].

All these examples suggest that, as a next step in the study of electron thermal transport, heat and particle convection should be taken into account. The reason that this is not already common practice is that it is very difficult to experimentally separate contributions of different nature to a net flux. However, perturbative transport studies in principle offer the possibility to carry out such an analysis.

8.5.2 Stepped $\chi_e(q)$ and big tokamaks

Strictly speaking, we have proven the existence of the stepped $\chi_e(q)$ for RTP only. RTP is one of the smallest tokamaks that is currently being operated, and the question whether our results are relevant for big tokamaks is valid. In Chap. 5 we argued that RTP-discharges are fitted equally good by the ITER L-mode scaling as discharges of bigger tokamaks, indicating that similar turbulent mechanisms are active in machines of different dimensions. We also mention that, except for the exotic post ECH state II Ohmic discharges, the phenomenology of Ohmic discharges (LOC at low values for n_e and saturation of τ_{Ee} at higher values) in RTP is consistent with that in bigger tokamaks.

We note that, although the majority of publications on barrier formation discuss $E \times B$ sheared velocity decorrelation of turbulence, other teams published data that could fit into our scheme. The transport barrier for the electrons and ions in JET optimised shear discharges forms only when the $q = 2$ surface is in the plasma [3]. TFTR published the 'type two' transition, [4] in which barriers in the electron and ion channel form when the decreasing minimum in q approaches 2. JT-60 [5] published the observation of a barrier around $q = 3$. DIII-D [6] presented the correlation between sudden changes in $\partial T_e / \partial t$ and low order rational values of the evolving minimum in of q.

These data suggest that also in big tokamaks, stepped $\chi_e(q)$ profiles influence the transport. This motivates the continuation of our experimental work in larger devices. In collaboration with our TEC partners, the Rijnhuizen team will carry out transport studies in the TEXTOR tokamak in Jülich, Germany. Systems for ECE-imaging, Thomson scattering, ECH and ECCD are currently being mounted on TEXTOR.

In view of the new facility scheme for JET, a collaboration is set up to study advanced scenarios of tokamak operation. One of the issues that will be tackled is the optimisation of the $\chi(\rho)$ profile by non-inductive current drive.

Finally, we mention other tokamaks, that have installed, or will install sufficient EC-heating capacity to carry out similar experiments as we discussed in the chapters 4,5,6 and 7 of this thesis. Collaboration is envisaged with the teams of TCV (Lausanne), FTU (Frascati), T-10 (Moscow), Compass (Culham) and Tore Supra (Cadarache).

Bibliography

[1]   J.W. Connor, Physicalia magazine **20** 2 (1998) 145

[2]   P. Mantica, private communications

[3]   A.C.C. Sips *et al*, Plasma Phys. Control. Fusion **40** (1998) 647-652

[4]   R.E. Bell *et al*, Plasma Phys. Control. Fusion **40** (1998) 609-613

[5]   Y. Koide *et al*, Phys.Rev.Lett. **72** (1994) 366

[6]   M.E. Austin *et al.*, U.S. transport task force workshop (1998)

Summary

One of the most important problems in fusion research remains the anomalous radial heat conductivity via electrons and ions in in toroidally shaped confinement systems. The electron heat conductivity χ_e exceeds neo-classical predictions up to two orders of magnitude. The ion heat conductivity χ_i exceeds neo-classical predictions up to one order of magnitude. If the problem of anomalous heat conductivity is not tackled, fusion reactors will be big, complicated and expensive.

Anomalous transport is driven by turbulent processes. In specific regions of the plasma turbulence can be quenched, leading to a local improvement of the transport coefficents. These regions are referred to as transport barriers. In the literature examples have been presented of thermonuclear plasmas in which, transiently, the ion heat conductivity decreased below neo-classical predictions. In this phase fluctuations, associated with electrostatic turbulence, decreased below the detection limit. The electrons remained anomalous and showed only a modest improvement of χ_e.

RTP is a small tokamak featuring high resolution diagnostics for electron temperature T_e and density n_e. RTP features a system for dominant Electron Cyclotron Heating (ECH). The power deposition can be localised to < 10 % of the minor radius. For the conditions in this thesis, for central power deposition, the ratio $P_{ECH}/P_\Omega \approx 7$ and 4 for deposition at half radius. These specifications make RTP well-suited for its research target: the study of anomalous heat conductivity via the electrons.

A radial scan of the ECH deposition, with steps of $< 1\%$ of the minor radius, reveals a discretised response of the electron temperature. The central electron temperature shows sharp transitions between plateaux as a function of the ECH deposition radius. The transitions occur for a displacement of the deposition by less than 1 mm, and are much sharper than the power deposition profile. The transitions are associated with the crossing of the minimum value of q through integer and half-integer numbers. The phenomenology can be modeled with a heat diffusivity profile featuring transport barriers near integer and half integer values of q. This model

reproduces salient details of the experimental data, such as the sharpness of the transitions and the formation of pronounced off-axis temperature maxima for power deposition on top of a barrier. It is pointed out that the topology of the magnetic field of a tokamak under slight perturbation naturally has characteristics similar to this model.

The discrete response of the plasma is sustained in the Post-ECRH regime: Bifurcated states of plasmas in the Linear Ohmic Confinement regime are reported. One state is the usual Ohmic state featuring triangular profiles for temperature and pressure (state I). The second (state II), newly discovered, state features a much broader temperature profile, while the density has a very pronounced gradient near half-radius. The bifurcated states form after off-axis electron cyclotron heating (ECH) is switched off. Both states are stable until the end of the discharge, i.e. for many energy confinement and a few current diffusion times. The evolution of the discharge depends critically on the occurrence of an instability, in case of which the discharge relaxes to the normal Ohmic state. It is argued that also the two states come about through the layered structure of the heat-diffusivity. Such structure naturally reproduces the bifurcation itself, the critical dependence on the minimal value of q and related, the plasmas response to the instability.

In RTP, the EC-power can be coupled into the plasma under different angles. This provides the possibility of non-inductive current drive. A distinction is made between co ($\alpha > 0$) and counter ($\alpha < 0$) drive. In view of the interpretation that the electron transport barriers are q-related, by means of ECCD it can be tried to manipulate the q-profile such that confinement improvements can be invoked. We report on three experiments. For so-called dynamic scans a clear improvement of the confinement is observed with non-inductively driven current.

An apparent paradox is that this improvement of confinement is not reflected in steady-state scans of the deposition radius. Finally, it was tried to exploit the strongest barrier, by creating a low shear region in the vicinity of $q = 1$ by means of counter drive in high I_p discharges. Although we obtained high central electron temperatures, also these experiments were unsuccesful: MHD-activity indicates that in stead of flat shear, we created a region of shear reversal.

Model calculations indicate that the paradox that no steady-state confinement improvement was forthcoming, is due to profile self-organisation: The inductively driven component of the current density profile is organised such that the desired flat shear regions are expelled from the barrier

relevant q-values. In discharges in which a large fraction of the current is driven non-iductively, the coupling is broken and steady state improvements of the thermal conductivity can be expected.

Samenvatting

In het onderzoek naar thermonucleaire fusie wordt gepoogd met behulp van magneetvelden een plasma op te sluiten onder hoge druk, bij een zo lang mogelijke energiebehoudstijd. De hoogste waarden voor het produkt van druk en energiebehoudstijd worden bereikt in de zogenaamde toka-mak. Idealiter bestaat het magneetveld in een tokamak uit een verza-meling van geneste oppervlakken van constante magnetische flux. Deze oppervlakken worden fluxoppervlakken genoemd. Fluxoppervlakken kun-nen worden gekenmerkt door hun radiële coördinaat. De geladen deeltjes 'kleven' vast op de fluxoppervlakken, hetgeen aanleiding zou moeten geven tot een zeer beperkt transport in de richting loodrecht op deze opper-vlakken (radieel).

Een van de belangrijkste problemen om tot fusiecondities te komen is het onverwacht hoge (anomale) warmtetransport via electronen en ionen in tokamaks. Het laagst haalbare warmtetransport in tokamaks wordt beschreven door de neo-klassieke theorie, waarin alleen Coulomb botsin-gen in acht worden genomen om de deeltjes van hun oppervlak te stoten. De warmtegeleidingscoefficient voor electronen χ_e blijkt twee ordes van grootte belangrijker te zijn dan voorspeld door neo-klassieke theorie. De warmtegeleidingscoefficient voor ionen χ_i blijkt minder dan een orde van grootte belangrijker te zijn dan voorspeld door neo-klassieke theorie. Indien het warmtetransport niet gereduceerd wordt, zullen fusiereactoren groot, complex en duur zijn.

Het anomale transport in tokamaks vindt plaats in de radiële richting. Het wordt gedreven door turbulente processen. Men maakt onderscheid tussen twee families van turbulentie: de electrostatische en de magneti-sche turbulentie. In electrostatische turbulentie worden perfecte fluxopper-vlakken verondersteld, waarbij het transport wordt vergroot door een extra netto drift van deeltjes loodrecht op de fluxoppervlakken. In magnetische turbulentie bestaat de perfecte topologie niet, maar wisselen 'goede' en 'aangetaste' oppervlakken elkaar af.

Het blijkt mogelijk in bepaalde gebieden van het plasma de turbulentie aanzienlijk te verminderen. Deze gebieden worden transportbarrières genoemd. Recent zijn voorbeelden gevonden van thermonucleaire plasma's waarbij het warmtetransport via de ionen tijdelijk neo-klassieke waarden bereikte. In deze fase verdwenen fluctuaties die geassociëerd worden met electrostatische turbulentie beneden het detectieniveau. Barrières in het electronen kanaal zijn geobserveerd, maar het transport via de electronen bleef in veel gevallen anomaal en vertoonde slechts een beperkte verlaging van χ_e. Dit geeft aan dat de mechanismen die de turbulentie drijven voor de ionen fundamenteel anders zijn dan de mechanismen die de turbulentie drijven voor de electronen.

RTP is een kleine tokamak met meetapparatuur (diagnostieken) voor de electronentemperatuur T_e en dichtheid n_e. Deze diagnostieken hebben een hoge plaats,- en/of tijdsresolutie. Een bijzondere eigenschap van RTP is de verhouding tussen het additionele verhittingsvermogen en het verhittingsvermogen door resistieve dissipatie van de stroom in het plasma. Het additionele vermogen wordt verkregen via microgolven die resonant met de 2^e harmonische van de electron cyclotron frequentie in het plasma worden gekoppeld. Men spreekt daarom van electron cyclotron (EC) verhitting. Door de grootte van het toroidale magneetveld te variëren is het mogelijk om de positie van warmtedepositie (ρ_{dep}) te variëren. Op RTP is de EC-vermogensdepositie sterk gelocaliseerd. Al deze eigenschappen maken RTP uitermate geschikt voor haar taakstelling: het onderzoek naar de warmtegeleiding via electronen in thermonucleaire plasma's.

Een radiële scan van ρ_{dep}, met stapjes $< 1\%$ van de kleine straal, onthult een discrete respons van T_e. De centrale electronentemperatuur, $T_e(0)$, vertoont, als functie van ρ_{dep}, scherpe transities tussen plateau's van constante $T_e(0)$. De transities vinden plaats voor veranderingen van de depositie die kleiner zijn dan 1 mm en zijn veel scherper dan het profiel van de EC-vermogensdepositie. De transities houden verband met het verlies van barrières in het electronen transport. De barrières verdwijnen als speciale waarden van het magnetisch winding getal q uit het plasma verdwijnen. Een familie van instabiliteiten treedt op voor waarden van ρ_{dep} die dicht bij de transities zitten. Analyse van deze instabiliteiten leert ons dat de barrières geassociëerd worden met $q = 1, 4/3, 3/2, 2, 5/2$ en 3.

Een model met een warmte diffusiviteitsprofiel als functie van q, met transportbarrières bij $q = 1, 4/3, 3/2, 2, 5/2$ en 3 reproduceert in het oog springende details van de experimentele data. We noemen hier de scherpte

van de transities en de vorming van geprononceerde 'oren' in de profielen van T_e als het EC-vermogen precies in een barriére wordt gedeponeerd.

De discrete respons van het plasma als functie van q is ook geobserveerd in het plasma zonder EC-verhitting (Ohmse plasma). Twee stabiele, discrete toestanden van het Ohmse plasma worden gerapporteerd. De eerste is de gebruikelijke toestand (I) die gekenmerkt wordt door driehoeksvormige profielen van T_e en n_e. De tweede, nieuw ontdekte toestand (II) wordt gekenmerkt door een veel breder T_e-profiel en een sterk gepiekt n_e-profiel. De evolutie van de ontlading hangt kritisch af van een instabiliteit. Als de instabiliteit plaatsvindt, ontstaat toestand I. Als de instabiliteit niet plaatsvindt, ontstaat toestand II. We beargumenteren dat de twee Ohmse toestanden, hun kritsche gedrag ten aanzien van instabiliteiten en de gevoeligheid voor de minimum waarde van $q(0)$ samenhangen met de lagen van hoog en laag transport. De waarnemingen spreken eerder gepubliceerde verklaringen voor het transport in het Ohmse plasma tegen.

In RTP kan het EC-vermogen onder verschillende hoeken in het plasma worden gekoppeld. Hierdoor ontstaat de mogelijkheid van niet-inductieve stroomdrijving (ECCD). Er wordt onderscheid gemaakt tussen co drive (met de richting van de inductief gedreven stroom mee) en counter drive (tegen de richting van de inductief gedreven stroom in).

De sterkste barrière van de reeks bevindt zich bij $q = 1$. In het licht hiervan is gepoogd, met behulp van ECCD, het q-profiel zodanig te manipuleren dat de barrière bij $q = 1$ extra versterkt wordt. In dynamische situaties wordt een duidelijke verbetering van de opsluiting waargenomen in geval van co-drive. Een paradoxaal resultaat is echter dat de verbetering van de opsluiting met stroomdrijving niet geobserveerd is in stationaire toestanden.

Modelberekeningen geven aan dat de paradox van de niet verbeterde stationaire opsluiting moet worden geweten aan de koppeling tussen T_e en de electrische conductiviteit. De hoge centrale temperaturen die bereikt zouden worden met sterke barrières leiden tot aanzuigen van stroomdichtheid naar het centrum, met als gevolg dat het gebied met lage shear precies buiten de voor barrière relevante q-waarden wordt geduwd. Dit effect zou teniet gedaan kunnen worden in ontladingen waarin een grote fractie van de stroom niet inductief gedreven wordt.

Dankwoord

Rijnhuizen is een perfecte plek om als fysicus te werken. Je weet je omringd door enthousiaste (soms zelfs gedreven) collega's. Zij stimuleren je om nog nauwkeuriger naar je metingen te kijken. Ze geven je informatie en achtergrondinformatie. Ze zijn kritisch, en dwingen je daardoor om het beter te doen. Bovenal geven ze, door hun aandacht, het vertrouwen dat het van belang is wat je doet. Ik wil Niek Lopes Cardozo, Chris Schüller, Dick Hogeweij en Noud Oomens bedanken voor de warme belangstelling die zij getoond hebben in mijn werk en voor de vele stimulerende discussies.

De dinsdagochtend-taart (het ingekomen stuk) wordt weggespoeld met te sterke koffie. Voor het bord staat een OiO met een stift te knoeien. Hij rapporteert zijn recente bevindingen en lanceert een wild idee om de data te interpreteren. Hij wordt niet gespaard, maar het blijft net nog fair. Zweet staat op zijn voorhoofd, en de stapel grafieken op tafel wordt steeds onoverzichtelijker. Totdat hij geen een grafiek meer kan vinden, en de meeting voorbij is. Ik zal het allemaal missen! De vriendschappelijke sfeer, en de onderlinge steun die de OiO's elkaar gegeven hebben, zijn goud waard. In dit verband wil ik Hans, Jeroen, Machiel, Michiel, Boudewijn en Joop (de vorige generatie) en Peter, Ingeborg, Jos, Frank, Mark, Arnold, Oktay, Jaco, Leon, Erik en Francisco (de huidige generatie) bedanken. Leon wil ik in het bijzonder bedanken voor het werk dat hij verrichtte aan centraal verhitte RTP plasmas. Erik wil ik bedanken voor het werk aan barrière manipulatie met ECCD. Arnold en Jos hielpen me vaak met LaTex en IDL. Naast het werk dat beschreven is in dit proefschrift, had ik het voorrecht betrokken te zijn bij metingen aan de off-axis zaagtanden. Deze sessies met Ralph, Attila en Hugo waren altijd geweldig gezellig en verrassend!

Het succes van mijn werk is voor een belangrijk deel bepaald door de de excellente meetapparatuur en de sterke ECH die op RTP geinstaleerd zijn, het mooie data-viewing systeem en de goede machine-maintenance. In het bijzonder wil ik de RTP-operatoren Cor, Paul en Jeroen, de ECH-operatoren Marlies, Raymond en Ogé, en de data-aquisiteurs Peter, Wim

Curriculum Vitae

Ik ben geboren op 31 mei 1967 te Woerden. Mijn middelbare school-
opleiding volgde ik aan het 'Christelijk Lyceum' te Zeist (eerst HAVO,
later VWO). Na het behalen van mijn VWO-diploma in 1987 volbracht
ik mijn militaire dienst als plaatsvervangend commandant van een gemo-
toriseerde infanteriegroep. Van 1988 tot 1994 studeerde ik experimentele
natuurkunde aan de Rijksuniversiteit Utrecht. Mijn afstudeeronderzoek,
het met behulp van een neuraal netwerk interpreteren van data van de 4
kanaals pulsed radar, voerde ik uit op het FOM instituut voor plasmafysica
Rijnhuizen onder dagelijkse begeleiding van Dr. S. Heynen. Op 1 oktober
1994 begon ik aan mijn promotie-onderzoek, dat ik ook uitvoerde op het
FOM instituut voor plasmafysica Rijnhuizen. Mijn promotie-onderzoek
richtte zich op de mogelijkheid dat in een thermonucleair tokamak plasma
het radiële transport van warmte via de electronen inhomogeen is.

STELLINGEN

bij het proefschrift

Electron Transport Barriers in Tokamak Plasmas

M.R. de Baar

Eindhoven, 6 Januari 1999

1. Een tokamakplasma organiseert zich in schillen met afwisselend goede en slechte warmtegeleiding via de electronen. De isolerende schillen, de zgn. transport barrières, bevinden zich in de nabijheid van de waarden van het magnetisch windingsgetal $q = 1, 4/3, 3/2, 2, 5/2$ en 3. De dikte van de barrières wordt bepaald door de lokale afschuiving van het magnetische veld.
   Dit proefschift, chapter 4 en 5

2. In een tokamakplasma bevinden zich schillen met slechte warmtegeleiding via de electronen, de zgn. transport barrières. Om actieve barrière-verbreding mogelijk te maken, dient een belangrijk deel van de plasma-stroom niet-inductief gedreven te worden.
   Dit proefschrift, chapter 7

3. Zaagtandachtige oscillaties die kunnen optreden bij rationale waarden van het magnetisch windingsgetal bieden een goede mogelijkheid voor het verwijderen van Helium-as uit de kern van het plasma in een tokamak-reactor.
   J. Rapp et al., Plasma Phys. Control. Fusion **39** (1997) 1615-1634
   H.R. Koslowski et al., Plasma Phys. Control. Fusion **39** (1997) B325-B336

4. De meting van de evolutie van filamenten in tokamakplasmas door middel van snel opeenvolgende metingen van het temperatuurprofiel wordt bemoeilijkt door de rotatie van het plasma en de geringe afmetingen van de filamenten.
   M.N.A. Beurskens et al., 'Filamentation of the RTP tokamak plasma,' in voorbereiding

5. Het feit dat de depositiesnelheid in VHF-silaan ontladingen toeneemt met toenemende frequentie bij constant toegevoegd vermogen is toe te schrijven aan veranderingen in de energieverdeling van de ionen.
   M. Yan and W.J. Goedheer, 'A PIC simulation on the effect of frequency on the characteristics of VHF SiH_4/H_2 discharges', submitted for publication in Plasma Sources Science and Technology

6. De interpretatie van 'pulsed radar' signalen in termen van de posities van lagen van kritische dichtheid in een tokamakplasma zou aanzienlijk verbeterd kunnen worden als, naast de vluchttijd, ook de vorm van de gereflecteerde pulsen werd gemeten.

7. Het zgn. 'Porter-model' voor het formuleren van bedrijfsstrategieën voldoet niet.
   M.E. Porter, Harvard Buisiness Review, March-April (1979)
   K.P. Coyne and S. Subramaniam, The McKinsey Quarterly **4** (1996) 14-25

8. Het 'super slow protocol' is, naast een 'brutally hard' trainingsroutine voor krachtsporters, een eenvoudige, goedkope en effectieve methode om botontkalking bij ouderen tegen te gaan.
   E. Darden, 'Bulk-builders instructional guide,' ISBN 0-399-51630-1
   Dr. P. Bertina, private communications

9. De Koraalspecht gevangenis (Willemstad, Curaçao, N.A.) voldoet niet aan de eisen op het gebied van veiligheid en mensenrechten zoals geformuleerd in het Europees Verdrag voor de Rechten van de Mens (Rome) en het Internationaal Verdrag Burgelijke Politieke Rechten (New York). De houding van de Nederlandse overheid in deze is in flagrante tegenspraak met het uitgangspunt dat een actief mensenrechtenbeleid gevoerd dient te worden.

10. Het feit dat het basisonderwijs op de Nederlandse Antillen nog steeds plaatsvindt met Nederlands lesmateriaal, met de weinig aansprekende voorbeelden van ijspret, sneeuwballen en sproetjes, leidt tot een verhoogd percentage van vroege drop-outs.